The rate and effect of *de novo* mutations in a colonizing lineage of *Arabidopsis thaliana*

Moises Exposito-Alonso[1,2†], Claude Becker[1†], Verena J. Schuenemann[3,4], Ella Reiter[3], Claudia Setzer[5], Radka Slovak[5], Benjamin Brachi[6§], Jörg Hagmann[1§], Dominik G. Grimm[1§], Chen Jiahui[6,7], Wolfgang Busch[5], Joy Bergelson[6], Rob W. Ness[8], Johannes Krause[3,4,9], Hernán A. Burbano[2,*], Detlef Weigel[1,*]

[1]Department of Molecular Biology, Max Planck Institute for Developmental Biology, 72076 Tübingen, Germany

[2]Research Group for Ancient Genomics and Evolution, Max Planck Institute for Developmental Biology, 72076 Tübingen, Germany

[3]Institute of Archaeological Sciences, University of Tübingen, 72070 Tübingen, Germany

[4]Senckenberg Center for Human Evolution and Paleoenvironment, University of Tübingen, 72070 Tübingen, Germany

[5]Gregor Mendel Institute, Austrian Academy of Sciences, 1030 Vienna, Austria

[6]Department of Ecology and Evolution, University of Chicago, Chicago, Illinois 60637, USA

[7]Institute of Tibet Plateau Research, Chinese Academy of Sciences, Beijing 100101, China

[8]Department of Biology, University of Toronto Mississauga, Mississauga, Ontario L5L IC6, Canada.

[9]Max Planck Institute for the Science of Human History, 07743 Jena, Germany

[†]Co-first authors

[§]Current addresses: INRA, UMR 1202 Biodiversité Gènes & Communautés, 69 route d'Arcachon, 33610 CESTAS, France (B.B.); Computomics, 72072 Tübingen, Germany (J.H.); Department of Biosystems Science and Engineering, ETH Zurich, 4058 Basel, Switzerland (D.G.G).

*Correspondence to: hernan.burbano@tuebingen.mpg.de, weigel@weigelworld.org

Keywords: colonization, mutation, selection, herbarium genomes, aDNA, phylogenomics, population genomics, association mapping, *Arabidopsis thaliana*

Because colonizations and invasions are often associated with genetic bottlenecks, they offer an opportunity to directly observe de novo mutations and their subsequent fate. North America has recently been colonized by *Arabidopsis thaliana*, and many of the individuals found today belong to a single lineage, HPG1. To determine substitution rates under natural conditions in this lineage, we have sequenced 100 HPG1 genomes from plants collected between 1863 and 2006. We infer that the last common HPG1 ancestor lived in the early 17th century, most likely the time when HPG1 began to colonize N. America. Demographic reconstructions infer substantial population size fluctuations during the past four centuries. Even though changing demographics can undermine the effect of natural selection, we observed that mutations at coding sites were at lower frequency than mutations at other sites, consistent with the effect of purifying selection. Exceptionally, some mutations rose to high frequency and some had measurable effects in root development, consistent with positive selection acting over mutations with an adaptive value. Our work showcases how by applying genomics methods to a combination of modern and historic samples we can learn about plant colonisations and invasions and observe "evolution in action".

Knowledge of mutation rates and efficacy of selection, which together determine the substitutions that can be observed in a population, is essential for understanding evolution[1]. Mutation rates are required to estimate the effective diversity of populations[2], to date historic population splits[3], and to predict what opportunities there are for rapid novel adaptations, for instance, to drugs or pesticides[4,5]. Two extreme approaches to discover these parameters are either short-term mutation accumulation experiments in the laboratory[6] and pedigree-based estimates[7], or interspecific phylogenomic comparisons over millions of years[8]. Since mutation rates are generally studied independently of natural selection and population dynamics contexts, the two approaches often yield estimates that do not coincide, which has generated a heated controversy[9,10]. An alternative not exploited so far is the analysis of naturally occurring "evolutionary experiments" such as colonizing or invasive populations associated with a recent and strong genetic bottleneck[11,12]. Both colonizations and invasions are increasingly common due to human movement[13,14]. The study of these natural experiments is especially powerful when time-stamped samples from historic specimens can be used as internal calibration points[15,16]. Colonizing populations often start with very few individuals and therefore have low genetic diversity. The N. American population of the self-fertilizing plant *Arabidopsis thaliana* is no exception, with many individuals belonging to a genetically very similar lineage, haplogroup-1 (HPG1), that spread over large geographic areas[17]. The study of the origin along with demographic and selective dynamics of mutations in HPG1 can further help us solve the current paradox generated by two evolutionary conjectures: "Baker's law", inspired by the observation that selfing species are more successfully colonizing new environments than outcrossing ones, and "Muller's ratchet", which posits that selfing populations are evolutionary dead ends, since low diversity and accumulation of more deleterious mutations should hinder their ability to adapt to new environments[18–21].

To better understand the evolution of HPG1, we sequenced 27 herbarium specimens, from 1863–1993, and 76 live isolates of this lineage collected 1993–2006 (Fig. 1; Table S1). DNA retrieved from herbarium specimens showed biochemical features typical of ancient DNA[22], which indicates that the DNA recovered from historic samples is authentic (Fig. S1, see Supplementary Online Material [SOM] for details). We mapped reads against an HPG1 pseudo-reference genome[23], focusing on single nucleotide

73 polymorphisms (SNPs) because the short sequence reads of herbarium samples preclude accurate calling
74 of structural variants. Genome sequences were of high quality, with herbarium samples covering
75 96.8–107.2 Mb of the 119 Mb reference, and modern samples covering 108.0–108.3 Mb (Table S1). Pairs
76 of herbarium genomes differed on average by 109-222 SNPs, and pairs of modern genomes by 186-299
77 SNPs, that is, they ranged from 99.9997 to 99.9999 % identity .

78 A neighbor joining tree (Fig. 2A), multi-dimensional scaling (MDS) (Fig. 2B), and a parsimony
79 network (Fig. 2C) confirmed very close relatedness of the HPG1 genomes, with only three apparent
80 intra-HPG1 recombinants (Fig. 2C). Removing these resolved the reticulations in the parsimony network
81 (Fig. 2D). The remaining 100 samples (Table S1) constitute a quasi-clonal lineage mostly devoid of
82 effective recombination and population structure, and without SNPs in organellar genomes. The very low
83 genome-wide nuclear diversity (π = 0.000002, θ_W = 0.00001, 5,013 segregating sites) is two orders of
84 magnitude lower than in the native range of the species (θ_W = 0.007) (ref. [24]) (Table S1). The enrichment
85 of low frequency variants in the site frequency spectrum (Tajima's *D* = -2.84; global= -2.04) (ref. [24]) and
86 low levels of polymorphism are consistent with a recent bottleneck followed by population expansion
87 (Fig. 3). The obvious explanation is that the bottleneck corresponds to a colonization founder event,
88 likely by very few closely related individuals, or perhaps only a single plant. To describe intra-HPG1
89 relationships in a more sophisticated manner, we used Bayesian phylogenetic inference, exploiting
90 collection dates for tip calibration of phylogenetic trees. The 76 modern individuals formed a largely
91 monophyletic clade, with only four interspersed herbarium samples from the second half of the 20th
92 century (Fig. 3A, B). Long branches reflected an abundance of singletons, typical of expanding
93 populations after bottlenecks.

94 To estimate the substitution rate in the HPG1 lineage, we used distance- and phylogeny-based
95 methods that take advantage of the known collection dates. One has to distinguish between the
96 *mutation rate*, which is the rate at which genomes change due to DNA damage, faulty repair, gene
97 conversion and replication errors, and *substitution rate*, which is the rate at which mutations survive and
98 accumulate after demographic and natural selective processes[25]. Under neutral evolution, mutation and
99 substitution rates should be equal[26]. The simple evolutionary history of the HPG1 natural population
100 enables direct estimates of substitution rates, and by comparing these with mutation rates calculated in
101 controlled conditions, we can learn about demographic and selective forces. In the distance method, the
102 substitution rate is calculated from correlation between differences in collection time in historic-modern
103 sample pairs, and the number of changes between those pairs relative to a reference (Fig. 3C), scaled to
104 the size of the genome accessible to Illumina sequencing. This method resulted in an estimated rate of
105 $2.11*10^{-9}$ substitutions site^{-1} year^{-1} (95% bootstrap Confidence Interval [CI]: $1.88–2.33*10^{-9}$) using
106 rigorous SNP calling quality thresholds. Relaxing the quality thresholds for base calling and minimum
107 genotyped rate affects both the number of called SNPs and the length of the interrogated reference
108 sequence[27]. These largely cancelled each other out, and our estimates were relatively stable, between
109 $2.1–3.2*10^{-9}$ substitutions site^{-1} year^{-1} (Table S3). The Bayesian phylogenetic approach, which uses the
110 collection years for tip calibration and assumes a relaxed molecular clock, yielded a similar estimate,
111 $4.0*10^{-9}$, with confidence ranges overlapping the above estimates (95% Highest Posterior Probability
112 Density [HPPD]: $3.2–4.7*10^{-9}$). Based on the results obtained with different methods, we can confidently
113 say that the substitution rate in the wild should be between 2 to 5 $*10^{-9}$ site^{-1} year^{-1}. We recommend

114 that these rates be used to date temporal splits between populations. To be able to compare our
115 substitution rate with the mutation rate, both need to be expressed per generation. While *A. thaliana* is
116 an annual plant, seed bank dynamics generate a delay of average generation time at the population
117 scale. A comprehensive study of multiple *A. thaliana* populations reports an average generation time of
118 1.3 years[28], with a notable variance across populations. Re-scaling with the mean generation time led to
119 an adjusted substitution rate of $2.7*10^{-9}$ substitutions site^{-1} generation^{-1} (95% CI $2.4-3.0*10^{-9}$) (Fig. 3E).
120 This is much lower than the rate of $7.1*10^{-9}$ mutations site^{-1} generation^{-1} (95% CI $6.3–7.9*10^{-9}$) (Tables
121 S2, S3) that one can calculate from resequencing data for mutation accumulation (MA) lines in the Col-0
122 reference background grown in the greenhouse[29].

123 Differences in "per generation" rates could be caused by several factors, such as an imperfect
124 knowledge of the generation time in the wild (for rates using different generation times, see Fig. 3E). In
125 addition, mutagenic environmental factors, genome background, mutation spectrum, or methodological
126 idiosyncrasies can affect the estimates. For example, transposons, which comprise ~8% of the genome
127 and ~19% of the SNPs in greenhouse MA lines, had fewer SNPs called than expected in HPG1 (~13%).
128 This is likely due to difficulties when mapping reads to genomic areas with extensive   structural
129 variation[30,30a30d30] could have contributed to the lower substitution rate estimates for HPG1 (Fig. 3E,
130 Fig S3C, Table S3). In addition, the substitution spectrum in HPG1 is shifted to a lower
131 transition/transversion ratio compared to the MA lines (Fig. 3C and Fig. S3), which could be caused by
132 methylated cytosines (see Fig. S4 and SOM). Finally, an alternative evolutionary explanation for the rate
133 differences is that purifying selection slows the accumulation of mutations in the wild by removing
134 deleterious mutations (Fig. 3E). To find evidence of negative selection independently of dataset
135 comparisons, we looked at the site frequency spectrum of different annotations within the HPG1
136 dataset. Medium-frequency variants, which are more exposed to purifying selection[31], were more
137 sharply depleted in genomic regions expected to be under greater selection constraint (genic and
138 nonsynonymous sites) than in putatively more neutral ones (intergenic or synonymous sites) (Fisher's
139 Exact test, p-value <0.05 for both comparisons, see Fig. S5). Therefore, even if we cannot say with
140 certainty that purifying selection drives the differences between HPG1 and MA rates, it must be
141 responsible for the differences between different types of sites within HPG1.

142 The substitution rate allows dating of HPG1's origin. The mean estimate from Bayesian methods
143 was the year 1597 (HPPD 95%: 1519–1660) (Fig. 3A, B). We also used a non-phylogenetic method that
144 utilizes the relationship between the average genetic distance between any two individuals, with the
145 substitution rate multiplied by twice the divergence time and the genome size; solving by the divergence
146 time in the equation we obtained 353 years. When subtracted from the average collection date of our
147 samples, the corresponding point estimate is 1625, within the confidence interval of the Bayesian
148 estimate. This corresponds to the date of the last common ancestor of HPG1, and should thus be close to
149 the time of introduction of HPG1 to N. America. (The date is older than our previous estimate, for which
150 we had naively applied the higher greenhouse mutation rate[23]). Inference of N_e through time suggested
151 exponential population growth until the early 19th century (Fig 3B, Fig S6C). During the 20th century the
152 N_e trajectory showed oscillating patterns between growth and bottlenecks, which are typical of selfing
153 organisms [32], and which likely led to a replacement of most HPG1 sublineages, as the modern samples
154 are all very closely related (Fig. 3 A, B).

Since we knew both the collection years and locations of origin of the HPG1 samples, we could also analyze the migration dynamics of HPG1. Although unknown sources of sampling bias could affect our analyses[16], the phylogeographic models suggested that HPG1 came to cover much of its modern range soon after its introduction to N. America (Fig. S6 A,B). We found a significant correlation between collection date and both latitude and longitude (Fig. 1C) , which we interpret as a net, highly dispersed, movement in a northwestern direction over time. Additional support for this hypothesis comes from an isolation-by-distance signal, which is most consistent with a historic westward migration and a more recent reverse eastward migration (Fig. S6 E,F). The apparent source of those new migrants now persisting along the East coast was the Lake Michigan area .

Finally, while we did not expect to easily find mutations that have helped the HPG1 lineage to adapt to its new N. American environment, we wanted to determine whether any of the mutations have measurable phenotypic effects. Focusing on flowering-related, reproductive and root traits of likely ecological relevance, we detected significant quantitative heritable variation (Table S4). We used an approach borrowed from GWAS to find SNPs that had increased in frequency (>5%) and were associated with these phenotypes. Because conventional GWAS relies on recombination, which is almost absent from our population, our approach could not identify individual SNPs, but only SNP cohorts distributed across the genome[33]. We found 79 SNPs associated with root traits, of which nine resulted in nonsynonymous changes. We did not find any SNPs associated with flowering time, even though it is thought to be a key player of rapid adaptation in many annual species[34,35]. Nineteen other SNPs, of which four were nonsynonymous, were associated with climate variables (www.worldclim.org) even after correction for latitude and longitude, and some of the hits overlapped between root traits and climate variables (Table 1, Table S5, Fig. S7). Although a good number of SNPs was associated with phenotypes and/or climate variables, it is not possible to confidently pinpoint individual candidate SNPs, since the extent of whole-genome linkage disequilibrium (LD) in HPG1 is high (Fig. S9 B,C). However, there is a gradient in the extent of LD between SNPs associated with root architecture, which could help to determine particularly promising candidates for molecular characterization and quantification of fitness in natural conditions (Table 1, Fig. S9 D-F). For example, the gene AT5G19330, overexpression of which confers salt tolerance[36], contains a SNP that was unlinked to other hits and that has risen in the last four centuries to a frequency of 40%. This SNP is likely to change protein function, as it leads to a substitution of cysteine for tryptophan. Another nonsynonymous SNP is located in AT2G38910, encoding a calcium dependent kinase that belongs to a family of factors involved in root hydraulic conductivity and phytohormone response[37,38]. Remarkably, most derived root-associated alleles, when compared with equally frequent neutral alleles, were first seen in older herbarium samples, most of which were collected near Lake Michigan, the apparent source of modern populations (Fig. S8). Altogether, the rise in frequency, older age of some *de novo* mutations, and their quantifiable phenotypic effects and climatic correlations strengthen the hypothesis that they might have an adaptive value and were under positive selection. These results favor Baker's law, which alleges that selfing species can often adapt to new environments, over the evolutionary dead-end hypothesis of Muller's ratchet. Furthermore, these suggestive signals of rapid adaptation via *de novo* mutations could change the current paradigm that invasive species adapt most often from sources of standing variation, either because an incomplete

bottleneck left residual variation or because there has been subsequent admixture with native species or secondary colonizers[39,40].

In summary, we have exploited whole-genome information from historic and contemporary collections of a herbaceous plant to empirically characterize the effect of evolutionary forces during a recent colonization. With this natural time series experiment, we could directly estimate the nuclear substitution rate in wild *A. thaliana* populations. This parameter, which provides immediate ability to date key events of populations, is only known for one other species: *Homo sapiens* [41]. We have presented evidence that purifying selection is perceptible already over time scales spanning only a few centuries. Although the colonizing population we have investigated has limited diversity and suffered rapid fluctuations in population size, there appear to be *de novo* mutations with phenotypic effects that contributed to rapid adaptation. While *A. thaliana* HPG1 is not an invasive species, it can teach us about fundamental evolutionary processes behind successful colonizations and adaptation to new environments. Our work should encourage others to search for similar natural experiments and to unlock the potential of herbarium specimens to study "evolution in action".

Online Content Methods, along with any additional Extended Data display items, are available in the online version of the paper; references unique to these sections appear only in the online paper.

Supplementary Information is available in the online version of the paper.

Author Contributions H.A.B. and D.W. conceived and supervised the project, and coordinated the collaborative effort. J.B. coordinated the collection of modern seed samples. C.J., B.B. and J.B. performed and analyzed flowering time and seed set greenhouse experiments. C.S. and R.S. performed and analyzed root assays and seed size measurements under the supervision of W.B.; C.B. and J.H. sequenced and curated modern samples, coordinated by D.W.; H.A.B. coordinated the collection and analysis of herbarium samples. J.K. coordinated the extraction of DNA and library preparation of herbarium samples. V.J.S. and E.R. prepared sequencing libraries from herbarium specimens. C.B. called variants in HPG1. J.H. called variants in mutation accumulation lines. M.E.A. performed the population and quantitative genomic analyses with supervision of R.N., C.B. and H.A.B. The paper was written by M.E.A., C.B., H.A.B. and D.W. with comments from all coauthors.

Author Information Reprints and permissions information is available at www.nature.com/reprints. The authors declare no competing financial interests. Readers are welcome to comment on the online version of the paper. Correspondence and requests for materials should be addressed to H.A.B. (hernan.burbano@tue.mpg.de) or D.W. (weigel@weigelworld.org).

235

REFERENCES

1. Lynch, M. *et al.* Genetic drift, selection and the evolution of the mutation rate. *Nat. Rev. Genet.* **17,** 704–714 (2016).

2. Leffler, E. M. *et al.* Revisiting an old riddle: what determines genetic diversity levels within species? *PLoS Biol.* **10,** e1001388 (2012).

3. Scally, A. & Durbin, R. Revising the human mutation rate: implications for understanding human evolution. *Nat. Rev. Genet.* **13,** 745–753 (2012).

4. Pennings, P. S. & Hermisson, J. Soft Sweeps II—Molecular Population Genetics of Adaptation from Recurrent Mutation or Migration. *Mol. Biol. Evol.* **23,** 1076–1084 (2006).

5. Karasov, T., Messer, P. W. & Petrov, D. A. Evidence that adaptation in Drosophila is not limited by mutation at single sites. *PLoS Genet.* **6,** e1000924 (2010).

6. Halligan, D. L. & Keightley, P. D. Spontaneous Mutation Accumulation Studies in Evolutionary Genetics. *Annu. Rev. Ecol. Evol. Syst.* **40,** 151–172 (2009).

7. Roach, J. C. *et al.* Analysis of genetic inheritance in a family quartet by whole-genome sequencing. *Science* **328,** 636–639 (2010).

8. Wolfe, K. H., Sharp, P. M. & Li, W.-H. Rates of synonymous substitution in plant nuclear genes. *J. Mol. Evol.* **29,** 208–211 (1989).

9. Subramanian, S. & Lambert, D. M. Selective constraints determine the time dependency of molecular rates for human nuclear genomes. *Genome Biol. Evol.* **4,** 1127–1132 (2012).

10. Gao, Z., Wyman, M. J., Sella, G. & Przeworski, M. Interpreting the Dependence of Mutation Rates on Age and Time. *PLoS Biol.* **14,** e1002355 (2016).

11. Sax, D. F. *et al.* Ecological and evolutionary insights from species invasions. *Trends Ecol. Evol.* **22,** 465–471 (2007).

12. G. F. Gauze. *The struggle for existence*. (The Williams & Wilkins company, 1934).

13. van Kleunen, M. *et al.* Global exchange and accumulation of non-native plants. *Nature* **525,** 100–103 (2015).

14. Razanajatovo, M. *et al.* Plants capable of selfing are more likely to become naturalized. *Nat. Commun.* **7,** 13313 (2016).

15. Green, R. E. & Shapiro, B. Human evolution: turning back the clock. *Curr. Biol.* **23,** R286–8 (2013).

16. Crawford, P. H. C. & Hoagland, B. W. Can herbarium records be used to map alien species invasion and native species expansion over the past 100 years? *J. Biogeogr.* **36,** 651–661 (2009).

17. Platt, A. *et al.* The scale of population structure in Arabidopsis thaliana. *PLoS Genet.* **6,** e1000843 (2010).

18. Barrett, S. C. H. Foundations of invasion genetics: the Baker and Stebbins legacy. *Mol. Ecol.* **24,** 1927–1941 (2015).

19. Stebbins, G. L. Self Fertilization and Population Variability in the Higher Plants. *Am. Nat.* **91,** 337–354 (1957).

20. Muller, H. J. THE RELATION OF RECOMBINATION TO MUTATIONAL ADVANCE. *Mutat. Res.* **106,** 2–9 (1964).

21. Lynch, M., Conery, J. & Burger, R. Mutation Accumulation and the Extinction of Small Populations. *Am. Nat.* **146,** 489–518 (1995).

22. Weiß, C. L. *et al.* Temporal patterns of damage and decay kinetics of DNA retrieved from plant herbarium specimens. *Royal Society Open Science* **3,** 160239 (2016).

23. Hagmann, J. *et al.* Century-scale Methylome Stability in a Recently Diverged Arabidopsis thaliana Lineage. *PLoS Genet.* **11,** e1004920–e1004920 (2015).

24. 1001 Genomes Consortium. 1,135 Genomes Reveal the Global Pattern of Polymorphism in Arabidopsis thaliana. *Cell* **0,** (2016).

25. Barrick, J. E. & Lenski, R. E. Genome dynamics during experimental evolution. *Nat. Rev. Genet.* **14,** 827–839 (2013).

280   26.   Kimura, M. On the evolutionary adjustment of spontaneous mutation rates. *Genet. Res.* **9,** 23–23 (1967).

281   27.   Ness, R. W., Morgan, A. D., Colegrave, N. & Keightley, P. D. Estimate of the spontaneous mutation rate in
282   Chlamydomonas reinhardtii. *Genetics* **192,** 1447–1454 (2012).

283   28.   Falahati-Anbaran, M., Lundemo, S. & Stenøien, H. K. Seed dispersal in time can counteract the effect of gene
284   flow between natural populations of Arabidopsis thaliana. *New Phytol.* **202,** 1043–1054 (2014).

285   29.   Ossowski, S. *et al.* The rate and molecular spectrum of spontaneous mutations in Arabidopsis thaliana. *Science*
286   **327,** 92–94 (2010).

287   30.   Treangen, T. J. & Salzberg, S. L. Repetitive DNA and next-generation sequencing: computational challenges and
288   solutions. *Nat. Rev. Genet.* **13,** 36–46 (2012).

289   31.   Charlesworth, B. & Charlesworth, D. *Elements of Evolutionary Genetics*. (Roberts and Company Publishers,
290   2010).

291   32.   Arunkumar, R., Ness, R. W., Wright, S. I. & Barrett, S. C. H. The evolution of selfing is accompanied by reduced
292   efficacy of selection and purging of deleterious mutations. *Genetics* **199,** 817–829 (2015).

293   33.   Templeton, A. R., Sing, C. F., Kessling, A. & Humphries, S. A cladistic analysis of phenotype associations with
294   haplotypes inferred from restriction endonuclease mapping. II. The analysis of natural populations. *Genetics*
295   **120,** 1145–1154 (1988).

296   34.   Franks, S. J., Sim, S. & Weis, A. E. Rapid evolution of flowering time by an annual plant in response to a climate
297   fluctuation. *Proceedings of the National Academy of Sciences* **104,** 1278–1282 (2007).

298   35.   Bradshaw, W. E. & Holzapfel, C. M. Genetic response to rapid climate change: it's seasonal timing that matters.
299   *Mol. Ecol.* **17,** 157–166 (2008).

300   36.   Kim, S. *et al.* ARIA, an Arabidopsis arm repeat protein interacting with a transcriptional regulator of abscisic
301   acid-responsive gene expression, is a novel abscisic acid signaling component. *Plant Physiol.* **136,** 3639–3648
302   (2004).

303   37.   Li, G. *et al.* The calcium-dependent protein kinase CPK7 acts on root hydraulic conductivity. *Plant Cell Environ.*
304   **38,** 1312–1320 (2015).

305   38.   Choi, H.-I. *et al.* Arabidopsis calcium-dependent protein kinase AtCPK32 interacts with ABF4, a transcriptional
306   regulator of abscisic acid-responsive gene expression, and modulates its activity. *Plant Physiol.* **139,**
307   1750–1761 (2005).

308   39.   Barrett, R. D. H. & Schluter, D. Adaptation from standing genetic variation. *Trends Ecol. Evol.* **23,** 38–44 (2008).

309   40.   Dlugosch, K. M. & Parker, I. M. Founding events in species invasions: genetic variation, adaptive evolution, and
310   the role of multiple introductions. *Mol. Ecol.* **17,** 431–449 (2008).

311   41.   Fu, Q. *et al.* Genome sequence of a 45,000-year-old modern human from western Siberia. *Nature* **514,**
312   445–449 (2014).

313

314

METHODS

Sample collection and DNA sequencing. Modern *A. thaliana* accessions were from the collection described by Platt and colleagues[17] which identified HPG1 candidates based on 149 genome-wide SNPs (Table S1). Herbarium specimens were directly sampled by Max Planck colleagues Jane Devos and Gautam Shirsekar, or sent to us by collection curators from various herbaria (Table S1). DNA from herbarium specimens was extracted as described[42] in a clean room facility at the University of Tübingen. Two sequencing libraries with sample-specific barcodes were prepared following established protocols, with and without repair of deaminated sites using uracil-DNA glycosylase and endonuclease VIII (refs. [43–45]) (see Supplementary Online Material [SOM]). DNA from modern individuals was extracted from pools of eight siblings using the DNeasy plant mini kit (Qiagen, Hilgendorf, Germany). Genomic DNA libraries were prepared using the TruSeq DNA Sample or TruSeq Nano DNA sample prep kits (Illumina, San Diego, CA), and sequenced on Illumina HiSeq 2000, HiSeq 2500 or MiSeq instruments. Paired-end reads from modern samples were trimmed and quality filtered before mapping using the SHORE pipeline v0.9.0 (ref. [46,47]). Because ancient DNA fragments are short (Fig. S1B), we merged forward and reverse reads for herbarium samples after trimming, requiring a minimum of 11 bp overlap[48], and treated the resulting as single-end reads. Reads were mapped with GenomeMapper v0.4.5s (ref. [49]) against an HPG1 pseudo-reference genome[23], and against the Col-0 reference genome, and SNPs were called with SHORE[23,50] using different thresholds. Samples JK2509 to JK2531 were only mapped to the HPG1 pseudo-reference genome. Average coverage depth, number of covered genome positions, and number of SNPs identified per accession relative to HPG1 are reported in Table S1. We also re-sequenced the genomes of twelve Col-0 MA lines[50,51] (Table S2).

Phylogenetic methods and genome-wide statistics. We used four methods to estimate the relationships among modern accessions, and between modern and herbarium HPG1 samples: (i) multidimensional scaling (MDS); (ii) construction of a neighbor joining tree with the adegenet package in R (ref. [52]), with branch support assessed with 1,000 bootstrap iterations and consensus reported; (iii) construction of a parsimony network using SplitsTree v.4.12.3 (ref. [53]), with confidence values calculated with 1,000 bootstrap iterations; (iv) performing a Bayesian phylogenetic analysis using BEAST v.1.8 (ref. [54]) (see below).

We estimated genetic diversity as Watterson´s θ (ref. [55]) and nucleotide diversity π, and the difference between these two statistics as Tajimas's *D* (ref. [56]) using DnaSP v5 (ref. [57]). We calculated the folded site frequency spectrum (SFS) as well as the unfolded SFS, for which we assigned the ancestral state using the *A. lyrata* genome[58]. We estimated pairwise linkage disequilibrium (LD) between all possible combinations of informative sites, ignoring singletons, by computing r^2, *D* and *D'* statistics. For the modern individuals, we calculated the recombination parameter rho ($4N_e r$) and performed the four-gamete-test[59] to identify the minimum number of recombination events. All LD and recombination related statistics were determined using DnaSP v5 (ref. [57]) (see SOM).

Substitution and mutation rate analyses. We used genome-wide nuclear SNPs to calculate pairwise "net" genetic distances using the equation $D'_{ij} = D_{ic} - D_{jc}$, where D'_{ij} is the net distance between a modern sample *i* and a herbarium sample *j*; D_{ic} the distance between the modern sample *i* and the reference

9

genome c; and D_{jc} is the distance between a modern sample (j) and the reference genome (c). We calculated a pairwise time distance in years between the collection times, $T'ij$, and calculated the linear regression: $D' = a+bT'$. The slope coefficient b describes the number of substitution changes per year. We used either all SNPs or subsets of SNPs at different annotations (genic, intergenic etc.) appropriately scaled by accessible genome length and with confidence intervals determined by bootstrap (see SOM and Fig. S3).

The second approach used Bayesian phylogenetics with the tip-calibration method implemented in BEAST v1.8 (ref. [54]). Our analysis optimized simultaneously and in an iterative fashion using a Monte Carlo Markov Chain (MCMC) a tree topology, branch length, substitution rate, and a demographic Skygrid model (Fig. 3 A,B; see SOM). The demographic model is a Bayesian nonparametric one that is optimized for multiple loci and that allows for complex demographic trajectories by estimating population sizes in time bins across the tree based on the number of coalescent - branching - events per bin (ref. [60]). We also performed a second analysis run using a fixed prior for substitution rate of $3*10^{-9}$ substitutions site^{-1} year^{-1} based on our previous net distance estimate to confirm that the MCMC had the same parameter convergence, e.g. tree topology, as in the first "estimate-all-parameters" run.

Inference of genome-wide selection. We separately analyzed sequences at different annotations, since certain regions regions should be under a different selection regime (less evolutionary constraint) than others. We compared the means and confidence intervals of substitution rates in the entire genome and in intergenic regions for both datasets, HPG1 population and laboratory Col-0 MA lines. Only within the HPG1 population, we also tested for an interaction between low and common allele frequency polymorphisms and putatively selected and putatively neutral annotations (comparisons: entire genome - intergenic, genic - intergenic, nonsynonymous - synonymous). The formal test was Fisher exact test and low and common frequency SNPs were defined in all possible cutoffs from 1 to 45% allele frequency (Fig. S5). The signal captured is based on the assumption that purifying selection is more efficient at intermediate frequencies, pushing deleterious variants towards lower frequency in the spectrum.

Association analyses and dating of new mutations. We collected flowering, seed and root morphology phenotypes for 63 accessions. For associations with climate parameters, we followed a similar rationale as described[61]. We extracted information from the bioclim database (http://www.worldclim.org/bioclim) at a 2.5 degrees resolution raster and intersected it with geographic locations of HPG1 samples (n = 100). We performed association analyses under several models and p-value corrections using the R package GeneABEL (ref. [62]), with phenotypes and climatic variables as response variables and SNPs as explanatory variables; appropriately correcting for covariates. Resulting p-values were adjusted with an empirical p-value distribution generated from 1,000 permuted datasets, or with a double Bonferroni correction: 5% / (number of SNPs + number of phenotypes tested).

Accession numbers. Short reads have been deposited in the European Nucleotide Archive under the accession number XXXXX.

METHODS REFERENCES

42.   Yoshida, K. *et al.* The rise and fall of the Phytophthora infestans lineage that triggered the Irish potato famine.

392   *Elife* **2,** e00731 (2013).

393 43. Meyer, M. & Kircher, M. Illumina sequencing library preparation for highly multiplexed target capture and
394   sequencing. *Cold Spring Harb. Protoc.* **2010,** db.prot5448 (2010).

395 44. Briggs, A. W. *et al.* Removal of deaminated cytosines and detection of in vivo methylation in ancient DNA.
396   *Nucleic Acids Res.* **38,** e87 (2010).

397 45. Kircher, M. in *Ancient DNA* (eds. Shapiro, B. & Hofreiter, M.) 197–228 (Humana Press, 2011).

398 46. Hagmann, J. *et al.* Century-scale Methylome Stability in a Recently Diverged Arabidopsis thaliana Lineage. *PLoS*
399   *Genet.* **11,** e1004920–e1004920 (2015).

400 47. Ossowski, S. *et al.* Sequencing of natural strains of Arabidopsis thaliana with short reads. *Genome Res.* **18,**
401   2024–2033 (2008).

402 48. Yoshida, K. *et al.* The rise and fall of the Phytophthora infestans lineage that triggered the Irish potato famine.
403   *eLife* **2,** e00731 (2013).

404 49. Schneeberger, K. *et al.* Simultaneous alignment of short reads against multiple genomes. *Genome Biol.* **10,** R98
405   (2009).

406 50. Becker, C. *et al.* Spontaneous epigenetic variation in the Arabidopsis thaliana methylome. *Nature* **480,**
407   245–249 (2011).

408 51. Shaw, R. G., Byers, D. L. & Darmo, E. Spontaneous mutational effects on reproductive traits of arabidopsis
409   thaliana. *Genetics* **155,** 369–378 (2000).

410 52. Jombart, T. adegenet: a R package for the multivariate analysis of genetic markers. *Bioinformatics* **24,**
411   1403–1405 (2008).

412 53. Huson, D. H. & Bryant, D. Application of phylogenetic networks in evolutionary studies. *Mol. Biol. Evol.* **23,**
413   254–267 (2006).

414 54. Drummond, A. J., Suchard, M. A., Xie, D. & Rambaut, A. Bayesian phylogenetics with BEAUti and the BEAST
415   1.7. *Mol. Biol. Evol.* **29,** 1969–1973 (2012).

416 55. Watterson, G. A. On the number of segregating sites in genetical models without recombination. *Theor. Popul.*
417   *Biol.* **7,** 256–276 (1975).

418 56. Tajima, F. Statistical method for testing the neutral mutation hypothesis by DNA polymorphism. *Genetics* **123,**
419   585–595 (1989).

420 57. Librado, P. & Rozas, J. DnaSP v5: a software for comprehensive analysis of DNA polymorphism data.
421   *Bioinformatics* **25,** 1451–1452 (2009).

422 58. Hu, T. T. *et al.* The Arabidopsis lyrata genome sequence and the basis of rapid genome size change. *Nat. Genet.*
423   **43,** 476–481 (2011).

424 59. Hudson, R. R. & Kaplan, N. L. Statistical properties of the number of recombination events in the history of a
425   sample of DNA sequences. *Genetics* **111,** 147–164 (1985).

426 60. Gill, M. S. *et al.* Improving Bayesian population dynamics inference: a coalescent-based model for multiple
427   loci. *Mol. Biol. Evol.* **30,** 713–724 (2012).

428 61. Hancock, A. M. *et al.* Adaptation to climate across the Arabidopsis thaliana genome. *Science* **334,** 83–86
429   (2011).

430 62. Aulchenko, Y. S., Ripke, S., Isaacs, A. & van Duijn, C. M. GenABEL: an R library for genome-wide association
431   analysis. *Bioinformatics* **23,** 1294–1296 (2007).

432

433

FIGURE LEGENDS

Figure 1. Geographic location and temporal distribution of HPG1 samples.

(A) Sampling location of herbarium (blue) and modern individuals (green). **(B)** Temporal distribution of samples (random vertical jitter for visualization purposes). Stars indicate four herbarium accessions that nest within the clade of modern accessions (see Fig. 3). **(C)** Linear regression of latitude and longitude as a function of collection year (p-value of the slope and Pearson correlation coefficient are indicated)

Figure 2. Relationship among herbarium and modern HPG1 samples.

(A) Neighbor joining tree, consensus of 1,000 bootstrap replicates. Branch lengths indicate number of base substitutions (colors represent herbarium (blue) and modern individuals (green)). Scale line shows the equivalent branch length of 80 nucleotide changes. Note that no outgroup was included. **(B)** First two dimensions of a multidimensional scaling plot based on pairwise identity-by-state distances. Fraction of variance explained given in parentheses. **(C, D)** Network of all samples using the parsimony splits algorithm, before **(C)** and after **(D)** removing intra-HPG1 recombinants (in red).

Figure 3. Substitution rates and demographic history.

(A) Bayesian phylogenetic analyses employing the tip calibration methodology. A total of 10,000 trees were superimposed as transparent lines, and the most common topology was plotted solidly. Tree branches were calibrated with their corresponding collection dates. **(B)** Maximum Clade Credibility (MCC) tree summarizing the trees in (A). The demographic model underlying the phylogenetic analysis, Bayesian Skygrid reconstruction, is superimposed; the mean N_e over time is shown as a dotted line and the 95% HPD is shaded grey. Note the scale line shows the equivalent branch length of 50 nucleotide changes. **(C)** Regression between pairwise net genetic and time distances. The slope of the linear regression line corresponds to the genome substitution rate per year. **(D)** Substitution spectra in HPG1 samples, compared to greenhouse-grown mutation accumulation (MA) lines. **(E)** Comparison of genome-wide, intergenic, intronic, and genic substitution rates in HPG1 and mutation rates in greenhouse-grown MA lines. Substitution rates for HPG1 were re-scaled to a per generation basis assuming different generation times. Confidence intervals in HPG1 substitution rates were obtained from 95% confidence intervals of the slope from 1,000 bootstrap (see Table S4 for actual values).

Table 1. Genic SNPs associated with different traits.

Most SNPs first appeared in sample JK2530 collected 1922 in Indiana. For non-synonymous SNPs, the amino acid change and the Grantham score (ranging from 0 to 215), which measures the physico-chemical properties of the amino acids, are reported. All SNPs in the table were significant ($p < 0.05$) after raw p-values were corrected by an empirical p-value distribution from a permutation procedure. * highlights those that also passed a double Bonferroni threshold, correcting by number of SNPs and number of phenotypes ($p < 0.0001$). LD corresponds to how many other SNP hits are in high
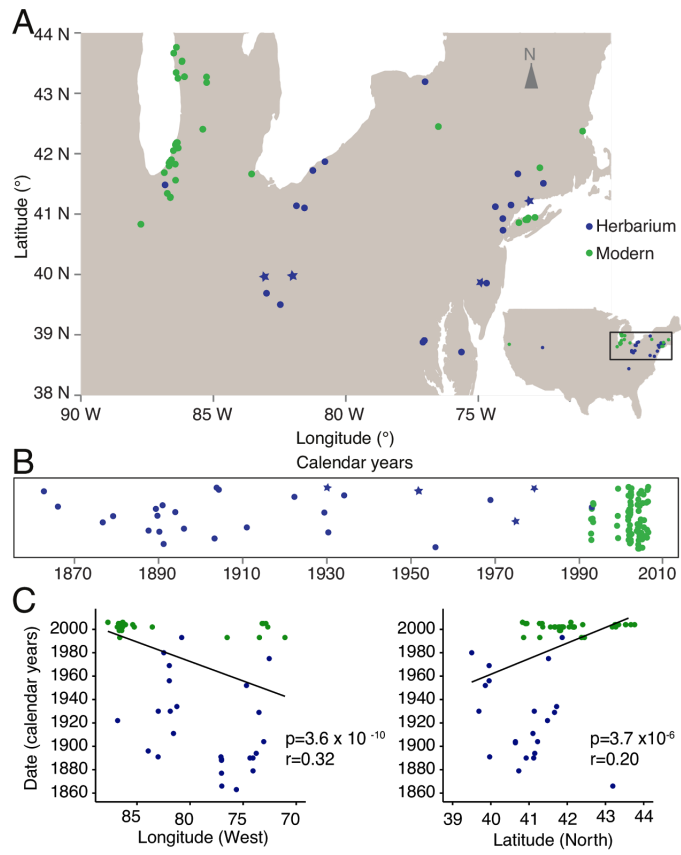
468   linkage (r^2>0.5). See Table S5 for information on all significant SNPs and Table S4 for details on

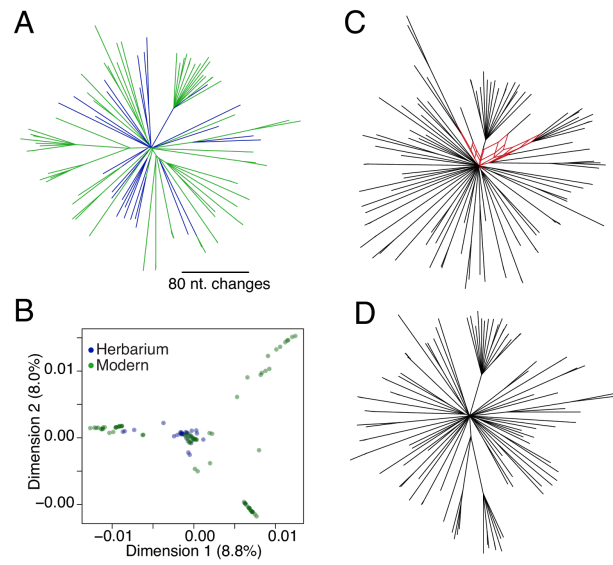469   phenotypes and climatic variables.

470

471

472   **Figure 1**

473

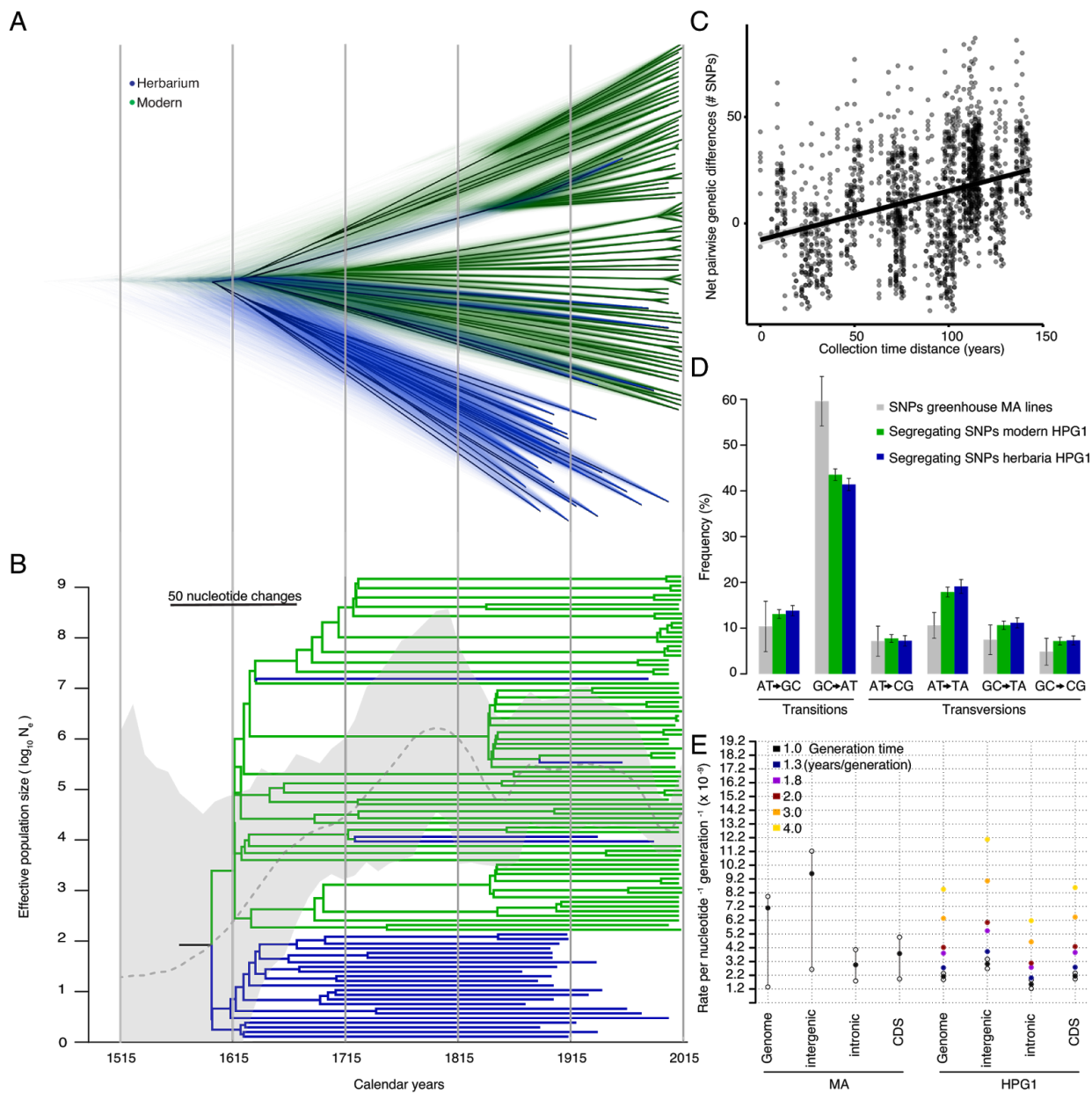
474

475   **Figure 2**

476

477

479   **Figure 3**

480

481

482

483

484

Table 1

485

Trait[†]	Location (chr-bp)	Gene	Anno–tation	Protein	aa change	LD	Bonf.
G	1-958,948	AT1G03810	nonsyn	Oligonucleotide/ oligosaccharide binding	A>P, 27	53	
D	1-13,994,958	AT1G36933	transposon	Copia		49	
S	1-20,324,050	AT1G54440	intronic	RRP6-LIKE 1		11	*
D	1-23,648,407	AT1G63740	nonsyn	TIR-NLR family	Y>S, 144	46	
G	2-358,395	AT2G01820	syn	RLK family		43	*
G	2-585,918	AT2G02220	syn	PSKR1		42	*
G	2-6,034,545	AT2G14247	syn	Expressed protein		38	*
G	2-7,047,529	AT2G16270	nonsyn	Unknown protein	P>A, 27	37	*
G	2-7,186,220	AT2G16580	intronic	SAUR8		36	*
G	2-10,495,275	AT2G24680	intronic	B3 family		34	*
G	2-12,415,084	AT2G28900	intronic	OEP16		32	
S	2-16,039,488	AT2G38290	3' UTR	AMT2		8	*
S	2-16,247,290	AT2G38910	nonsyn	CPK20	A>G, 60	7	*
G	2-16,333,662	AT2G39160	nonsyn	Unknown protein	A>G, 60	29	
G	3-2,500,258	AT3G07830	syn	PGA3		28	*
G	3-3,629,794	AT3G11530	intronic	VPS55		26	*
G	3-4,269,626	AT3G13229	5' UTR	DUF868 domain		25	*
D	3-11,873,293	AT3G30219	transposon	Gypsy		0	
G & D	4-4,228,138	AT4G07440	transposon	Oligonucleotide/ oligosaccharide binding		19	
G & D	4-9,046,942	AT4G15960	nonsyn	Alpha/beta-hydrolase superfamily	A>Q, 24	18	
G & D	4-15,646,341	AT4G32410	syn	ANY1		15	
G	4-15,845,001	AT4G32840	3' UTR	PFK6		14	
D	5-4,245,213	AT5G13260	syn	Unknown protein		12	
D	5-4,500,202	AT5G13950	nonsyn	Unknown protein	A>G, 60	11	
G	5-4,797,923	AT5G14830	transposon	Retrotransposon		10	
G	5-6,508,329	AT5G19330	nonsyn	ARIA	C>W, 215	0	
G	5-11,090,365	AT5G29037	transposon	Gypsy		4	
G	5-12,312,975	AT5G32630	pseudogene	–		3	
G	5-12,358,159	AT5G32825	transposon	CACTA		2	
S	5-16,024,197	AT5G40020	intronic	Thaumatin superfamily		2	*

[†]Traits with significant associations were root gravitropism (G), root size (S), or summer precipitation, related to drought conditions.

Supplementary Information Guide for

Exposito-Alonso, Becker et al.: **THE RATE AND EFFECT OF *DE NOVO* MUTATIONS IN A COLONIZING LINEAGE OF *ARABIDOPSIS THALIANA***

49   **SUPPLEMENTAL TEXT**

50   **1. Sample collection and preparation**

51   Seeds from modern accessions (Table S1) were bulked at the University of Chicago. Progeny for DNA

52   extraction was grown at the Max Planck Institute for Developmental Biology. We used 2 to 8 mm^2 of

53   dried tissue for destructive sampling from the herbarium specimens (Table S1).

54

55   **2. Authenticity of aDNA**

56   First, unrepaired sequencing herbarium libraries were screened for authenticity by sequencing at low

57   coverage on Illumina HiSeq 2500 or MiSeq instruments. To verify the DNA retrieved from historical

58   samples of *A. thaliana* was authentic, we checked the percentage of endogenous DNA of the sample

59   (Fig. S1A) as well as typical postmortem DNA damages: high fragmentation of DNA (Fig. S1B),

60   enrichment of substitution from C to T at the first base pair (Fig. S1C) as well as purine enrichment at

61   breakpoints of DNA fragments (Fig. S1D) (for details see [1]). Sequencing to produce the final genomes

62   (101 bp paired end) was carried out on an Illumina HiSeq 2000 instrument after DNA repair by

63   uracil-DNA glycosylase[2–4].

64

65   **3. SNP calling thresholds**

66   To asses the effect of SNP calling thresholds on the mutation rate, we employed three different

67   SHORE v0.9.0 quality thresholds following previous work (see Table S4 from ref. [5]): allowing at most

68   one intermediate penalty in all strains (most stringent threshold; "32-32"); requesting that at least

69   one strain had at most one intermediate penalty, while all others were allowed up to two high and

70   one intermediate penalties (intermediate stringency, "32-15"); and finally allowing one high and one

71   intermediate penalty for all strains (most lenient stringency, "24-24"). On top of that, we would

72   either allow missing information per SNP in up to 50% of accessions, or request complete

73   information (0% missing rate). Thus, the most rigorous case would be 32-32 quality and 0% missing

74   rate, and the most relaxed 24-24 quality and 50% maximum missing rate. Substitution rate

75   calculations (section 7.2) were done for datasets from all combinations of these quality parameters

76   (Fig. S3), and we chose the regular 32_15 quality threshold and complete information for the final

77   estimate (Fig 3 C, E).

78

79   **4. Resequencing of Col-0 Mutation Accumulation lines**

80   We also sequenced the genomes of twelve greenhouse-grown mutation accumulation (MA) lines,

81   including ten that had been sequenced at lower coverage before[5,6] (Table S2). We called SNPs, indels

82   and structural variants (SVs), following the workflow and parameters described[7], but without

83   iterations. This procedure resulted in 2,203 polymorphisms shared by all lines, indicating errors in the

84   reference sequence (12% of variants replaced N's in the TAIR9 genome) or genetic differences in the

85   founder plant of the MA population compared to the Col-0 reference genome. In addition, we

86   identified 388 segregating variants across the twelve lines (Table S2), of which 350 were singletons.

87   This analysis revealed on average 25.5 SNPs, 4.9 deletions and 3.2 insertions per MA line at the 31st

88   generation (Table S2), compared to 19.6 SNPs, 2.4 deletions and 1.0 insertions previously detected in

89   the 30th generation with shorter read length and lower read depth[8]. The genome length accessed in

90   this sequencing effort, 115,954,227 bp, was used to scale the number of point mutations to a rate of

91   7.1×10^{-9} mutations site^{-1} generation^{-1} (Table S3, Fig. 3E).

92

93   **5. Identification of *bona fide* HPG1 accessions and mutations**

94   Before we could work with the colonizer group HPG1, we needed to carefully identify individuals that

95   belong to other haplogroups or that have introgressions from them. We established the relationships

96   among all samples at three levels of resolution: (i) the 149 nuclear SNPs used originally to define the

97   HPG1 haplogroup in a global screening[9] (Fig. S2A), (ii) SNPs in the chloroplast genome (where we did

98   not find any variants within HPG1), (iii) and all nuclear genome SNPs (Fig. S2B-C). At these three

99   levels we performed a multidimensional scaling (MDS) analysis and built a neighbor-joining tree

100   using the adegenet package in R (ref. [10]).

101   Having identified these *bona fide* HPG1 individuals, we wanted to confirm that the diversity

102   has a legitimate origin from *de novo* mutations. For that we used the 1001 Genomes resource

103   (1001genomes.org) to verify that the majority of HPG1-specific variants did not originate in the

104   native Eurasian range. Subsetting the genomes from this resource to only European accessions, and

105   limiting the SNP set to those with ≥1% frequency of alternative alleles, there were 338 variants out of

106   all 5,181 HPG1 variants that were also found in Europe or Asia (6%). Only one of the reported SNPs

107   associated with phenotypes (see section 10) was among these shared variants.

108   There are several scenarios that can explain these shared SNPs. One is that some HPG1

109   individuals were moved back to Europe by humans. Another one is that parallel mutations occurred

110   in North America and Eurasia or that a reversion-mutation happened in some HPG1 individuals.

111   Given that 10% of all sites in the genome are variable in the 1001 Genomes collection, this is not an

112   implausible scenario for at least a fraction of shared SNPs. Two additional scenarios involve an origin

113   from standing European variation: (1) the shared variants come from small introgression events that

114   passed our filters above, or (2) the bottleneck was not complete, and while it left no diversity in the

115   chloroplast genome, a few hundred SNPs were passed on in the nuclear genome (given the low

116   number of variants, the colonizers could have been as many as two dozen seeds)

117

6. Extent of linkage disequilibrium and recombination

We estimated pairwise linkage disequilibrium (LD) between all possible combinations of informative sites, ignoring singletons, by computing r^2, D and D' statistics. LD decay was estimated using a linear regression approach. Linkage disequilibrium parameter D' did not decay with physical distance (intercept = 0.99, slope = 0.00, p < 0.0001) among all SNP pairs. Furthermore, only 0.02% of the nonsingleton SNP pairs were not in complete linkage disequilibrium (D'<1), indicating extensive linkage between chromosomes. We also formally estimated recombination within HPG1. The estimate was much lower ($4N_er$ = ρ = 3.0 x 10^{-6} cM bp^{-1}) than for a similar-sized collection of diverse *A. thaliana* individuals from the native range[11] (ρ = 7.5 x 10^{-2} cM bp^{-1}). The four-gamete test[12], which determines whether all four possible gametes (ab, aB, Ab, AB) are observed for two segregating loci, revealed that all configurations of SNPs could be explained with as few as 38 recombination events for the 100 genomes. We argue that this number of potential recombination events is sufficiently small to use phylogenetic methods with the 100 HPG1 genomes, even though such methods are normally not appropriate for genome-wide analyses. Indeed, other sources of failure of the four-gamete test and the violation of phylogenetic assumptions could be sequencing errors, or lineage sorting of segregating sites from the ancestral population. LD and recombination related statistics were determined using DnaSP v5 (ref. [13]) or plink v1.90b2n (ref.[14]).

7. Substitution and mutation rate analyses

7.1 Greenhouse grown MA lines

Mutation rates were estimated for each 31st generation greenhouse-grown MA line[5] as the number of mutations divided by the total bp length of the genome (or a given annotation) and by 31 generations (the two MA lines with only three generations were excluded from this analysis). Mean and confidence intervals across lines are reported (Table S3). The genome length was determined as all base pairs with coverage higher or equal to 3, and a SHORE mapping quality score of at least 32 in one sample (Table S2).

7.2 Natural populations of HPG1

7.2.1 Net distances

For the "net genetic distances" method, we computed confidence intervals of the *b* regression slope coefficient (D' = $a+bT'$) using a bootstrap with replacement of 1,000 samples to avoid over-confident confidence intervals due to lack of independence of points[15]. We used either all SNPs or SNPs at specific annotations to calculate different substitution rates and scaled the slope into a per-base rate using all positions (of the given annotation) that passed alternative or reference call quality

4

152 thresholds rather than using a single value of genome length (Table S3). For all annotations we

153 calculated substitution rates with three quality thresholds and either full information per SNP or

154 allowing a maximum of 50% missing accessions per SNP (see section 3 and Fig. S3C). For some

155 annotations substitution rates were not reliable. For instance, in 3' and 5' UTR regions, we did not

156 have enough mutations (on average ~1 SNP difference between any pair), and thus do not report

157 these regions' rates. Transposons showed unstable substitution rate estimates that we attribute to

158 structural variation relative to the reference genome. This likely decreased our ability to map

159 transposon reads correctly and subsequently call SNPs[16]. In contrast, in the MA dataset, transposon

160 structural variation was probably fairly low since only 31 generation separate the Col-0 reference

161 genome with each of the ten derived MA lines. This can be the reason that the number of

162 transposon SNPs identified in the MA dataset is proportionally larger than in HPG1 (Table S2 and S3).

163 Therefore, transposon substitution rates in HPG1 cannot be trusted.

164

165 *7.2.2 Bayesian tip-calibration*

166 For the second approach to estimate a substitution rate, the Bayesian phylogenetics tip-calibration

167 approach, we performed systematic runs and chain convergence assessments of different

168 demographic and molecular clock models. We found the Skygrid demographic model[17] and the

169 lognormal relaxed molecular clock[18 18] the most appropriate models. Under a relaxed molecular

170 clock, the substitution rate is allowed to vary across branches with a lognormal distribution. The prior

171 used for molecular clock was a Continuous-Time Markov Chain (CTMC)[17,19]. The analysis was carried

172 out remotely at CIPRES PORTAL (v3.1 www.phylo.org) using uninformative priors. The run took about

173 1,344 CPU hours and performed 1,000 million steps in a Monte Carlo Markov Chain (MCMC),

174 sampling every 100,000 steps. Burn-in was adjusted to 10% of the steps. To visualize the tree output

175 we produced a Maximum Clade Credibility (MCC) tree with a minimum posterior probability

176 threshold of 0.8 and a 10% burn-in using TreeAnnotator (part of BEAST package), and visualized the

177 MCC tree using FigTree (tree.bio.ed.ac.uk/software/figtree/) (Fig. 3B). Additionally, we used

178 DensiTree[20] to simultaneously draw the 10,000 BEAST trees with the highest posterior probability

179 (Fig. 3A). Since all trees were drawn transparently, agreements in both topology and branch lengths

180 appear as densely colored regions, while areas with little agreement appear lighter.

181

182 *7.2.3 Methylation status of mutated sites*

183 As in many other species, the spectrum of *de novo* mutations in the greenhouse-grown *A. thaliana*

184 MA lines is biased towards G:C→A:T transitions[8], leading to an inflated transition-to-transversion

185 ratio (Ts/Tv). This bias is less pronounced in recent mutations in a Eurasian collection of natural

186 accessions[21] and in HPG1 accessions (Fig. 3D). A recent multigenerational salt stress experiment in

187 the greenhouse also showed a more balanced Ts/Tv (ref. [22]). These findings indicate that less benign

188 conditions might promote a lower Ts/Tv, and one possible cause are methylation patterns, known to

189 change under different environments[23].

190   We interrogated the potential evolutionary role of cytosine methylation in the mutability of

191 cytosine bases in the HPG1 accessions. For reference DNA methylation data, we used previously

192 generated bisulfite-sequencing data of HPG1 strains[7] and of Col-0 MA lines[5], respectively. For both

193 datasets, methylation status was calculated as the fraction of reads with methylated cytosines by the

194 total number of reads at a certain cytosine position in the genome. Our rationale was that if

195 methylation affected mutability, the degree of methylation at positions were we find a new mutation

196 should be higher. To be sure that a given site in HPG1 was a new mutation, we only considered

197 positions for which we could determine that state by alignment to the *A. lyrata* genome[24]. The

198 "tested sites" were positions in HPG1 that had a mutation both from *A. lyrata* and *A. thaliana* Col-0.

199 These positions can be of two kinds, "fixed" if all HPG1 individuals carry the alternative, or

200 "segregating" if both reference and alternative alleles exist in HPG1. As control, "control set", we

201 used cytosine positions that did not vary across HPG1, *A. lyrata* and *A. thaliana*. To produce the

202 methylation distribution of the control set we randomly chose 1,000 invariant cytosine positions. For

203 the test sets, we averaged the methylation degree and compared it with the control distribution.

204   Ancestral cytosines with higher methylation in both *A. thaliana* Col-0 reference and HPG1

205 pseudo-reference methylome datasets were more likely to mutate to thymines in HPG1 (Fig. S4 A-D).

206 Additionally, the methylation degree at substitutions inside genes was higher in the HPG1

207 methylome (Fig. S4 B,D). While some C→T changes could be explained by higher spontaneous

208 deaminations known to happen more often at methylated cytosines, also C→A/G substitutions were

209 more likely to have been methylated. If this process is common enough, the Ts/Tv ratio should

210 decrease. We are far from understanding differences in Ts/Tv in natural and controlled conditions,

211 but definitely methylation status seems to have a strong statistical connection with mutability.

212

213 **8. Inference of genome-wide selection**

214 Since we observed differences between the two mutation accumulation (MA) datasets (the

215 laboratory Col-0 MA lines and the wild HPG1 lines), we tried to infer selection based on differences in

216 polymorphisms and substitution rates. We compared the different substitution rates and the 95%

217 bootstrap confidence intervals to assess how identical they were (Table S3). Genome-wide

218 substitution rate in the HPG1 dataset was significantly lower than that in controlled greenhouse

219 conditions, even after correcting by the mean generation time of 1.3 years[25] (Table S3). However,

220 these differences could be due to differences in individual genomic annotations. For instance, coding

221 regions and introns were virtually identical between the two datasets, but transposons and

222 intergenic were much lower in HPG1. Furthermore, if the true generation time is about 2-3 years (Fig.

223 3), differences in the mentioned annotations would also disappear. Therefore, we tried to investigate

224 the existence of purifying selection based on frequency equilibriums only within the HPG1

225 population. We did comparisons between pairs of annotation categories and between pairs of

226 frequency classes (i.e., low and common). In this way, genome-wide, genic and non-synonymous

227 polymorphisms were compared to matched putatively neutral annotations: intergenic and

228 synonymous sites (Fig. S5). We tested for an interaction using a Fisher's Exact test on 2x2 table

229 counts as:

230

Neutral annotation & low frequency	Neutral annotation & common frequency
Selected annotation & low frequency	Selected annotation & common frequency

235

236   Because any frequency cut-off is arbitrary, we computed the test with all cutoffs from 0 to

237 50% frequencies in 1% steps (Fig. S5). This test, which resembles in concept the MK or HKA tests,

238 evidences that there is a depletion of common frequency polymorphisms, which are more exposed

239 to selection, at the three putatively selected genomic levels compared to control (quasi-neutral)

240 regions: genome-wide, genes and nonsynonymous sites.

241

242 **9. Demography and migration of HPG1**

243 9.1 Skygrid coalescent

244 From the Bayesian phylogenetic analyses described previously (section 7.2.2), we studied the

245 demographic model estimated via Skygrid. We reconstructed a skyline plot that depicts changes in

246 effective population size, a measure of relative diversity, through time[26] (Fig. 3B). Sampling biases

247 could produce artefactual effects in the Skygrid plot. Nevertheless we expect these to be minor since

248 our dataset has a continuous sampling over a century (>2 samples per decade) instead of a

249 two-timepoints sampling, as it is common in ancient DNA studies where the rarity of the samples are

250 a limiting factor[27]. An additional BEAST run was performed only with modern samples to verify that

251 the corresponding part of the tree and population sizes matched (data not shown). Implementation

252 of non-phylogenetic methodologies for demographic inference exist, e.g. Multiple Sequentially

253 Markovian Coalescent (MSMC)[28], but after exploring them we concluded their resolution was

254 insufficient for analyses of the last several centuries. In order to compare with another method, we

255 got rough estimates of the diversity per decade as the average genetic differences between any two

256 samples per decade (Fig S6C).

257

258   9.2. Phylogeography

259   We performed another Bayesian phylogenetic analysis incorporating a geographic location trait[29,30].

260   For this, Brownian diffusion parameters are estimated by fitting a continuous gradient of geographic

261   locations along tree branches, starting from the leaves of the tree for which geographic locations are

262   known, i.e., the collection sites of our samples. We excluded three samples from the West coast of

263   the United States, separated over three thousand kilometers from the rest, since these do not fit a

264   gradual propagation by Brownian diffusion. We ran this analysis with the parameters described

265   previously (section 7.2.2) and sliced the resulting 3D (temporal and geographical) phylogeny at the

266   early 16th and late 18th century using SPREAD software[31] (Fig. S6B). Similar to before, we roughly

267   estimated "local diversity" for each sampling location by computing the average genetic differences

268   to the 10 closest neighbours (Fig. S6D).

269

270   9.3. Isolation by distance

271   We employed a heuristic search[32] using an isolation-by-distance pattern to find the origin of

272   diffusion of HPG1 in North America, and compared it to the phylogeography analyses. We performed

273   a regression between genetic distances on geographic distances for all pairs of samples (*genetic*

274   *distance ~ Euclidean geographic distances*). This pattern, known as isolation by distance pattern,

275   reflects that as individuals are more geographically apart, they differ more genetically. We evaluated

276   whether this relationship was still significant for each of our samples separately (i.e., from a focal

277   sample, does genetic distance increase as geographic distance increases?). Only the significant

278   samples were retained and plotted since those points are the expected origins of migrations (Fig. S6

279   E,F). Arrows can be plotted in the direction of the maximum slope to illustrate migration trajectories.

280   This was done separately for historic and modern samples.

281

282   **10. Phenotypic association analyses and dating of newly arisen mutations**

283   10.1. Phenotyping

284   *10.1.1 Root*

285   Fifteen root phenotypes were scored for ≥ 10 replicates per genotype over a time-series experiment

286   at the Gregor Mendel Institute in Vienna, using image analysis as described in detail elsewhere[33]. We

287   used the means per genotypes and per time series for association analyses.

288

289   *10.1.2 Seed size*

290   We spread the seeds of given genotypes on separate plastic square 12 x 12 cm Petri dishes. For faster

291   image acquisition we used a cluster of eight Epson V600 scanners. The scanner cluster was operated

292   by   the   BRAT   Multiscan   image   acquisition   tool

293   (www.gmi.oeaw.ac.at/research-groups/wolfgang-busch/resources/brat/). The resulting 1600 dpi

294   images were analyzed in Fiji software. Scans were converted to 8-bit binary images, thresholded

295   (parameters: setAutoThreshold("Default dark"); setThreshold(20, 255)) and particles analyzed

296   (inclusion parameters: size=0.04-0.25 circularity=0.70-1.00). The 2D seed size was measured in

297   square millimeters (parameters: distance=1600 known=25.4 pixel=1 unit=mm) for 2 plants per

298   genotype, > 500 seeds per plant.

299

300   *10.1.3 Flowering in the growth chamber*

301   We estimated the flowering time in growth chambers under four vernalization treatments (0, 14, 28

302   and 63 days of vernalization). We grew 6 replicates per accession divided between two complete

303   randomized blocks for each treatment. Seeds were sown on a 1:1 mixture of Premier Pro-Mix and

304   MetroMix and cold stratified for 6 days (6°C, no light). We then let plants germinate and grow at

305   18°C, 14 hours of light, 65% humidity. After 3 weeks, we transferred the plants to vernalization

306   conditions (6°C, 8 hours of light, 65% humidity). After vernalization, plants were transferred back to

307   long day conditions. Trays were rotated around the growth chambers every other day throughout the

308   experiment, under both vernalization and ambient conditions. Germination, bolting and flowering

309   dates were recorded every other day until all plants had flowered. Days till flowering or bolting times

310   were calculated from the germination date until the first flower opened and until the first flower bud

311   was developed, respectively. The average flowering time and bolting time per genotype were used

312   for association analyses.

313

314   *10.1.4 Fecundity in the field*

315   To investigate variation in fecundity in natural conditions, we grew three replicates of each accession

316   in a field experiment following a completely randomized block design. Seeds were sown from

317   09/20/2012 to 09/22/2012 in 66-well trays (well diameter = 4 cm) on soil from the field site where

318   plants were to be transplanted. The trays were cold stratified for seven days before being placed in a

319   cold frame at the University of Chicago (outdoors, no additional light or heat, but watered as needed

320   and protected from precipitation). Seedlings were transplanted directly into tilled ground at the

321   Warren Wood field station (41.84° N., 86.63° W.), Michigan, USA on 10/13/2012 and 10/14/2012.

322   Seedlings were watered-in and left to overwinter without further intervention. Upon maturation of

323   all fruits, stems were harvested and stored between sheets of newsprint paper. To estimate the

324   fecundity, stems were photographed on a black background and the size of each plant was estimated

325   as the number of pixels occupied by the plant on the image. This measure correlates well with the

326   total length of siliques produced, a classical estimator of fecundity in *A. thaliana* (Spearman's

327   rho=0.84, *p*-value<0.001, data not shown).

328

10.2 Quantitative genetic analyses

For 63 modern accessions, we measured time to bolting and flowering, seeds per plant, seed size, and 15 root phenotypes in common chamber or common garden settings. For all 100 accessions, climatic information from the bioclim database (http://www.worldclim.org/bioclim) was extracted using their geographic coordinates. For historic samples, some locations were only known by county name. In this case we assigned the geographic coordinate location of the centroid of the county.

10.2.1 Heritability

We performed association analyses using the R package GenABEL[34], with measured phenotypes (p = 25) and climatic variables (c = 18) as response variables and SNPs as explanatory variables. A Minimum Allele Frequency (MAF) cutoff of 5% was used. The number of assessed SNPs was 391 in a dataset of only modern samples but with imputed genotypes for missing data using Beagle v4.0 (ref. [35]), and 456 SNPs with a dataset of modern and historic samples, without imputation. For all associations, at least 63 individuals were genotyped for a specific SNP. We first investigated broad sense heritability (H^2) of each trait using ANOVA partition of variance between and within lines using replicates (Table S4). Significance was obtained by common F test in ANOVA. Secondly we used the *polygenic_hglm* function to fit a genome wide kinship matrix to calculate a narrow sense heritability estimate (h^2). Significance was calculated employing a likelihood ratio test comparing with a null model. In principle, h^2 is a component of H^2, then its values should theoretically be $h^2 < H^2$; that is not our case. Our result cannot be interpreted in this framework, since the calculation of both was not done with the same samples: for the h^2 calculation we employed genotype means whereas for the H^2 we used multiple replicated measurements per genotype. The averaging of replicates per genotype in h^2 reduced environmental and developmental noise and thus we would expect $h^2 > H^2$. We did this so the climatic estimates of h^2, for which we only have one value per genotype, would be comparable with the phenotypic h2 ones (Table S4).

10.2.2 Linear Models

For association analyses we first employed a linear mixed model that fitted the kinship matrix using the *mmscore* function, and only three significant SNP hits were discovered using a 5% significance threshold after False Discovery Rate correction (FDR). This was expected since we have few variants and these would have originated in an approximated phylogeny structure. We concluded that fitting the kinship matrix in our model was not appropriate since there would be no residual variation for association with specific SNPs. With this rationale we employed a fixed effects linear model using the *qtscore* function[36]. To reduce the false-positive rate we took a conservative permutation strategy by

363 carrying out association with over 1,000 randomized datasets (permuting phenotypes across

364 individuals) and used the resulting p-value distribution to correct p-values estimated with the original

365 dataset. SNPs with p-values below 5% in the empirical p-value distribution were considered

366 significant (Table S5). In climatic models, we included longitude and latitude as covariates to correct

367 for any spurious association between SNPs and climate gradients created by the migratory pattern of

368 isolation by distance.

369

370 *10.2.3 Evaluation of significance*

371 Significant SNPs were interspersed throughout the genome (Fig. S7) and their p-values and

372 phenotypic effects did not correlate with the minimum age of the SNPs nor with their allele

373 frequency (Fig. S10), something that could have indicated that the significance was merely driven by

374 the higher statistical power of intermediate frequency variants. Using QQ plots to assess inflation or

375 deflation of p-values, we observed generally that permutation corrected p-values were deflated.

376 Straight series of points in QQ plots indicate identical p-values for multiple SNPs, a pattern that we

377 attributed to long range LD, i.e. lack of independence (see Graphic Table S7 for trait distributions and

378 QQ plots from each association analysis). We also used a False Discovery Rate correction for the raw

379 p-values using *p.adjust* in R and, as a sanity check, we used a Bonferroni-corrected threshold, a

380 procedure considered over-stringent in association analyses (Table S5). This was calculated as: 5% /

381 (number of SNPs + number of traits) ~ 0.01%.

382

383 *10.2.4 Context of de novo mutations associated with phenotypes*

384 For each SNP in our dataset, we determined the ancestral and derived states, by identifying which

385 allele was found in the oldest herbarium samples. We compared the time of emergence and the

386 centroid of geographic distribution of the alternative alleles of SNP hits to random draws of SNPs

387 with the same MAF filtering (5%) (Fig. S8).

388

389 *10.2.5 Functional information*

390 On top of phenotypic and climatic associations of SNP hits, we also provide a likely functional effect

391 employing a commonly used amino acid matrix of biochemical effects[37]. Functional information of

392 gene   name   and   ontology   categorization   of   SNP   hits   was   obtained   from

393 www.arabidopsis.org/portals/genAnnotation/gene_structural_annotation/annotation_data.jsp   and

394 www.arabidopsis.org/tools/bulk/go/ (Table 1 and Table S5).

395

396   *10.2.6 Proof of concept examples*

397   We argue that the power of an association approach relies on the fact that HPG1 lines resemble Near

398   Isogenic Lines (NILs) produced by experimental crosses[38] (Fig. S9A). Similar to genome-wide

399   association studies (GWA), power depends on many factors, namely the noise of phenotype under

400   study, architecture of phenotypic trait, quality of genotyping, population structure, sample diversity,

401   sample size, allele frequency, and recombination. On one hand, association analyses in NILs suffer

402   from large linkage blocks, but confident results can be achieved due to accurate measurement of

403   phenotypes, limited genetic differences between any two lines, and high quality genotypes. In

404   common GWA studies such as in humans, there are multiple confounding effects. Among the

405   confounders are (1) that any two samples differ in hundreds of thousands of SNPs, and (2) that

406   historical and geographic stratification produce non-random correlations among those SNP

407   differences. This considerably complicates the identification of phenotypic effects at specific genes,

408   and power relies greatly on large sample sizes to achieve the sufficient number of recombination

409   between markers.

410   To provide support for the non-synonymous SNP on chromosome 5, at position 6,508,329 in

411   AT5G19330, we looked for pairs of lines that carry the ancestral and the derived allele, but that differ

412   in few (or no other) SNPs in the genome. When considering all genic substitutions with a minimum

413   allele frequency of 5% (Fig. S9A), we identified 20 pairs of lines differing only in the AT5G19330 SNP

414   and another linked SNP (located on a different chromosome, association p-value > 0.4). The

415   phenotypic differences in mean gravitropic score of these almost-identical pairs were significantly

416   higher than phenotypic differences among all pairs of HPG1 lines, and genetically identical pairs

417   attending to substitutions inside genes (Fig. S9A). Furthermore, this SNP was not in complete linkage

418   with any other SNP hit (r^2 < 0.5) (Fig. S7D). The same approach was used to examine the SNPs in

419   AT1G54440 (Fig. S7E) and AT2G16580 (Fig. S7F), which represent an intermediate and a high LD

420   example.

421

REFERENCES

422   1.   Weiß, C. L. *et al.* Temporal patterns of damage and decay kinetics of DNA retrieved from plant

423   herbarium specimens. *Royal Society Open Science* **3,** 160239 (2016).

424   2.   Meyer, M. & Kircher, M. Illumina sequencing library preparation for highly multiplexed target

425   capture and sequencing. *Cold Spring Harb. Protoc.* **2010,** db.prot5448 (2010).

426   3.   Briggs, A. W. *et al.* Removal of deaminated cytosines and detection of in vivo methylation in

427   ancient DNA. *Nucleic Acids Res.* **38,** e87 (2010).

428   4.   Kircher, M. in *Ancient DNA* (eds. Shapiro, B. & Hofreiter, M.) 197–228 (Humana Press, 2011).

429   5.   Becker, C. *et al.* Spontaneous epigenetic variation in the Arabidopsis thaliana methylome.

430   *Nature* **480,** 245–249 (2011).

431   6.   Shaw, R. G., Byers, D. L. & Darmo, E. Spontaneous mutational effects on reproductive traits of

432   arabidopsis thaliana. *Genetics* **155,** 369–378 (2000).

433   7.   Hagmann, J. *et al.* Century-scale Methylome Stability in a Recently Diverged Arabidopsis

434   thaliana Lineage. *PLoS Genet.* **11,** e1004920–e1004920 (2015).

435   8.   Ossowski, S. *et al.* The rate and molecular spectrum of spontaneous mutations in Arabidopsis

436   thaliana. *Science* **327,** 92–94 (2010).

437   9.   Platt, A. *et al.* The scale of population structure in Arabidopsis thaliana. *PLoS Genet.* **6,**

438   e1000843 (2010).

439   10.   Jombart, T. adegenet: a R package for the multivariate analysis of genetic markers.

440   *Bioinformatics* **24,** 1403–1405 (2008).

441   11.   Choi, K. *et al.* Arabidopsis meiotic crossover hot spots overlap with H2A.Z nucleosomes at gene

442   promoters. *Nat. Genet.* **45,** 1327–1336 (2013).

443   12.   Hudson, R. R. & Kaplan, N. L. Statistical properties of the number of recombination events in the

444   history of a sample of DNA sequences. *Genetics* **111,** 147–164 (1985).

445   13.   Librado, P. & Rozas, J. DnaSP v5: a software for comprehensive analysis of DNA polymorphism

446   data. *Bioinformatics* **25,** 1451–1452 (2009).

447   14.   Purcell, S. *et al.* PLINK: a tool set for whole-genome association and population-based linkage

448   analyses. *Am. J. Hum. Genet.* **81,** 559–575 (2007).

449   15.   Drummond, A., Pybus, O. G. & Rambaut, A. Inference of viral evolutionary rates from molecular

450   sequences. *Adv. Parasitol.* **54,** 331–358 (2003).

451   16.   Treangen, T. J. & Salzberg, S. L. Repetitive DNA and next-generation sequencing: computational

452   challenges and solutions. *Nat. Rev. Genet.* **13,** 36–46 (2012).

453   17.   Gill, M. S. *et al.* Improving Bayesian population dynamics inference: a coalescent-based model

454   for multiple loci. *Mol. Biol. Evol.* **30,** 713–724 (2012).

455   18.   Drummond, A. J., Ho, S. Y. W., Phillips, M. J. & Rambaut, A. Relaxed phylogenetics and dating

456   with confidence. *PLoS Biol.* **4,** e88–e88 (2006).

457   19.   Ferreira, M. a. R. & Suchard, M. a. Bayesian analysis of elapsed times in continuous-time

458   Markov chains. *Can. J. Stat.* **36,** 355–368 (2008).

459   20.   Bouckaert, R. R. DensiTree: making sense of sets of phylogenetic trees. *Bioinformatics* **26,**

460   1372–1373 (2010).

461   21.   Cao, J. *et al.* Whole-genome sequencing of multiple Arabidopsis thaliana populations. *Nat.*

462   *Genet.* **43,** 956–963 (2011).

463   22.   Jiang, C. *et al.* Environmentally responsive genome-wide accumulation of de novo Arabidopsis

464   thaliana mutations and epimutations. *Genome Res.* **24,** 1821–1829 (2014).

465   23.   Wibowo, A. *et al.* Hyperosmotic stress memory in Arabidopsis is mediated by distinct

466   epigenetically labile sites in the genome and is restricted in the male germline by DNA

467   glycosylase activity. *eLife Sciences* **5,** e13546 (2016).

468   24.   Hu, T. T. *et al.* The Arabidopsis lyrata genome sequence and the basis of rapid genome size

469   change. *Nat. Genet.* **43,** 476–481 (2011).

470   25.   Falahati-Anbaran, M., Lundemo, S. & Stenøien, H. K. Seed dispersal in time can counteract the

471   effect of gene flow between natural populations of Arabidopsis thaliana. *New Phytol.* **202,**

472   1043–1054 (2014).

473   26.   Drummond, A. J., Suchard, M. A., Xie, D. & Rambaut, A. Bayesian phylogenetics with BEAUti and

474   the BEAST 1.7. *Mol. Biol. Evol.* **29,** 1969–1973 (2012).

475   27.   Fu, Q. *et al.* A revised timescale for human evolution based on ancient mitochondrial genomes.

476   *Curr. Biol.* **23,** 553–559 (2013).

477   28.   Schiffels, S. & Durbin, R. Inferring human population size and separation history from multiple

478   genome sequences. *Nat. Genet.* **46,** 919–925 (2014).

479   29.   Lemey, P., Rambaut, A., Welch, J. J. & Suchard, M. A. Phylogeography takes a relaxed random

480   walk in continuous space and time. *Mol. Biol. Evol.* **27,** 1877–1885 (2010).

481   30.   Barton, N. H. & Wilson, I. Genealogies and geography. *Philos. Trans. R. Soc. Lond. B Biol. Sci.*

482   **349,** 49–59 (1995).

483   31.   Bielejec, F., Rambaut, A., Suchard, M. A. & Lemey, P. SPREAD: spatial phylogenetic

484   reconstruction of evolutionary dynamics. *Bioinformatics* **27,** 2910–2912 (2011).

485   32.   Handley, L. J. L., Manica, A., Goudet, J. & Balloux, F. Going the distance: human population

486   genetics in a clinal world. *Trends Genet.* **23,** 432–439 (2007).

487   33.   Slovak, R. *et al.* A Scalable Open-Source Pipeline for Large-Scale Root Phenotyping of

488   Arabidopsis. *Plant Cell* **26,** 2390–2403 (2014).

489   34.   Aulchenko, Y. S., Ripke, S., Isaacs, A. & van Duijn, C. M. GenABEL: an R library for genome-wide

490   association analysis. *Bioinformatics* **23,** 1294–1296 (2007).

491   35.   Browning, B. L. & Browning, S. R. Genotype Imputation with Millions of Reference Samples. *Am.*

492   *J. Hum. Genet.* **98,** 116–126 (2016).

493   36.   Aulchenko, Y. S., de Koning, D.-J. & Haley, C. Genomewide rapid association using mixed model

494   and regression: a fast and simple method for genomewide pedigree-based quantitative trait loci

495   association analysis. *Genetics* **177,** 577–585 (2007).

496   37.   Grantham, R. Amino acid difference formula to help explain protein evolution. *Science* **185,**

497   862–864 (1974).

498   38.   Weigel, D. Natural variation in Arabidopsis: from molecular genetics to ecological genomics.

499   *Plant Physiol.* **158,** 2–22 (2012).

500

501   SUPPLEMENTAL FIGURES

502
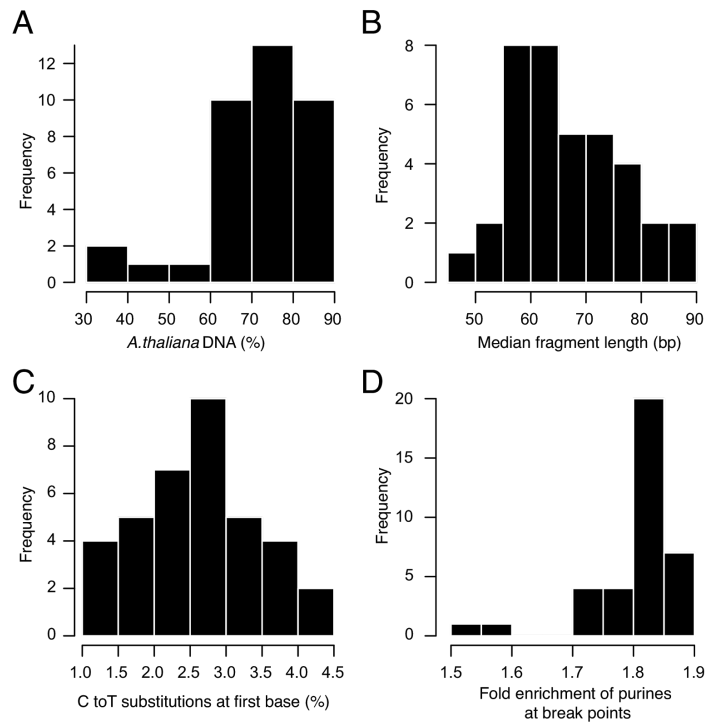
503   Figure S1. Ancient-DNA-like characteristics of unrepaired herbarium libraries.

504   **(A)** Fraction of *A. thaliana* DNA in sample. **(B)** Median length of merged reads. **(C)** Fraction of

505   cytosine to thymine (C-to-T) substitutions at first base (5' end). **(D)** Relative enrichment of purines

506   (adenine and guanine) at 5' end breaking points. Position -1 is compared with position -5 (negative

507   numbers indicate genomic context before upstream reads' 5' end).

508

509
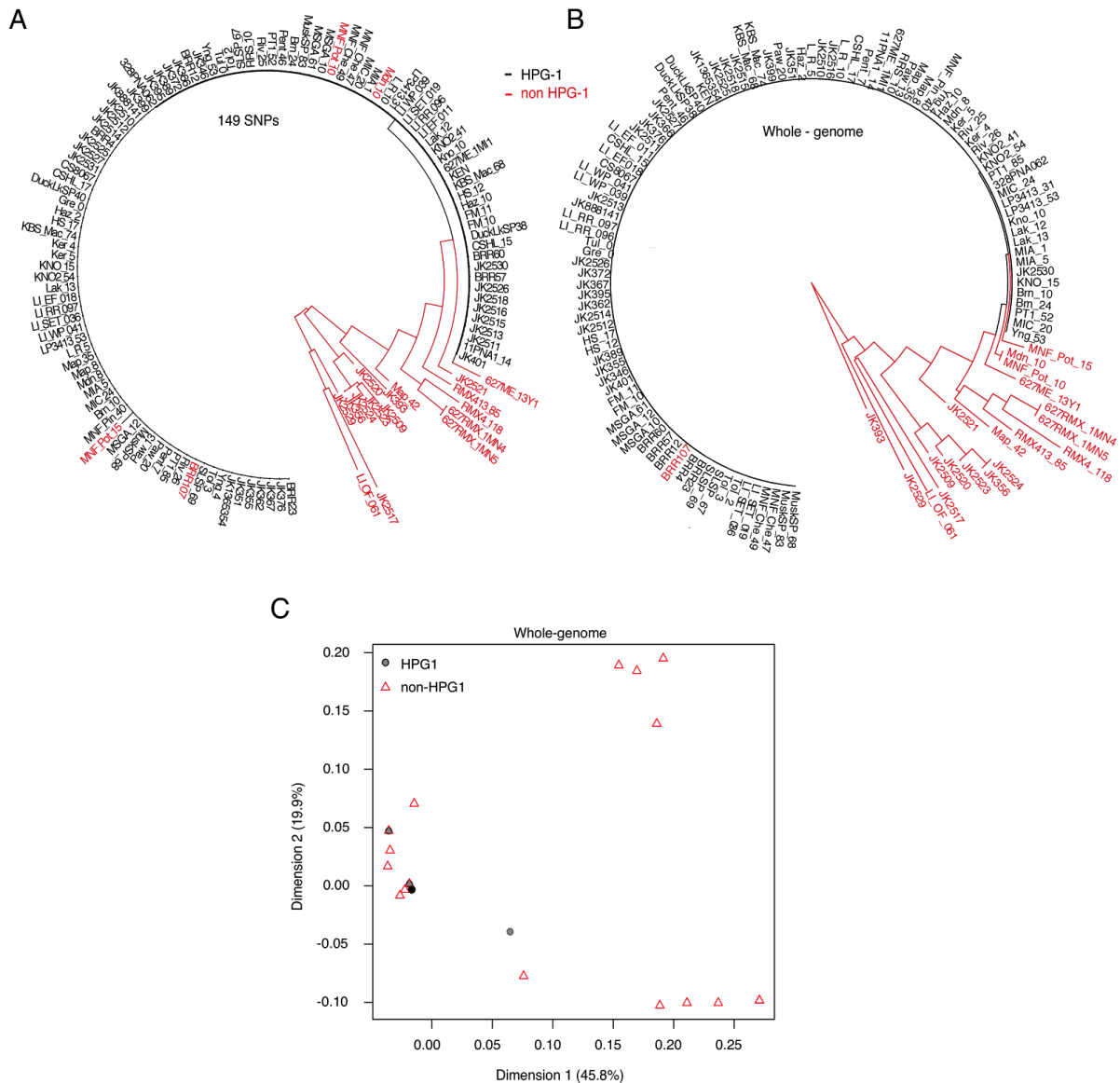
Figure S2. Separation between HPG1 and other North American lineages.

(A) Neighbor-joining tree built using Illumina-based SNP calls at the 149 genotyping markers originally used to identify HPG1 candidates (consensus of 1,000 replicates). HPG1 accessions are shown in black, whereas other North American lineages are depicted in red (see explanation below for four HPG1-like accessions). **(B)** Neighbor-joining tree based on genome-wide SNPs (consensus of 1,000 replicates). Accessions colored as in (A). Note that three accessions originally classified as HPG1 based on 149 SNPs (A) are placed outside this clade. A further accession (BRR7) within the HPG1 main branch was a recombinant removed from the analysis. **(C)** First two dimensions of a multidimensional scaling plot based on identity-by-state pairwise distances. Notice that black dots represent multiple transparent dots overlaid, a result of multiple almost-identical HPG1 genomes. Percentage of the variance explained by each dimension given in parentheses.

521

522
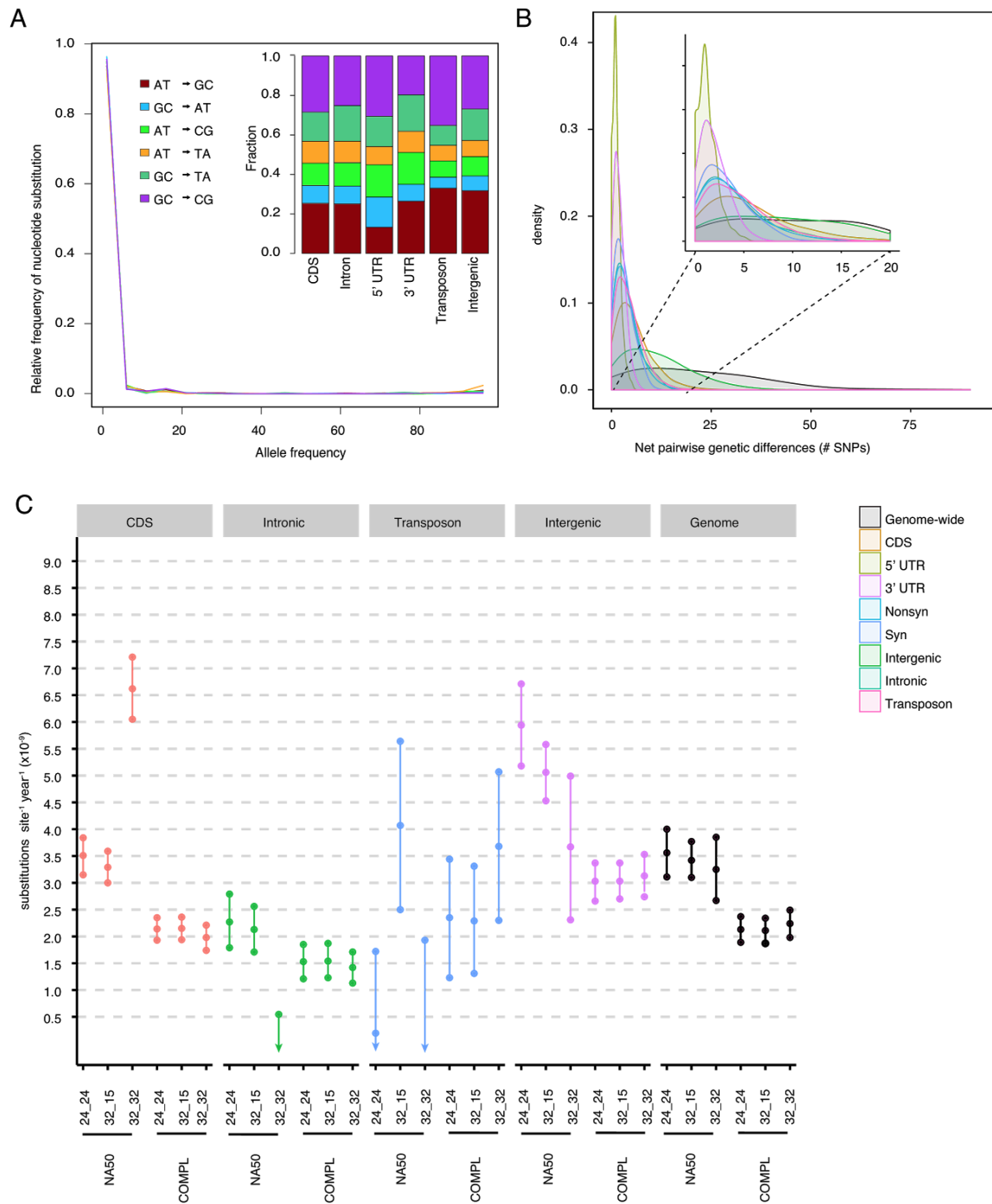
523

524 **Figure S3. Substitution spectrum and rates.**

525 **(A)** "Unfolded" site frequency spectrum using *Arabidopsis lyrata* as outgroup for all transitions and

526 transversions. Bar plot shows proportions of different types of substitutions divided by genomic

527 annotation. **(B)** Distributions of "net" pairwise genetic distances between historic and modern

528 samples used to calculate mutation rates (from quality 32_15 and complete information per site).

529 UTRs were excluded because of the small number of SNPs. **(C)** Mutation rates calculated for different

530 genomic annotations and quality thresholds (32_32, 32_15, 24_24) and missing values (NA50:

531   maximum 50% missing data per SNP; COMPL: missing data 0%). Mean and 95% confidence intervals

532   are shown.

533

534

535
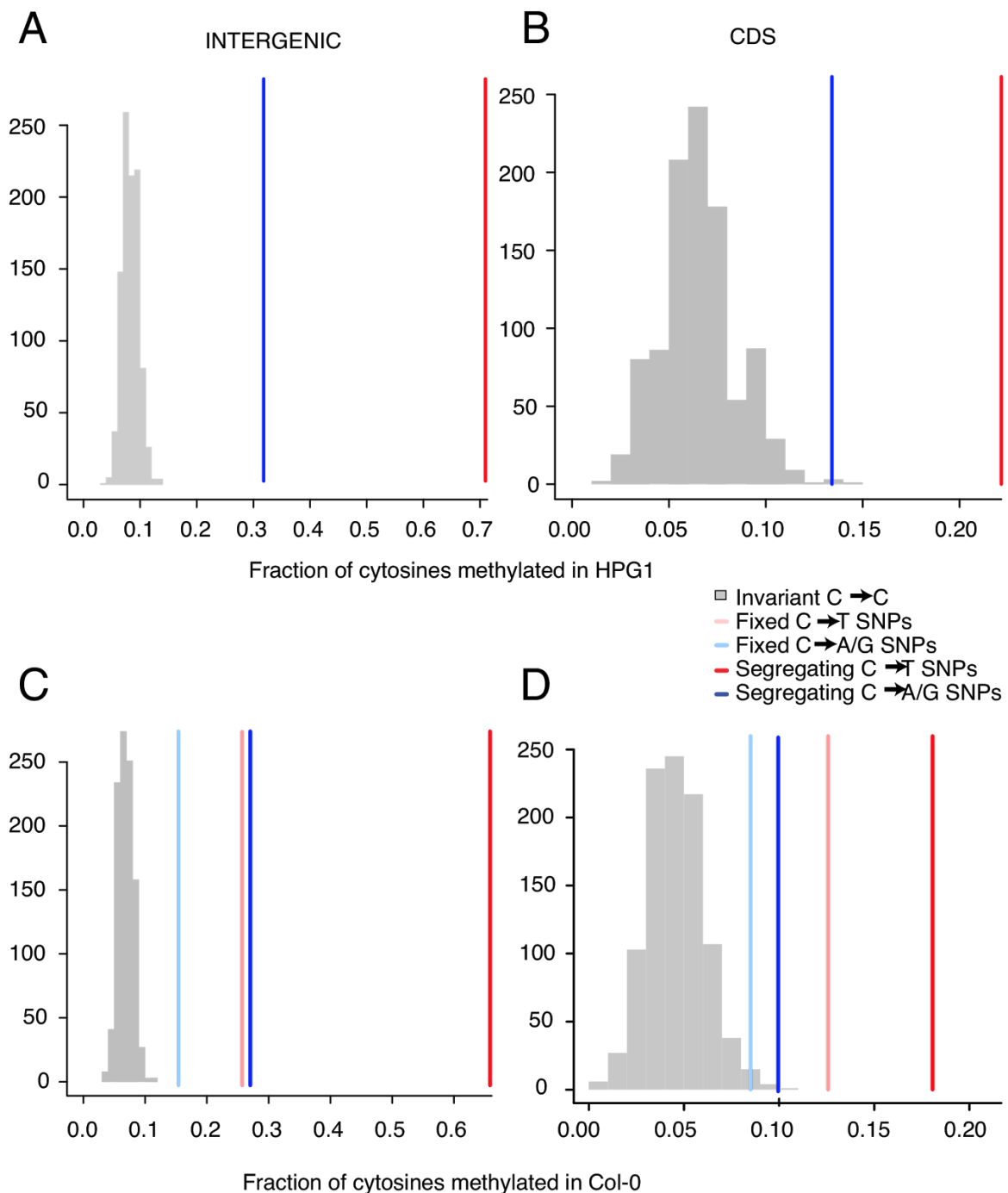
Figure S4. Relationship between methylation and substitutions.

(A, B) Fraction of methylation of cytosines in HPG1 pseudo-reference[7] at intergenic (A) or coding regions (B). **(C, D)** Fraction of methylation of cytosines in Col-0 reference genome[5] at intergenic (C) or coding regions (D). In each of the four comparisons, a grey histogram represents distribution of methylation of 1,000 random sets of invariant cytosines. Lines represent average methylation degree at those sites in HPG1 that changed from cytosine to thymine (red). We differentiate those substitutions that are shared - fixed - across all individuals (light red) or whose allele are present at

543   an intermediate - segregating - frequency (dark red). Likewise, average methylation is shown for sites

544   that changed from cytosine to adenine (blue) that that are fixed (light blue) or segregating (dark

545   blue). The fact that the average methylation is higher in new substitutions than in invariant positions

546   supports a connection between methylation and mutability of sites.

547

548

549

550
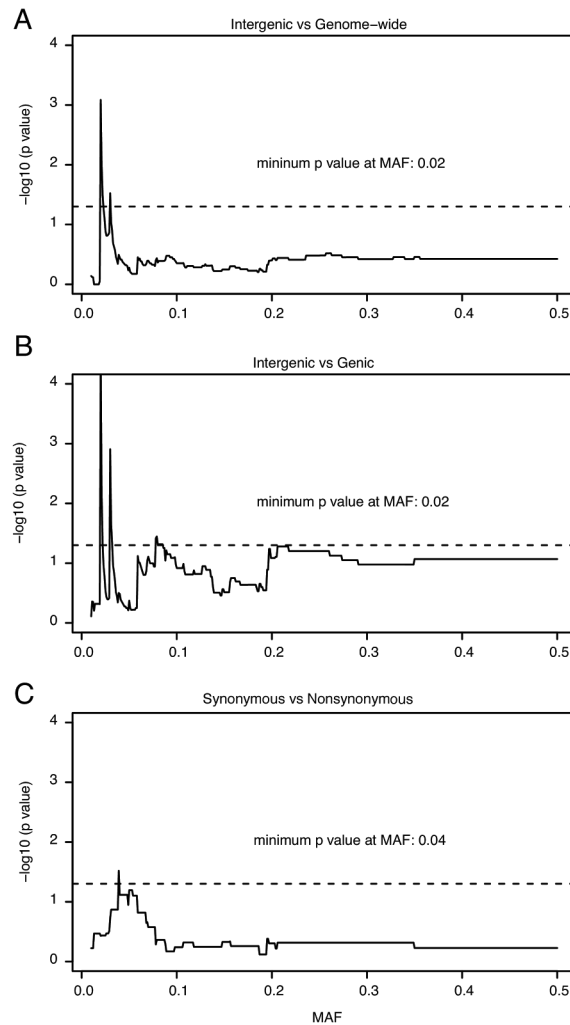
Figure S5. Enrichment of low variants at putatively selected annotations.
We tested for an interaction in a 2x2 table of counts of SNPs using Fisher's Exact Test. The tables were built with the number of SNPs falling into each of the two annotations: genome - intergenic **(A)**, genic - intergenic **(B)**, and synonymous - non-synonymous **(C)**; and two discrete allele groups assuming a minimum allele frequency (MAF) cutoff. We repeated the test by sliding the cut-off from 0 to 50% allele frequency (x axis) and we show the corresponding p-value (y axis). The dashed line indicates the 5% significance threshold.

558
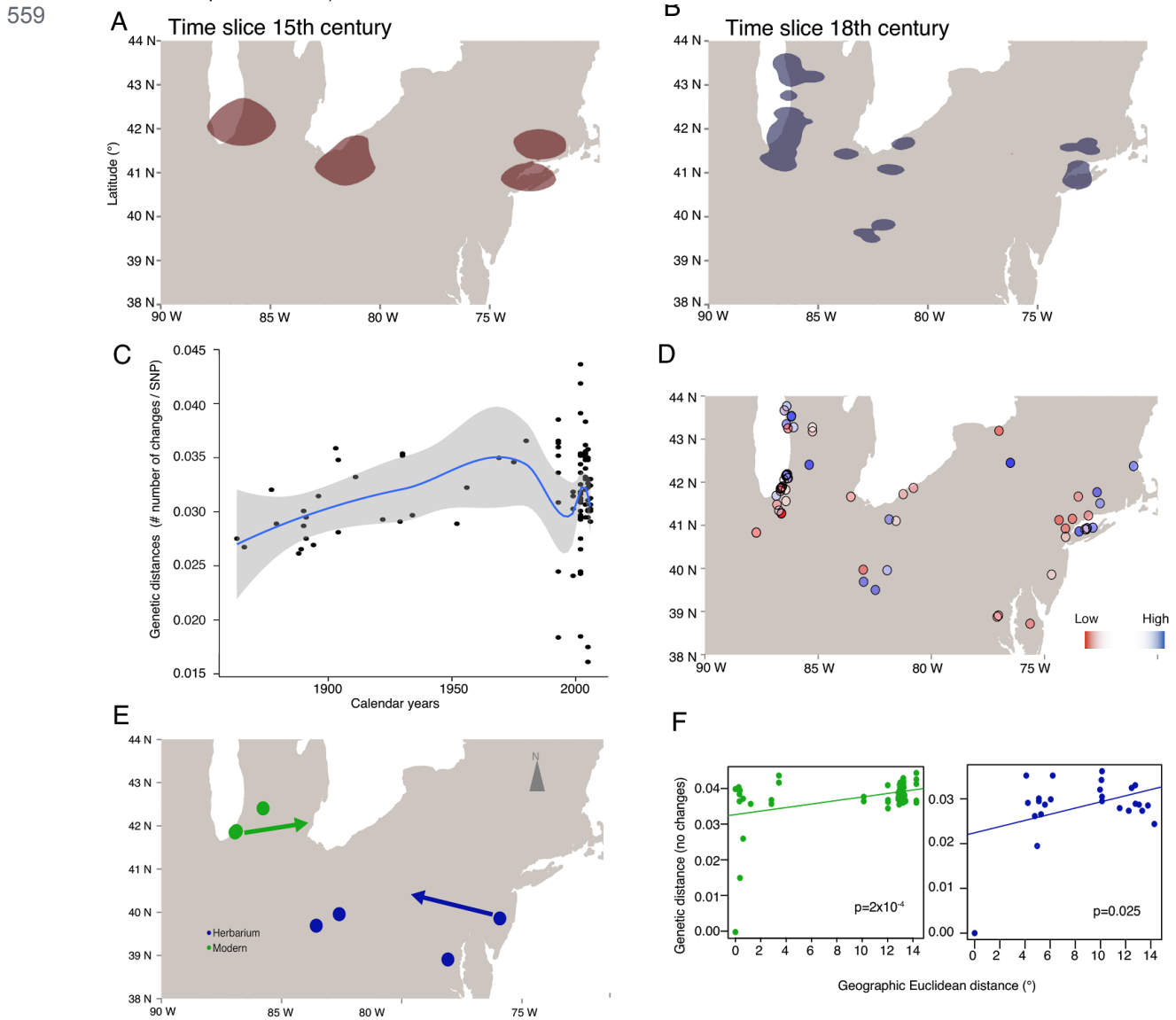
Figure S6. Phylogeographic inference in HPG1.

(A, B) The model infers the most probable geographic location of each of the nodes of the phylogeny in Figure 3. **(A)** Ancestral distribution map (dark red/brown) summarizing the first ~100 years of the phylogenetic tree. Clouds represent the 95% interval of the Highest Posterior Probability Density of locations. **(B)** Current distribution map (dark blue) summarizing the last ~100 years. Clouds as in (A).

(C) Diversity in time. Each point represents the average number of genetic changes between a sample and the other samples within a decade. The blue line shows the fit using a generalized additive model and the grey shaded area the 95% confidence interval. **(D)** Diversity in space. Each point represents the average number of genetic changes among the 10 geographically closest neighbors. Genetic distances are shown qualitatively from a red (low) to blue (high) gradient. **(E)** Origin of herbarium and modern geographic spread, determined using separate heuristic searches of

23

571   isolation-by-distance patterns. Three locations of modern samples and four locations of herbarium

572   samples showed significant slopes (p < 0.05) in the isolation-by-distance pattern. That is, genetic

573   distance increased when moving away from these geographic locations. For one sample of each

574   subset, herbarium **(F)** and modern **(G),** a likely migration trajectory is depicted by an arrow and its
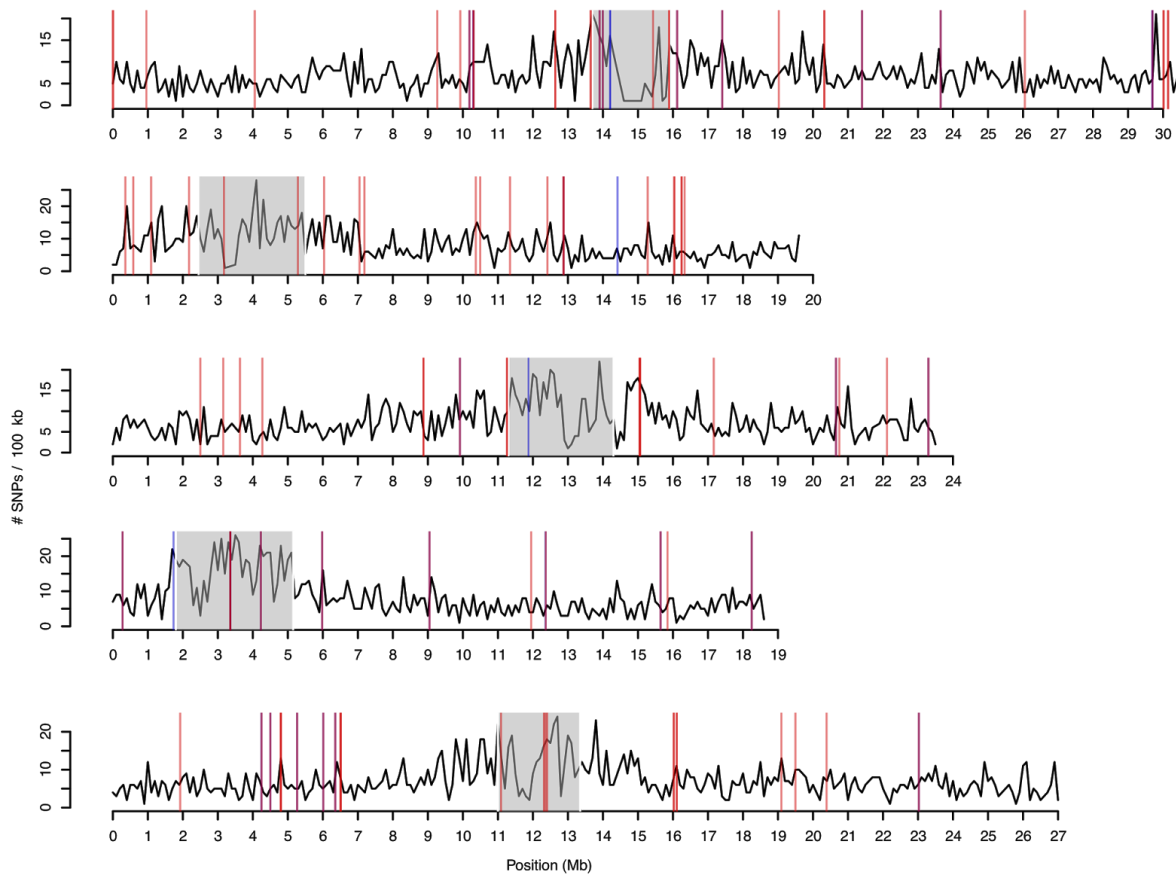
575   isolation-by-distance pattern is shown.

576

577

578

579

580 **Figure S7. Density of SNPs along all chromosomes and location of SNP hits.**

581 Black line shows number of SNPs per 100 kb window. Centromere locations are indicated by grey

582 shading. Vertical lines indicate SNPs associated with root phenotypes (red) and climatic variables

583 (blue) (see Table S5).

584

585

586

A

B
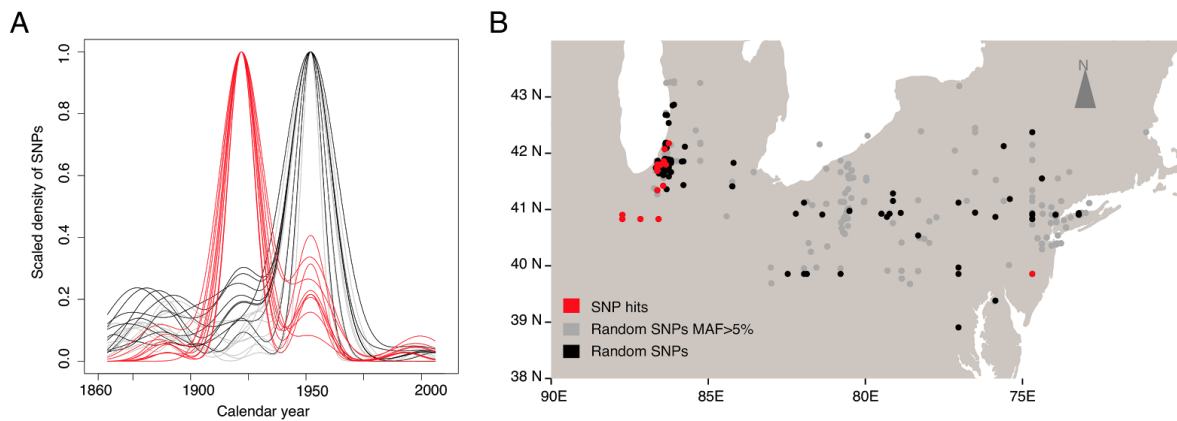
Figure S8. Spatial and temporal emergence of root-associated mutations.

(A) Age distribution of derived SNPs with a significant trait association (the herbarium sample in which they were first recorded) (red), compared with genome-wide SNPs with at least 5% minor allele frequency (grey), or without frequency cutoff (black). **(B)** Spatial centroid of all samples carrying a derived allele. Since it is an average location, centroids can be in a body of water. Ten random draws of 50 SNPs for each category were used to produce the density lines in (A) and points in (B).

594

595

596

597

598
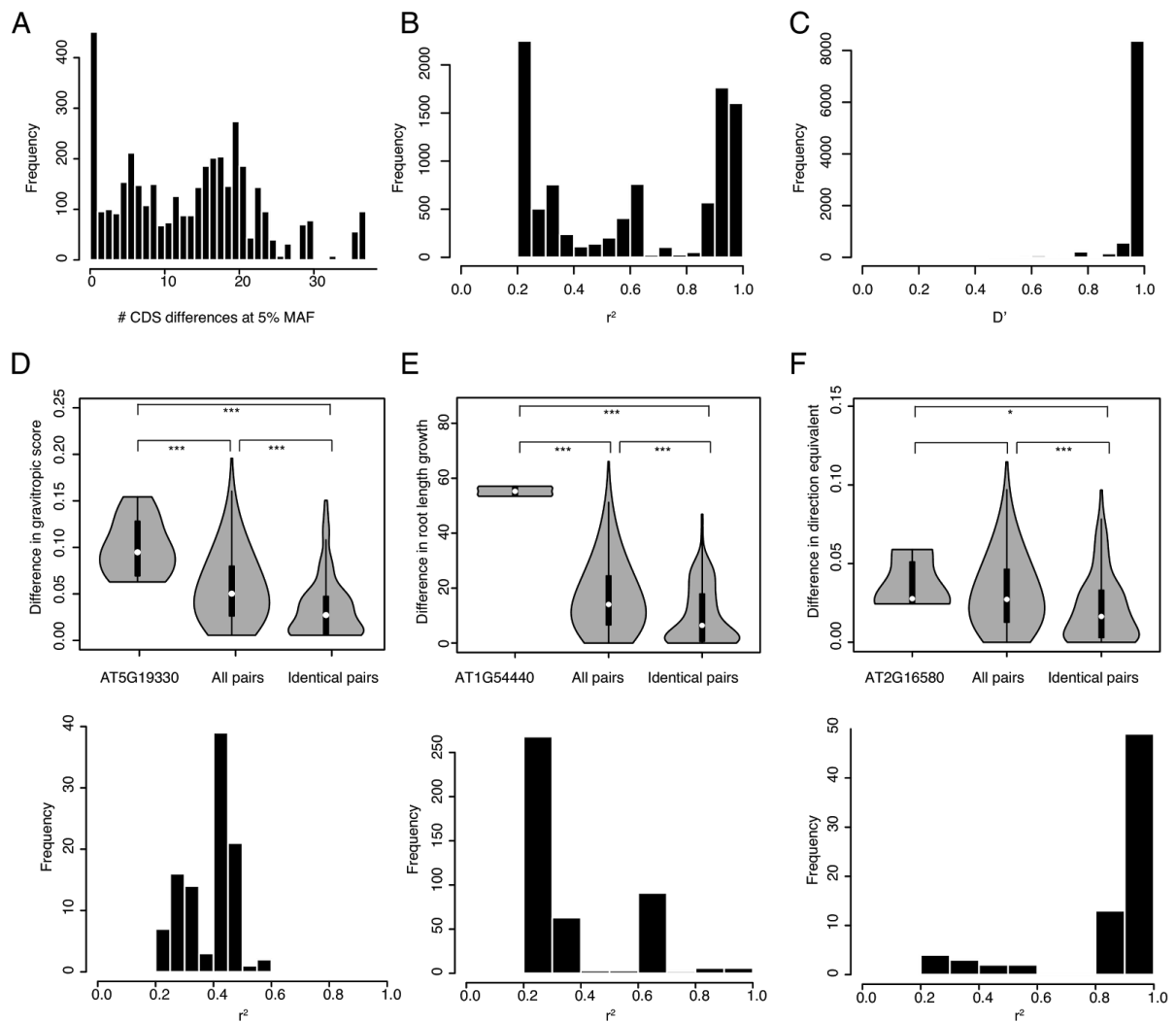
Figure S9. Linkage disequilibrium between SNPs with significant trait associations.

(A-F) Linkage disequilibrium between SNPs with significant trait associations. Histogram of genetic distances **(A)** between samples when evaluating only coding regions at 5% minimum allele frequency. Linkage disequilibrium between SNP hits measured as r^2 **(B)** and D' **(C)**. Three significant SNPs were further studied to exemplify the power of association analyses with HPG1. For each, phenotypic differences between accessions that differ in the focal SNP and that are otherwise virtually genetically identical are compared both with all pairs of accessions and with pairs of accessions completely identical for coding regions. Below each violin plot is the histogram of linkage disequilibrium of the focal SNP with all other SNP hits. The three focal SNPs evaluated are located in AT5G19330 **(D)**, AT1G54440 **(E)** and AT2G16580 **(F)**.

609

610

611

612
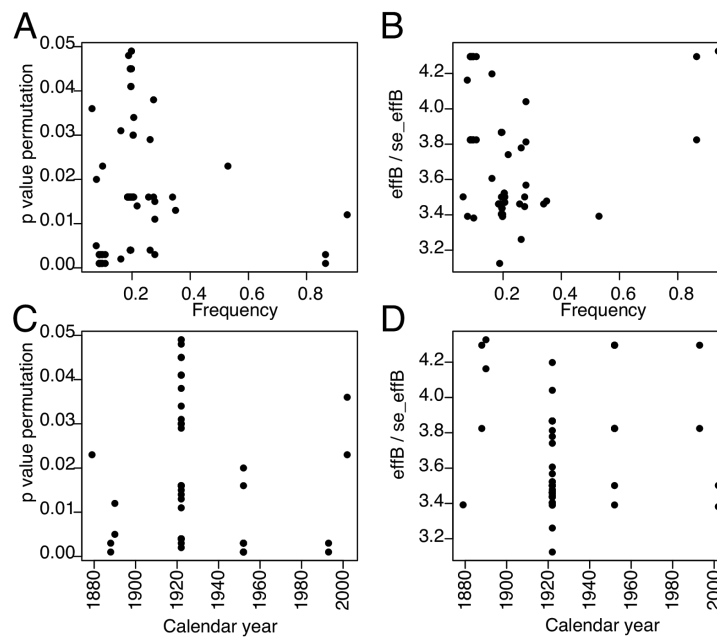
Figure S10. Correlations of SNP effects and p-values with frequency and age.

Correlation between SNP frequency and p-value **(A)**, frequency and effect **(B)**, age and p-value **(C)**, age and effect **(D)**. All cases were non-significant.

616

617

618   **SUPPLEMENTAL TABLES**

619   See appended .**pdf** file for **Tables S1-5**.

620   See appended .**pdf** file for **Graphic Table S7**: For each trait employed in association analyses, we

621   report the histogram distribution and the QQ plot of p-values to ensure that no trait departs

622   exaggeratedly from the normal distribution, and that no inflation of p-values is observed (when

623   lambda ≤ 1, there is no inflation of false positives).

624

625

Table S1. Sample information.

(Abbreviation H* indicates herbarium samples that cluster with the modern HPG1 clade rather than the historic HPG1 clade in Fig. 3., highlighted as a star in the map from Fig. 1. Abbreviations of herbarium collections or seed sources: UCONN = University of Connecticut Herbarium; CFM = Chicago Field Museum; NY = New York Botanical Garden; ABRC = Arabidopsis Biological Resources Center; OSU = Ohio State University.)

Accession	Latitude (ºN)	Longitude (º E)	State	Date collected	Alternative name	Collector/ Herbarium	Average coverage (x)	Number of covered positions (≥3x) (mapped against HPG1 reference)	Number of covered positions (≥3x) (mapped against Col_0 reference)	SNPs vs HPG1 reference	Belongs to HPG1	Modern/ Herbarium	Column number in the available genome matrix
JK399	38.7155	-75.635591	DE	1863	888124	NY	9	105,053,631	99,889,683	142	yes	H	101
JK366	43.1921	-77.0102	NY	1866	888144	NY	6.8	100,379,839	95,118,236	123	yes	H	94
JK395	38.9068	-77.036667	DC	1877	888134	NY	10.3	103,620,791	98,888,406	167	yes	H	100
JK888141	40.732007	-74.068455	NJ	1879	888141	NY	42	107,211,409	102,634,255	161	yes	H	103
JK389	38.9068	-77.036667	DC	1888	1365363	NY	9.9	106,042,465	100,826,958	151	yes	H	98
JK362	38.9068	-77.036667	DC	1889	1365364	NY	8.8	103,997,716	98,876,320	153	yes	H	93
JK367	40.9249	-74.0755	NJ	1890	1365344	NY	16.7	107,236,732	102,176,782	181	yes	H	95
JK372	41.1222	-74.3569	NJ	1890	1365332	NY	14.8	106,285,178	101,480,369	163	yes	H	96
JK1365354	38.8782	-77.09048	VA	1891	1365354	NY	36.4	106,718,326	102,458,166	169	yes	H	88
JK376	39.97	-83.01	NY	1891	1365337	NY	12.3	105,962,154	100,840,125	145	yes	H	97
JK351	41.15	-73.766667	NY	1894	1365333	NY	16.1	106,531,302	101,841,156	153	yes	H	90
JK355	35.99	-83.94	TE	1896	1365374	NY	14.3	106,391,637	101,455,311	192	yes	H	91
JK356	n/a	n/a	GA	1897	1365375	NY	5.3	90,426,010	89,296,191	n/a	no	H	92
JK393	n/a	n/a	NC	1897	1365370	NY	30.4	102,894,430	101,298,068	n/a	no	H	99
JK346	40.643136	-111.95177	UT	1903	102365	NY	29.1	107,223,283	102,450,446	222	yes	H	89
JK2525	41.224343	-73.06021	CT	1904	79391	UNCONN	12.5	105,025,845	n/a	138	yes	H	118
JK2529	n/a	n/a	OH	1904	176849	CFM	11.4	100,620,441	n/a	n/a	no	H	121

JK401	40.643136	-111.95177	UT	1904	102364	NY	10.4	99,572,736	94,661,828	216	yes	H	102
JK2513	41.102121	-81.560547	OH	1911	25	OSU	18.2	106,309,854	n/a	176	yes	H	108
JK2509	n/a	n/a	CT	1917	11	OSU	15.1	102,169,546	n/a	n/a	no	H	104
JK2530	41.482862	-86.822602	IN	1922	531679	CFM	22.2	107,043,540	n/a	161	yes	H	122
JK2526	41.666667	-73.508455	CT	1929	79409	UNCONN	16.3	107,026,827	n/a	161	yes	H	119
JK2515	41.137296	-81.863779	OH	1930	30	OSU	21.3	106,893,416	n/a	193	yes	H	110
JK2511	41.721618	-81.243317	OH	1934	14	OSU	5.6	95,822,372	n/a	109	yes	H	106
JK2523	n/a	n/a	OH	1940	25707	UNC	13.1	101,421,749	n/a	n/a	no	H	116
JK2520	n/a	n/a	OH	1945	54051	UNC	20.3	102,831,697	n/a	n/a	no	H	114
JK2524	39.856783	-74.686954	NJ	1952	63978	UNC	13.8	100,778,282	n/a	n/a	no	H	117
JK2512	39.95607	-81.953309	OH	1956	21	OSU	16.7	106,801,844	n/a	189	yes	H	107
JK2514	39.95607	-81.953309	OH	1969	27	OSU	28.4	107,044,415	n/a	219	yes	H	109
JK2517	n/a	n/a	OH	1981	34	OSU	21.7	102,643,436	n/a	n/a	no	H	112
JK2521	n/a	n/a	OH	1992	565960	UNC	2.9	62,673,938	n/a	n/a	no	H	115
JK2518	41.867643	-80.789021	OH	1993	40	OSU	14.8	106,578,197	n/a	177	yes	H	113
JK2531	39.856783	-74.686954	NJ	1952	1507461	CFM	15.1	106,158,181	n/a	177	yes	H*	123
JK2510	39.688861	-82.993218	OH	1930	13	OSU	21	106,305,970	n/a	178	yes	H*	105
JK2527	41.509059	-72.543694	CT	1975	79389	UNCONN	8.3	104,089,205	n/a	200	yes	H*	120
JK2516	39.500862	-82.472413	OH	1980	32	OSU	18.1	106,464,569	n/a	198	yes	H*	111
CSHL_15	40.8585	-73.4675	NY	1993	CSHL-15	ABRC	39.3	108,189,771	105,955,885	243	yes	M	16
CSHL_17	40.8585	-73.4675	NY	1993	CSHL-17	ABRC	41.5	108,194,960	105,982,511	240	yes	M	17
FM_10	42.4489	-76.5072	NY	1993	FM-10	ABRC	44.6	108,203,215	106,052,866	269	yes	M	20
FM_11	42.4489	-76.5072	NY	1993	FM-11	ABRC	44.4	108,214,008	106,040,276	288	yes	M	21
HS_12	42.373	-71.0627	MA	1993	HS-12	ABRC	48.8	108,230,030	106,124,249	251	yes	M	25
HS_17	42.373	-71.0627	MA	1993	HS-17	ABRC	55.3	108,242,062	106,155,362	254	yes	M	26
Kno_10	41.2816	-86.621	IN	1993	Kno-10	ABRC	39.4	108,198,601	105,985,288	226	yes	M	32
KNO_15	41.2816	-86.621	IN	1993	KNO-15	ABRC	43.6	108,219,683	106,069,077	231	yes	M	33
Gre_0	43.178	-85.2532	MI	1995	Gre-0	ABRC	44.6	108,209,345	106,032,827	207	yes	M	22
Tul_0	43.2708	-85.2563	MI	1995	CS6877	ABRC	31.2	108,140,393	105,806,418	221	yes	M	85
CS8067	41.3599	-122.755	CA	1996	Buckhorn Pas:	ABRC	66.4	108,260,489	106,243,277	294	yes	M	15
Tol_2	41.6639	-83.5553	OH	1996	CS8022	ABRC	61	108,241,333	106,194,209	238	yes	M	83
Tol_3	41.6639	-83.5553	OH	1996	CS8023	ABRC	40.2	108,184,749	105,953,559	232	yes	M	84
MIA_1	41.7976	-86.6691	MI	1999	MIA-1	ABRC	73.1	108,279,881	106,291,612	234	yes	M	56

MIA_5	41.7976	-86.6691	MI	1999	MIA-5	ABRC	62.9	108,263,557	106,250,560	235	yes	M	57
MIC_20	41.8266	-86.4366	MI	1999	MIC-20	ABRC	39.9	108,200,416	106,010,135	237	yes	M	58
MIC_24	41.8266	-86.4366	MI	1999	MIC-24	ABRC	33.8	108,176,527	105,728,326	237	yes	M	59
Brn_10	41.9	-86.583	MI	2002	Brn-10	ABRC	33.3	108,177,381	105,905,097	243	yes	M	7
Brn_24	41.9	-86.583	MI	2002	Brn-24	ABRC	38.4	108,208,482	105,951,803	228	yes	M	8
Haz_10	41.879	-86.607	MI	2002	Haz-10	ABRC	33.8	108,154,100	105,903,700	230	yes	M	23
Haz_2	41.879	-86.607	MI	2002	Haz-2	ABRC	39.7	108,201,103	106,004,251	288	yes	M	24
Ker_4	42.184	-86.358	MI	2002	Ker-4	ABRC	32.1	108,132,127	105,806,486	261	yes	M	30
Ker_5	42.184	-86.358	MI	2002	Ker-5	ABRC	62.9	108,259,905	106,246,278	259	yes	M	31
L_R_10	41.847	-86.67	MI	2002	L-R-10	ABRC	22.4	108,062,944	105,496,224	186	yes	M	49
L_R_5	41.847	-86.67	MI	2002	L-R-5	ABRC	60.6	108,255,795	106,209,826	299	yes	M	50
Lak_12	41.8	-86.67	MI	2002	Lak-12	ABRC	37.8	108,176,901	105,775,999	237	yes	M	36
Lak_13	41.8	-86.67	MI	2002	Lak-13	ABRC	28.5	107,955,559	105,553,559	226	yes	M	37
Map_35	42.166	-86.412	MI	2002	Map-35	ABRC	64.7	108,265,863	106,224,216	290	yes	M	51
Map_42	42.166	-86.412	MI	2002	Map-42	ABRC	46	107,303,032	106,093,945	n/a	no	M	52
Map_8	42.166	-86.412	MI	2002	Map-8	ABRC	33.4	108,155,999	105,921,907	287	yes	M	53
Mdn_10	42.051	-86.509	MI	2002	Mdn-10	ABRC	34.9	108,106,772	105,906,924	n/a	no	M	54
Mdn_8	42.051	-86.509	MI	2002	Mdn-8	ABRC	37.4	108,199,679	105,940,666	266	yes	M	55
Paw_13	42.148	-86.431	MI	2002	Paw-13	ABRC	43	108,159,739	105,980,721	267	yes	M	70
Paw_20	42.148	-86.431	MI	2002	Paw-20	ABRC	41.3	108,218,762	106,059,867	241	yes	M	71
Riv_25	42.184	-86.382	MI	2002	Riv-25	ABRC	36.8	108,186,632	105,779,717	273	yes	M	76
Riv_26	42.184	-86.382	MI	2002	Riv-26	ABRC	35.7	108,194,281	105,958,738	260	yes	M	77
Yng_4	41.865	-86.646	MI	2002	Yng-4	ABRC	41.3	108,182,789	106,000,003	289	yes	M	86
Yng_53	41.865	-86.646	MI	2002	Yng-53	ABRC	46	108,230,553	106,125,861	191	yes	M	87
RRS_10	41.5609	-86.4251	IN	2003	RRS-10	ABRC	41.8	108,208,144	106,033,465	274	yes	M	80
DuckLkSP38	43.3431	-86.4045	MI	2004	DuckLkSP38	ABRC	37.1	108,171,751	105,932,415	253	yes	M	18
DuckLkSP40	43.3431	-86.4045	MI	2004	DuckLkSP40	ABRC	39.6	108,204,654	105,969,244	257	yes	M	19
KBS_Mac_68	42.405	-85.398	MI	2004	KBS-Mac-68	ABRC	41.3	108,181,390	105,870,424	259	yes	M	27
KBS_Mac_74	42.405	-85.398	MI	2004	KBS-Mac-74	ABRC	37.7	108,160,645	105,801,702	265	yes	M	28
MNF_Che_47	43.5251	-86.1843	MI	2004	MNF-Che-47	ABRC	27.6	108,093,393	105,596,885	281	yes	M	60
MNF_Che_49	43.5251	-86.1843	MI	2004	MNF-Che-49	ABRC	28.5	108,082,202	105,661,610	274	yes	M	61
MNF_Pin_40	43.5356	-86.1788	MI	2004	MNF-Pin-40	ABRC	47.9	108,238,775	106,099,919	287	yes	M	62
MNF_Pot_10	43.595	-86.2657	MI	2004	MNF-Pot-10	ABRC	61.4	108,189,553	106,228,588	n/a	no	M	63

MNF_Pot_15	43.595	-86.2657	MI	2004	MNF-Pot-15	ABRC	25.2	108,543,185	107,022,924	n/a	no	M	64
MSGA_10	43.2749	-86.0891	MI	2004	MSGA-10	ABRC	41.9	108,191,659	106,019,404	233	yes	M	65
MSGA_12	43.2749	-86.0891	MI	2004	MSGA-12	ABRC	42.8	108,227,214	106,032,928	240	yes	M	66
MSGA_61	43.2749	-86.0891	MI	2004	MSGA-61	ABRC	45.5	108,210,152	106,077,183	247	yes	M	67
MuskSP_68	43.2483	-86.3368	MI	2004	MuskSP-68	ABRC	25.8	108,063,297	105,588,467	215	yes	M	68
MuskSP_83	43.2483	-86.3368	MI	2004	MuskSP-83	ABRC	29.9	108,099,368	105,721,042	222	yes	M	69
Pent_46	43.7623	-86.3929	MI	2004	Pent-46	ABRC	48.3	108,227,763	106,099,890	238	yes	M	72
Pent_7	43.7623	-86.3929	MI	2004	Pent-7	ABRC	55.7	108,220,625	106,144,167	240	yes	M	73
SLSP_67	43.665	-86.496	MI	2004	SLSP-67	ABRC	53.5	108,238,880	106,143,530	245	yes	M	81
SLSP_69	43.665	-86.496	MI	2004	SLSP-69	ABRC	35.5	108,160,835	105,899,252	249	yes	M	82
KNO2_41	41.273	-86.625	IN	2005	KNO2.41	ABRC	44.7	108,209,694	106,063,235	219	yes	M	34
KNO2_54	41.273	-86.625	IN	2005	KNO2.54	ABRC	44	108,212,430	105,903,373	218	yes	M	35
LI_EF_011	40.9064	-73.1493	NY	2005	LI-EF-011	ABRC	68.6	108,267,109	106,250,331	259	yes	M	38
LI_EF_018	40.9064	-73.1493	NY	2005	LI-EF-018	ABRC	39	108,244,306	105,898,497	230	yes	M	39
LI_OF_061	40.7777	-72.9069	NY	2005	LI-OF-061	ABRC	58	104,897,841	105,729,196	n/a	no	M	40
LI_RR_096	40.9447	-72.8615	NY	2005	LI-RR-096	ABRC	63.5	108,264,679	106,251,487	261	yes	M	41
LI_RR_097	40.9447	-72.8615	NY	2005	LI-RR-097	ABRC	40.8	108,211,310	105,992,095	249	yes	M	42
LI_SET_019	40.9352	-73.114	NY	2005	LI-SET-019	ABRC	29.9	108,085,297	105,737,781	259	yes	M	43
LI_SET_036	40.9352	-73.114	NY	2005	LI-SET-036	ABRC	41.5	108,216,592	106,006,605	238	yes	M	44
LI_WP_039	40.9076	-73.2089	NY	2005	LI-WP-039	ABRC	104.8	108,301,282	106,273,259	239	yes	M	45
LI_WP_041	40.9076	-73.2089	NY	2005	LI-WP-041	ABRC	76.5	108,287,248	106,322,146	235	yes	M	46
PT1_52	41.3423	-86.7368	IN	2005	PT1.52	ABRC	50.6	108,240,431	106,154,252	219	yes	M	74
PT1_85	41.3423	-86.7368	IN	2005	PT1.85	ABRC	46.1	108,220,150	106,097,633	233	yes	M	75
RMX4_118	42.036	-86.511	MI	2005	RMX4.118	ABRC	41.8	106,178,554	105,685,651	n/a	no	M	78
11PNA1_14	42.0945	-86.3253	MI	2006	11PNA1.14	ABRC	47.5	108,227,783	106,133,372	276	yes	M	1
328PNA062	42.0945	-86.3253	MI	2006	328PNA062	ABRC	47.3	108,221,709	106,127,272	223	yes	M	2
627ME_13Y1	42.093	-86.359	MI	2006	n/a	ABRC	53.4	107,908,679	106,148,671	n/a	no	M	3
627ME_1MI1	42.093	-86.359	MI	2006	627ME-1MI1	ABRC	57.8	108,252,617	106,173,403	281	yes	M	4
627RMX_1MN4	42.0333	-86.5128	MI	2006	n/a	ABRC	43.6	106,799,549	105,789,469	n/a	no	M	5
627RMX_1MN5	42.0333	-86.5128	MI	2006	n/a	ABRC	50.6	106,885,430	105,897,441	n/a	no	M	6
BRR107	40.8313	-87.735	IL	2006	BRR107	ABRC	28.5	108,896,513	107,320,745	n/a	no	M	9
BRR12	40.8313	-87.735	IL	2006	BRR12	ABRC	43.9	108,190,572	106,031,493	232	yes	M	10
BRR23	40.8313	-87.735	IL	2006	BRR23	ABRC	30.7	108,095,072	105,726,913	236	yes	M	11

BRR4	40.8313	-87.735	IL	2006	BRR4	ABRC	44.7	108,180,840	106,033,507	219	yes	M	12
BRR57	40.8313	-87.735	IL	2006	BRR57	ABRC	28.4	108,093,033	105,630,963	225	yes	M	13
BRR60	40.8313	-87.735	IL	2006	BRR60	ABRC	42.9	108,281,285	106,199,572	229	yes	M	14
KEN	41.767	-72.677	CT	n/a	KEN	ABRC	55.2	108,233,232	106,158,223	249	yes	M	29
LP3413_31	41.6862	-86.8513	IN	n/a	LP3413.31	ABRC	55.9	108,244,332	106,190,596	227	yes	M	47
LP3413_53	41.6862	-86.8513	IN	n/a	LP3413.53	ABRC	51.2	108,157,453	105,994,665	245	yes	M	48
RMX413_85	42.036	-86.511	MI	n/a	RMX413.85	ABRC	38	106,816,221	105,483,632	n/a	no	M	79

Table S2. Sample information for Col-0 mutation accumulation lines.

Information about each Mutation Accumulation (MA) line and their number of SNPs at different annotations. Also the total number of SNPs, average number of mutations and total bp covered in the genome per annotation are reported.

MA line	Read depth	Generation	Total	SNPs	Deletions	insertions	CDS	Nonsyn	Syn	Intron	5' UTR	3' UTR	TE	Intergenic
0-4-26	57	3	7	6	1	0	0	0	0	0	0	0	1	5
0-8-87	49	3	7	5	0	2	1	1	0	1	0	0	0	3
30-109	45	31	31	23	7	1	3	3	0	3	0	0	2	15
30-119	45	31	33	26	2	5	1	1	0	1	2	0	4	18
30-29	51	31	39	26	10	3	2	1	1	3	0	1	5	15
30-39	48	31	28	18	7	3	1	1	0	1	0	1	4	11
30-49	50	31	30	23	3	4	4	4	0	0	0	0	6	13
30-59	40	31	46	31	8	7	5	2	3	2	0	0	6	18
30-69	50	31	26	21	3	2	4	3	1	1	1	1	6	8
30-79	50	31	31	25	3	3	6	4	2	2	0	0	8	9
30-89	39	31	35	27	5	3	4	3	1	1	1	0	2	19
30-99	44	31	37	35	1	1	6	5	1	2	0	2	8	17
Total SNPs				274			38	28	10	17	4	5	52	158
average (31st)			33.6	25.5	4.9	3.2	3.6	2.7	0.9	1.6	0.4	0.5	5.1	14.3
stdev (31st)				5.9	4.9	3.0	1.8	1.8	1.4	1.0	1.0	0.7	0.7	2.1	3.9
Total bp			115,954,227				30,753,966			17,446,837	4,289,789	2,508,199	9,267,413	48,090,487

Table S3. Mutation rate estimates for different annotations in HPG1 and mutation accumulation lines.

Mutation rates from MA lines are compared to HPG1 substitution rates from the dataset of 32_15 quality filter and complete information (see SOM)
(Abbreviations: stat, descriptive statistic; bp, base pairs; lower and upper, lower and upper 95% CI; Nonsyn. and Syn., nonsynonymous and synonymous sites; UTR, untranslated region sites; HPG1 adj., substitution rate of HPG1 adjusted by a mean generation time of 1.3 years)

Dataset	stat	CDS	Syn.	Nonsyn.	Intronic	5' UTR	3' UTR	Transposon	Intergenic	Genome
MA	mean	3.776	n/a	n/a	2.958	3.008	6.431	17.752	9.592	7.094
MA	sem	1.928	n/a	n/a	1.786	5.258	9.094	7.420	2.628	1.352
MA	lower	2.581	n/a	n/a	1.851	-0.251	0.794	13.153	7.964	6.256
MA	upper	4.971	n/a	n/a	4.065	6.267	12.067	22.351	11.221	7.932
HPG1	mean	2.149	n/a	n/a	1.540	n/a	n/a	2.290	3.029	2.114
HPG1	sem	0.108	n/a	n/a	0.165	n/a	n/a	0.536	0.173	0.119
HPG1	lower	1.943	n/a	n/a	1.231	n/a	n/a	1.314	2.698	1.871
HPG1	upper	2.364	n/a	n/a	1.874	n/a	n/a	3.309	3.368	2.344
HPG1 adj.	mean	2.794	n/a	n/a	2.002	n/a	n/a	2.977	3.938	2.748
HPG1 adj.	sem	0.140	n/a	n/a	0.214	n/a	n/a	0.697	0.225	0.154
HPG1 adj.	lower	2.526	n/a	n/a	1.600	n/a	n/a	1.708	3.508	2.432
HPG1 adj.	upper	3.073	n/a	n/a	2.436	n/a	n/a	4.302	4.378	3.047
Distribution of pairwise SNP differences	min	0	0	0	0	0	0	0	0	0
	1st qu.	2	1	1	1	0	1	2	5	9
	median	5	3	3	3	1	2	4	10	18
	mean	5.6	3	3.1	3.8	1.2	1.9	4.3	11.3	21.1
	3rd qu.	8	5	4	5	2	3	6	16	31
	max.	27	17	11	15	5	7	22	43	87
Total number of SNPs		971	531	448	629	74	158	656	2498	5013
Total bp		32119233	n/a	n/a	18132262	2632130	4480510	6209512	43601507	108434034

Table S4. Description of phenotypic and climatic variables for association mapping analyses.

Mean and standard deviation (s.d.) across accessions for each phenotypic and climatic variables. Broad sense heritabilities (H2) were calculated from between line and within line (between replicate) variance in ANOVA. P-value corresponds to F test. Narrow sense heritabilities (h2) were calculated employing linear mixed models and kinship matrix from mean accession values. P-values correspond to Likelihood Ratio test.

Variable	Description	mean	s.d.	H2	p-value	h2	p-value
FT_V0	Time from germination until the first flower opens (days) under 0 days of vernalization	101	4.53	0.009	7.28E-03	0.017	1.97E-25
FT_V1	Time from germination until the first flower opens (days) under 14 days of vernalization	107	4.12	0.013	6.87E-04	0.395	1.83E-25
FT_V2	Time from germination until the first flower opens (days) under 28 days of vernalization	102	3.22	0.012	1.04E-03	0.429	3.37E-27
FT_V3	Time from germination until the first flower opens (days) under 63 days of vernalization	110	1.32	0.010	5.11E-03	0.226	9.52E-25
B_V0	Time from germination until the first developed bud (days) under 0 days of vernalization	88.8	4	0.013	8.99E-04	0.018	2.26E-25
B_V1	Time from germination until the first developed bud (days) under 14 days of vernalization	93.9	3.84	0.009	7.45E-03	0.340	3.98E-25
B_V2	Time from germination until the first developed bud (days) under 28 days of vernalization	89.2	2.13	0.005	6.92E-02	0.252	2.22E-25
B_V3	Time from germination until the first developed bud (days) under 63 days of vernalization	101	0.45	0.006	5.79E-02	0.177	1.99E-24
Fecundity	Pixel area of inflorescence (correlation with number of fruits, rho=0.84)	0.02	0.0042	0.001	3.56E-01	0.240	1.02E-22
seed_size	Average seed size (mm2)	0.134	0.0053	0.016	4.73E-03	0.149	3.58E-24
GR_rootLength	Average root growth rate	181	14.9	0.131	4.76E-77	0.640	3.13E-29
GR_shootArea	Average of shoot area growth rate	2279	253	0.053	2.33E-24	0.812	1.77E-31
rootLength	Average root length	467	35.8	0.048	2.01E-21	0.409	2.57E-28

dirEquivalent	Average root direction index. Score for average pixel-by-pixel deviations from growth relative to vector of gravity	0.393	0.0277	0.059	2.62E-28	0.544	1.14E-26
stdDevXY	Average root linearity coefficient of linear determination; R2 of linear regression line fitted to pixels of primary root skeleton	0.725	0.0429	0.018	4.54E-06	0.303	1.41E-25
meanRootWidth	Average root width	5.27	0.177	0.038	5.30E-16	0.359	1.52E-25
rootWidth20	Average width over first interval of the primary root length (0 to 20%) at hypocotyl/root junction	5.75	0.124	0.018	5.11E-06	0.166	3.37E-25
rootWidth40	Average width over first interval of the primary root length (20 to 40%) at hypocotyl/root junction	5.35	0.19	0.033	3.87E-13	0.291	1.76E-25
rootWidth60	Average width over first interval of the primary root length (40 to 60%) at hypocotyl/root junction	5.2	0.212	0.039	1.49E-16	0.405	6.51E-26
rootWidth80	Average width over first interval of the primary root length (60 to 80%) at hypocotyl/root junction	5.11	0.241	0.045	4.67E-20	0.381	5.47E-26
rootWidth100	Average width over first interval of the primary root length (80 to 100%) at hypocotyl/root junction	4.9	0.222	0.038	4.06E-16	0.351	8.81E-26
gravitropicDir	Average root angle between root vector and the vertical axis of the picture (assumed vector of gravity) (°)	-7.22	2.56	0.024	7.69E-09	0.210	4.68E-27
gravitropicScore	Average score for root angle intervals	0.1	0.0457	0.044	2.83E-19	0.642	7.56E-27
TotLen.EucLen	Average root tortuosity: Total root length divided by Euclidian length	1.1	0.0097	0.009	6.83E-03	0.422	2.53E-25
GR.TL	Average relative root growth rate: Root growth rate divided by total length at the earlier time point	0.673	0.0796	0.011	1.20E-03	0.393	2.69E-24
BIO1	Annual Mean Temperature (ºC x 10)	98.1	12.8	n/a	n/a	0.066	3.22E-40
BIO2	Mean Diurnal Range (Mean of monthly (max temp - min temp))	107	7.65	n/a	n/a	0.073	1.02E-40
BIO3	Isothermality (BIO2/BIO7) (x 100)	28.9	1.8	n/a	n/a	0.361	4.91E-39
BIO4	Temperature Seasonality (standard deviation x 100)	9169	483	n/a	n/a	0.383	4.68E-47
BIO5	Max Temperature of Warmest Month (ºC x 10)	283	10.1	n/a	n/a	0.152	3.78E-40
BIO6	Min Temperature of Coldest Month (ºC x 10)	-80.9	18	n/a	n/a	0.275	4.79E-42
BIO7	Temperature Annual Range (BIO5-BIO6) (ºC x 10)	364	17.5	n/a	n/a	0.239	6.31E-42
BIO8	Mean Temperature of Wettest Quarter (ºC x 10)	176	55.1	n/a	n/a	0.016	3.58E-43

BIO9	Mean Temperature of Driest Quarter (ºC x 10)	-7.11	48.7	n/a	n/a	0.000	3.58E-43
BIO10	Mean Temperature of Warmest Quarter (ºC x 10)	213	10.8	n/a	n/a	0.205	3.33E-40
BIO11	Mean Temperature of Coldest Quarter (ºC x 10)	-24.1	18.2	n/a	n/a	0.270	1.71E-41
BIO12	Annual Precipitation (mm)	990	109	n/a	n/a	0.219	3.94E-44
BIO13	Precipitation of Wettest Month (mm)	103	6.72	n/a	n/a	0.206	1.53E-40
BIO14	Precipitation of Driest Month (mm)	54.1	16.7	n/a	n/a	0.104	1.51E-40
BIO15	Precipitation Seasonality (Coefficient of Variation)	17.8	5.51	n/a	n/a	0.157	8.93E-40
BIO16	Precipitation of Wettest Quarter (mm)	291	19.7	n/a	n/a	0.269	1.55E-42
BIO17	Precipitation of Driest Quarter (mm)	191	44.8	n/a	n/a	0.084	3.67E-42
BIO18	Precipitation of Warmest Quarter (mm)	277	25.2	n/a	n/a	0.342	7.42E-44
BIO19	Precipitation of Coldest Quarter (mm)	197	47	n/a	n/a	0.022	2.68E-42

Table S5. SNP hits from association analyses and several descriptors.

SNP hits significant at the 5% level after permutation correction are shown. Additionally, if raw p-values pass a double Bonferroni threshold of 0.01% are marked with a "tick".
(Abbreviations: nonsyn. and syn., nonsynonymous and synonymous changes; regular one-letter abbreviation was used for amino acid changes)

Trait	Chromosome	Position	Ancestral	Derived	Effect	Effect standard error	Sample size	p - value raw	p - value false discovery rate	p - value permutation corrected	Allele frequency	Allele frequency in modern set	Oldest herbarium individual	Longitude	Latitude	Substitution type	AA change	Gene	Biochemical effect (Grantham score)	Significant permutation	Significant double Bonferroni	LD
dirEquivalent	1	958948	G	T	-0.014	0.004	63	5.30E-04	0.0052	0.018	0.186	0.227	1922	41.7	-85.3	nonsyn	A->P	AT1G03810	27	✓		53
gravitropicScore	1	9925177	C	T	0.033	0.010	63	7.10E-04	0.0651	0.016	0.078	0.092	1952	40.9	-82.3	interg.				✓		1
bio18	1	10187610	T	C	6.830	1.987	99	5.83E-04	0.0124	0.047	0.196	0.24	1922	41.7	-85.3	interg.				✓		52
GR_rootLength	1	12638692	C	T	-12.100	3.164	63	1.33E-04	0.0037	0.003	0.087	0.105	1952	40.9	-81.3	interg.				✓	✓	13
GR_shootArea	1	12638692	C	T	-231.000	53.774	63	1.75E-05	0.0005	0.001	0.087	0.105	1952	40.9	-81.3	interg.				✓	✓	13
GR_rootLength	1	13652509	C	A	-12.100	3.164	63	1.33E-04	0.0037	0.003	0.093	0.107	1952	40.9	-82.9	interg.				✓	✓	12
GR_shootArea	1	13652509	C	A	-231.000	53.774	63	1.75E-05	0.0005	0.001	0.093	0.107	1952	40.9	-82.9	interg.				✓	✓	12
bio18	1	13904611	C	T	6.570	1.756	90	1.83E-04	0.0124	0.016	0.217	0.237	1922	41.7	-85.3	interg.				✓		49
bio18	1	13994958	G	A	6.830	1.987	99	5.83E-04	0.0124	0.047	0.196	0.24	1922	41.7	-85.3	tranposon		AT1G36933		✓		49
bio18	1	17408807	C	T	6.830	1.987	99	5.83E-04	0.0124	0.047	0.196	0.24	1922	41.7	-85.3	interg.				✓		48
dirEquivalent	1	19024876	C	T	-0.014	0.004	63	5.30E-04	0.0052	0.018	0.19	0.23	1922	41.7	-85.3	interg.				✓		47
GR_shootArea	1	20324050	G	A	-231.000	53.774	63	1.75E-05	0.0005	0.001	0.087	0.105	1952	40.9	-82.9	interg.		AT1G54440		✓	✓	11
GR_rootLength	1	20324050	G	A	-12.100	3.164	63	1.33E-04	0.0037	0.003	0.087	0.105	1952	40.9	-82.9	interg.		AT1G54440		✓	✓	11
bio18	1	23648407	A	C	6.830	1.987	99	5.83E-04	0.0124	0.047	0.196	0.24	1922	41.7	-85.3	nonsyn	Y->S	AT1G63740	144	✓		46
dirEquivalent	1	26052913	A	T	-0.014	0.004	63	5.30E-04	0.0052	0.018	0.185	0.224	1922	41.7	-85.3	interg.				✓		45
GR_shootArea	1	29696198	G	A	-121.000	33.911	63	3.68E-04	0.0096	0.016	0.278	0.329	1922	41.5	-84.9	interg.				✓		42

Trait	Chr	Position	R	A	Effect	SE	N	P								Type	AA	Gene				
bio16	1	29696198	G	A	5.250	1.377	94	1.39E-04	0.0632	0.016	0.278	0.329	1922	41.5	-84.9	interg.					✓	42
bio18	1	29696198	G	A	6.340	1.569	94	5.36E-05	0.0124	0.004	0.278	0.329	1922	41.5	-84.9	interg.					✓	42
GR_rootLength	1	30015381	T	A	-12.100	3.164	63	1.33E-04	0.0037	0.003	0.087	0.105	1952	40.9	-82.9	interg.				✓	✓	10
GR_shootArea	1	30015381	T	A	-231.000	53.774	63	1.75E-05	0.0005	0.001	0.087	0.105	1952	40.9	-82.9	interg.				✓	✓	10
GR_rootLength	1	30143319	G	A	-12.100	3.164	63	1.33E-04	0.0037	0.003	0.088	0.105	1952	40.9	-82.9	interg.				✓	✓	9
GR_shootArea	1	30143319	G	A	-231.000	53.774	63	1.75E-05	0.0005	0.001	0.088	0.105	1952	40.9	-82.9	interg.				✓	✓	9
dirEquivalent	2	358395	C	T	-0.016	0.004	63	1.15E-04	0.0032	0.006	0.194	0.237	1922	41.7	-85.3	syn.	V->V	AT2G01820		✓	✓	43
dirEquivalent	2	585918	C	T	-0.016	0.004	63	1.15E-04	0.0032	0.006	0.194	0.237	1922	41.7	-85.3	syn.	G->G	AT2G02220		✓	✓	42
dirEquivalent	2	1093203	C	T	-0.016	0.004	63	1.15E-04	0.0032	0.006	0.194	0.237	1922	41.7	-85.3	interg.				✓	✓	41
dirEquivalent	2	2176891	T	C	-0.016	0.004	63	1.15E-04	0.0032	0.006	0.194	0.237	1922	41.7	-85.3	interg.				✓	✓	40
GR_rootLength	2	3174832	T	A	6.340	1.869	63	6.97E-04	0.017	0.017	0.529	0.566	1879	41.3	-84.3	interg.					✓	0
TotLen.EucLen	2	5285907	C	A	-0.006	0.002	63	3.05E-04	0.0241	0.037	0.162	0.194	1922	41.5	-85	interg.				✓	✓	39
dirEquivalent	2	5285907	C	A	-0.019	0.005	63	2.64E-05	0.0032	0.001	0.162	0.194	1922	41.5	-85	interg.				✓	✓	39
dirEquivalent	2	6034545	C	T	-0.016	0.004	63	1.15E-04	0.0032	0.006	0.194	0.237	1922	41.7	-85.3	syn.	S->S	AT2G14247		✓	✓	38
dirEquivalent	2	7047529	G	T	-0.016	0.004	63	1.15E-04	0.0032	0.006	0.194	0.237	1922	41.7	-85.3	nonsyn	P->A	AT2G16270	27	✓	✓	37
dirEquivalent	2	7186220	C	T	-0.016	0.004	63	1.15E-04	0.0032	0.006	0.194	0.237	1922	41.7	-85.3	intron		AT2G16580		✓	✓	36
dirEquivalent	2	10369545	T	C	-0.016	0.004	63	1.15E-04	0.0032	0.006	0.194	0.237	1922	41.7	-85.3	interg.				✓	✓	35
dirEquivalent	2	10495275	A	C	-0.016	0.004	63	1.15E-04	0.0032	0.006	0.196	0.237	1922	41.7	-85.3	intron		AT2G24680		✓	✓	34
dirEquivalent	2	11346211	C	A	-0.014	0.004	63	5.30E-04	0.0052	0.018	0.186	0.227	1922	41.7	-85.3	interg.					✓	33
dirEquivalent	2	12415084	T	A	-0.014	0.004	63	5.30E-04	0.0052	0.018	0.186	0.227	1922	41.7	-85.3	intron		AT2G28900			✓	32
dirEquivalent	2	12876361	A	C	-0.015	0.004	63	1.56E-04	0.0041	0.006	0.262	0.29	1922	41.7	-84.6	interg.					✓	31
gravitropicScore	2	12876361	A	C	-0.021	0.006	63	1.08E-03	0.0651	0.027	0.262	0.29	1922	41.7	-84.6	interg.					✓	31
bio13	2	14417366	A	G	3.990	0.959	64	3.22E-05	0.0147	0.004	0.077	0	1890	39.5	-77.9	interg.					✓	1
dirEquivalent	2	15278350	A	G	-0.014	0.004	63	5.30E-04	0.0052	0.018	0.186	0.227	1922	41.7	-85.3	interg.					✓	30
GR_shootArea	2	16039488	T	G	-231.000	53.774	63	1.75E-05	0.0005	0.001	0.087	0.105	1952	40.9	-82.9	3' UTR		AT2G38290		✓	✓	8
GR_rootLength	2	16039488	T	G	-12.100	3.164	63	1.33E-04	0.0037	0.003	0.087	0.105	1952	40.9	-82.9	3' UTR		AT2G38290		✓	✓	8
GR_rootLength	2	16247290	G	T	-12.100	3.164	63	1.33E-04	0.0037	0.003	0.088	0.105	1952	40.9	-82.9	nonsyn	A->G	AT2G38910	60	✓	✓	7
GR_shootArea	2	16247290	G	T	-231.000	53.774	63	1.75E-05	0.0005	0.001	0.088	0.105	1952	40.9	-82.9	nonsyn	A->G	AT2G38910	60	✓	✓	7
dirEquivalent	2	16333662	G	A	-0.014	0.004	63	5.30E-04	0.0052	0.018	0.186	0.227	1922	41.7	-85.3	nonsyn	A->G	AT2G39160	60	✓		29
dirEquivalent	3	2500258	C	A	-0.016	0.004	63	1.15E-04	0.0032	0.006	0.194	0.237	1922	41.7	-85.3	syn.	K->K	AT3G07830		✓	✓	28
dirEquivalent	3	3154804	C	T	-0.016	0.004	63	1.15E-04	0.0032	0.006	0.194	0.237	1922	41.7	-85.3	interg.				✓	✓	27
dirEquivalent	3	3629794	C	T	-0.016	0.004	63	1.15E-04	0.0032	0.006	0.194	0.237	1922	41.7	-85.3	intron		AT3G11530		✓	✓	26
dirEquivalent	3	4269626	G	T	-0.016	0.004	63	1.15E-04	0.0032	0.006	0.194	0.237	1922	41.7	-85.3	5' UTR		AT3G13229		✓	✓	25
GR_shootArea	3	8873116	C	T	-231.000	53.774	63	1.75E-05	0.0005	0.001	0.097	0.118	1952	40.9	-81.9	interg.				✓	✓	6
GR_rootLength	3	8873116	C	T	-12.100	3.164	63	1.33E-04	0.0037	0.003	0.097	0.118	1952	40.9	-81.9	interg.				✓	✓	6

Trait	Chr	Position	A1	A2	Effect	SE	N	p								Annot.	AA	Gene				Rank
GR_rootLength	3	11259214	A	T	-12.100	3.164	63	1.33E-04	0.0037	0.003	0.088	0.105	1952	40.9	-82.9	interg.				✓	✓	5
GR_shootArea	3	11259214	A	T	-231.000	53.774	63	1.75E-05	0.0005	0.001	0.088	0.105	1952	40.9	-82.9	interg.				✓	✓	5
bio8	3	11873293	A	G	37.800	8.736	65	1.52E-05	0.0069	0.006	0.939	1	1890	41.8	-83.7	tranposon		AT3G30219		✓		0
GR_rootLength	3	15050751	G	A	-12.100	3.164	63	1.33E-04	0.0037	0.003	0.108	0.105	1888	40.2	-82.5	interg.				✓	✓	4
GR_shootArea	3	15050751	G	A	-231.000	53.774	63	1.75E-05	0.0005	0.001	0.108	0.105	1888	40.2	-82.5	interg.				✓	✓	4
dirEquivalent	3	17164638	C	A	-0.014	0.004	63	5.30E-04	0.0052	0.018	0.19	0.227	1922	41.7	-85.3	interg.				✓		24
bio18	4	279210	T	G	6.830	1.987	99	5.83E-04	0.0124	0.047	0.196	0.24	1922	41.7	-85.3	interg.				✓		22
bio11	4	1732480	T	A	-5.550	1.564	79	3.89E-04	0.0195	0.045	0.063	0.068	2002	41	-87.5	interg.				✓		2
bio4	4	1732480	T	A	224.000	63.967	79	4.67E-04	0.0128	0.044	0.063	0.068	2002	41	-87.5	interg.				✓		2
dirEquivalent	4	3355152	C	G	-0.014	0.004	63	4.45E-04	0.0052	0.016	0.204	0.25	1922	41.7	-85.4	interg.				✓		21
bio18	4	3355152	C	G	6.850	1.944	##	4.25E-04	0.0124	0.035	0.204	0.25	1922	41.7	-85.4	interg.				✓		21
dirEquivalent	4	3355946	G	C	-0.014	0.004	63	4.45E-04	0.0052	0.016	0.204	0.25	1922	41.7	-85.4	interg.				✓		20
bio18	4	3355946	G	C	6.850	1.944	##	4.25E-04	0.0124	0.035	0.204	0.25	1922	41.7	-85.4	interg.				✓		20
dirEquivalent	4	4228138	A	G	-0.014	0.004	63	4.45E-04	0.0052	0.016	0.196	0.24	1922	41.7	-85.3	tranposon		AT4G07440		✓		19
bio18	4	4228138	A	G	6.830	1.987	99	5.83E-04	0.0124	0.047	0.196	0.24	1922	41.7	-85.3	tranposon		AT4G07440		✓		19
dirEquivalent	4	9046942	G	C	-0.014	0.004	63	4.45E-04	0.0052	0.016	0.204	0.25	1922	41.7	-85.4	nonsyn	H->Q	AT4G15960	24	✓		18
bio18	4	9046942	G	C	6.850	1.944	##	4.25E-04	0.0124	0.035	0.204	0.25	1922	41.7	-85.4	nonsyn	H->Q	AT4G15960	24	✓		18
dirEquivalent	4	11948961	T	A	-0.014	0.004	63	4.45E-04	0.0052	0.016	0.198	0.25	1952	41.7	-85.3	interg.				✓		17
dirEquivalent	4	12365323	C	T	-0.014	0.004	63	4.45E-04	0.0052	0.016	0.204	0.25	1922	41.7	-85.4	interg.				✓		16
bio18	4	12365323	C	T	6.850	1.944	##	4.25E-04	0.0124	0.035	0.204	0.25	1922	41.7	-85.4	interg.				✓		16
dirEquivalent	4	15646341	C	A	-0.014	0.004	63	4.45E-04	0.0052	0.016	0.206	0.25	1922	41.7	-85.4	syn.	E->E	AT4G32410		✓		15
bio18	4	15646341	C	A	6.720	1.936	99	5.14E-04	0.0124	0.042	0.206	0.25	1922	41.7	-85.4	syn.	E->E	AT4G32410		✓		15
dirEquivalent	4	15845001	A	T	-0.014	0.004	63	4.45E-04	0.0052	0.016	0.194	0.25	1922	41.8	-85.9	3' UTR		AT4G32840		✓		14
dirEquivalent	4	18249171	T	A	-0.014	0.004	63	4.45E-04	0.0052	0.016	0.274	0.328	1922	41.8	-85.9	interg.				✓		13
bio18	4	18249171	T	A	6.910	2.005	71	5.62E-04	0.0124	0.047	0.274	0.328	1922	41.8	-85.9	interg.				✓		13
bio18	5	4245213	A	T	6.830	1.987	99	5.83E-04	0.0124	0.047	0.196	0.24	1922	41.7	-85.3	syn.	I->I	AT5G13260		✓		12
bio18	5	4500202	G	A	6.830	1.987	99	5.83E-04	0.0124	0.047	0.196	0.24	1922	41.7	-85.3	nonsyn	A->G	AT5G13950	60	✓		11
dirEquivalent	5	4797923	A	T	-0.014	0.004	63	5.30E-04	0.0052	0.018	0.188	0.227	1922	41.7	-85.3	tranposon		AT5G14830		✓		10
dirEquivalent	5	4797976	G	A	-0.014	0.004	63	5.30E-04	0.0052	0.018	0.257	0.293	1922	41.7	-85.3	tranposon		AT5G14830		✓		10
dirEquivalent	5	4798526	A	G	-0.014	0.004	63	5.30E-04	0.0052	0.018	0.339	0.362	1922	41.7	-85.3	interg.				✓		9
gravitropicScore	5	6508329	A	G	-0.020	0.006	63	5.20E-04	0.0651	0.008	0.35	0.447	1922	42	-85	nonsyn	C->W	AT5G19330	215	✓		0
dirEquivalent	5	11090365	T	A	-0.014	0.004	63	5.30E-04	0.0052	0.018	0.186	0.224	1922	41.7	-85.3	TE		AT5G29037		✓		4
dirEquivalent	5	12312975	C	G	-0.014	0.004	63	5.30E-04	0.0052	0.018	0.185	0.224	1922	41.7	-85.3	TE		AT5G32630		✓		3
dirEquivalent	5	12358159	C	T	-0.014	0.004	63	5.30E-04	0.0052	0.018	0.186	0.224	1922	41.7	-85.3	tranposon		AT5G32825		✓		2
dirEquivalent	5	12409027	G	A	-0.014	0.004	63	5.30E-04	0.0052	0.018	0.185	0.224	1922	41.7	-85.3	interg.				✓		1

GR_rootLength	5	16024197	A	T	-12.100	3.164	63	1.33E-04	0.0037	0.003	0.098	0.118	1952	40.9	-81.9	intron	AT5G40020	✓	✓	2
GR_shootArea	5	16024197	A	T	-231.000	53.774	63	1.75E-05	0.0005	0.001	0.098	0.118	1952	40.9	-81.9	intron	AT5G40020	✓	✓	2
GR_shootArea	5	16109431	G	A	-231.000	53.774	63	1.75E-05	0.0005	0.001	0.865	0.877	1993	42.2	-84.4	interg.		✓	✓	1
GR_rootLength	5	16109431	G	A	-12.100	3.164	63	1.33E-04	0.0037	0.003	0.865	0.877	1993	42.2	-84.4	interg.		✓	✓	1
dirEquivalent	5	19099082	G	C	-0.014	0.004	63	5.30E-04	0.0052	0.018	0.186	0.227	1922	41.7	-85.3	interg.		✓		0
GR_rootLength	5	20388107	A	T	-10.700	3.164	63	6.94E-04	0.017	0.017	0.099	0.12	2002	41	-86.6	interg.		✓		0

Graphic Table S7

GR_rootLength
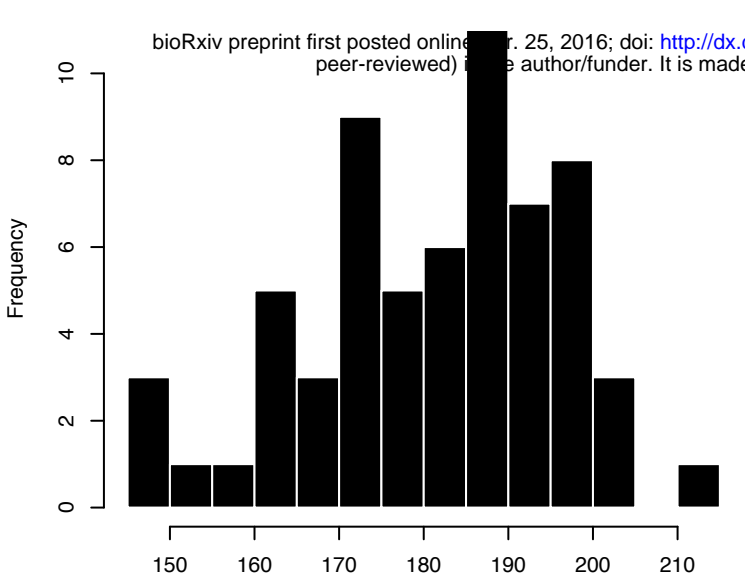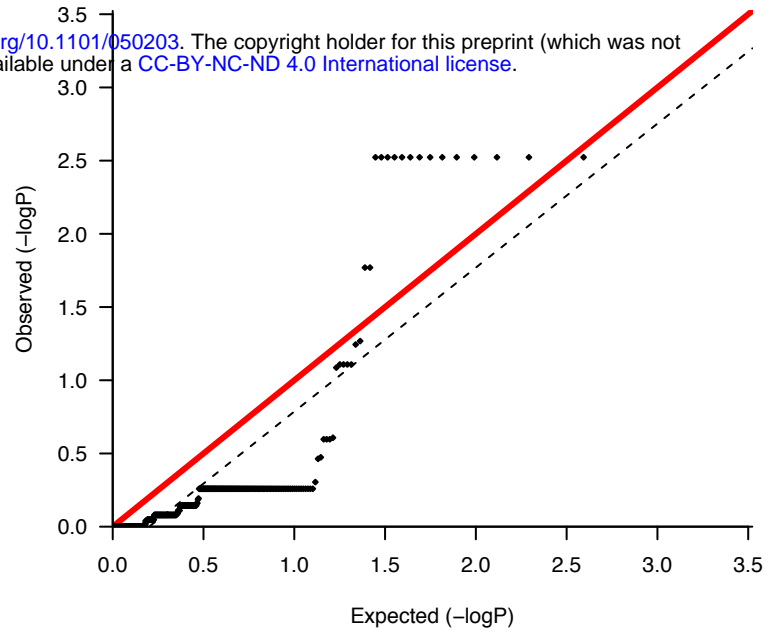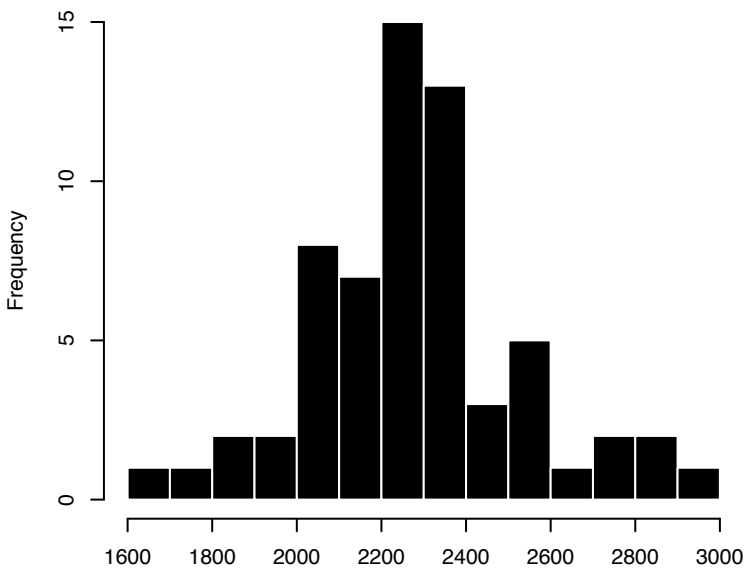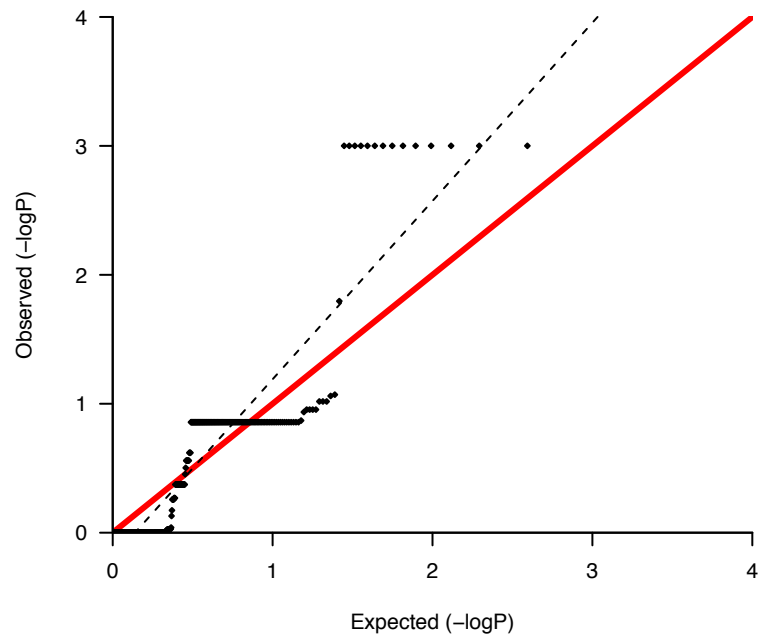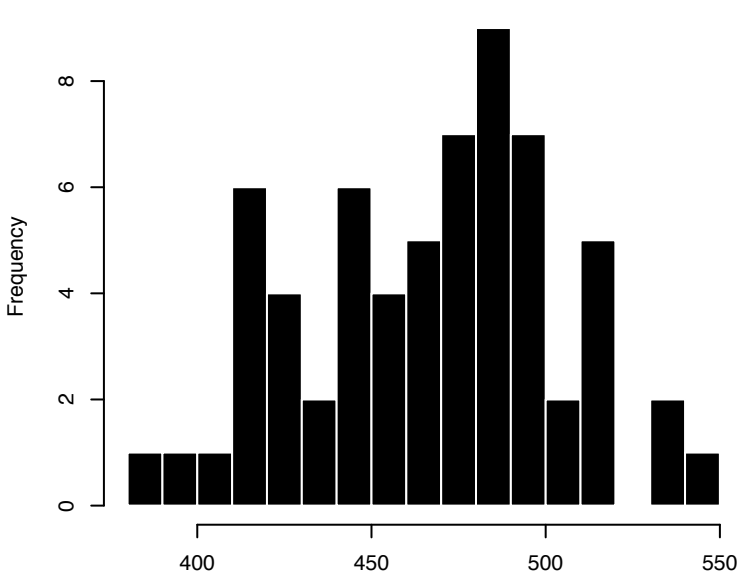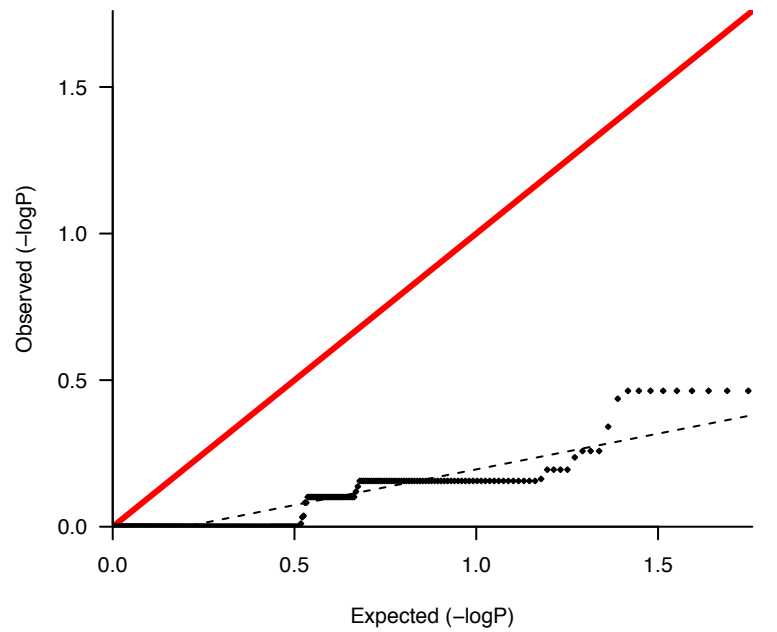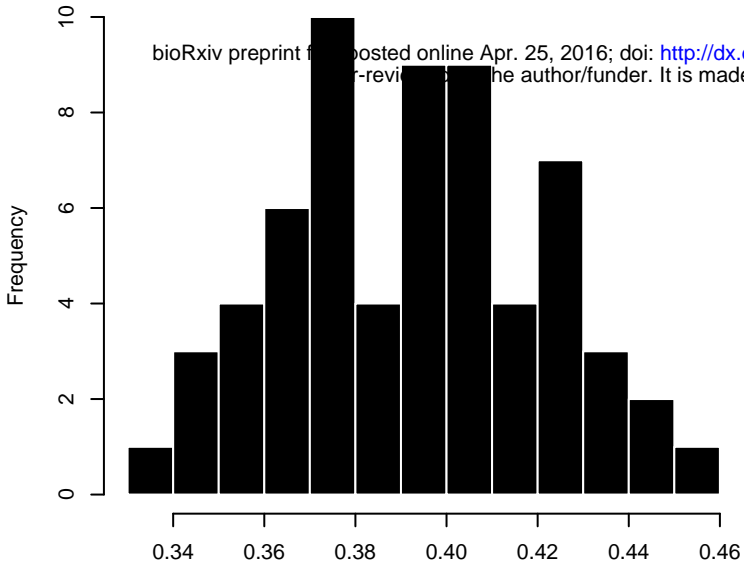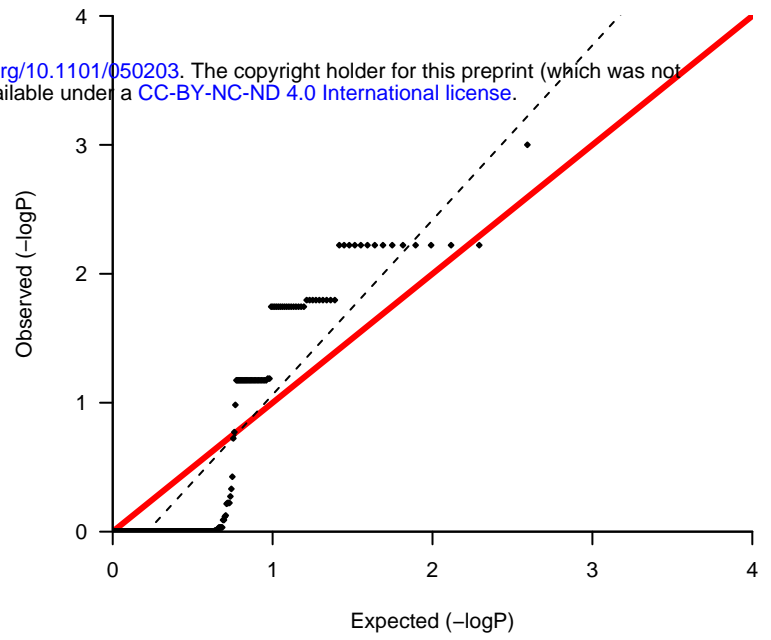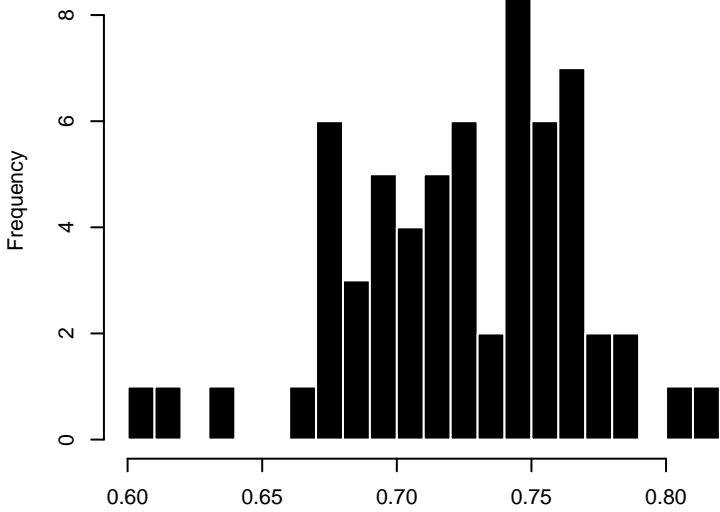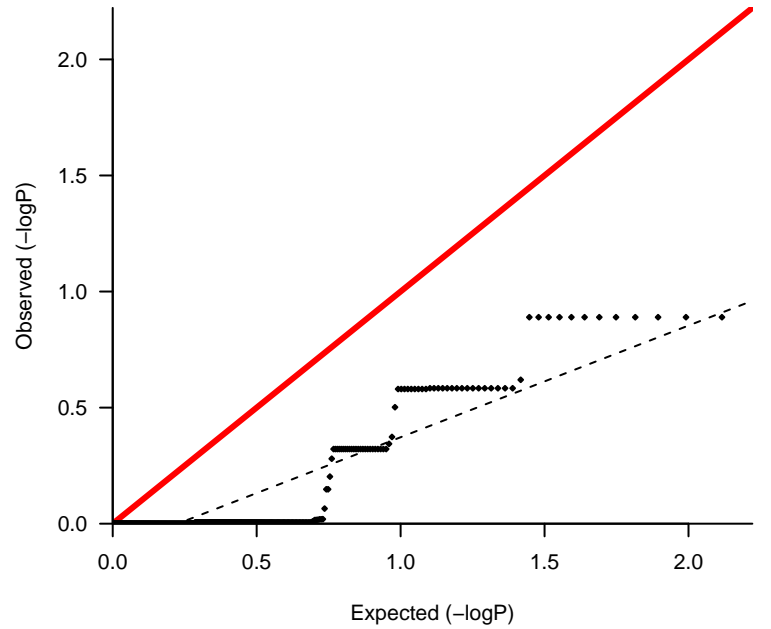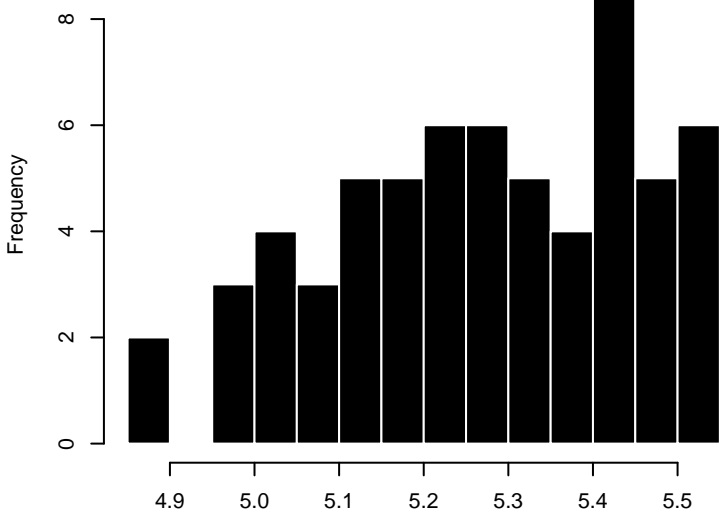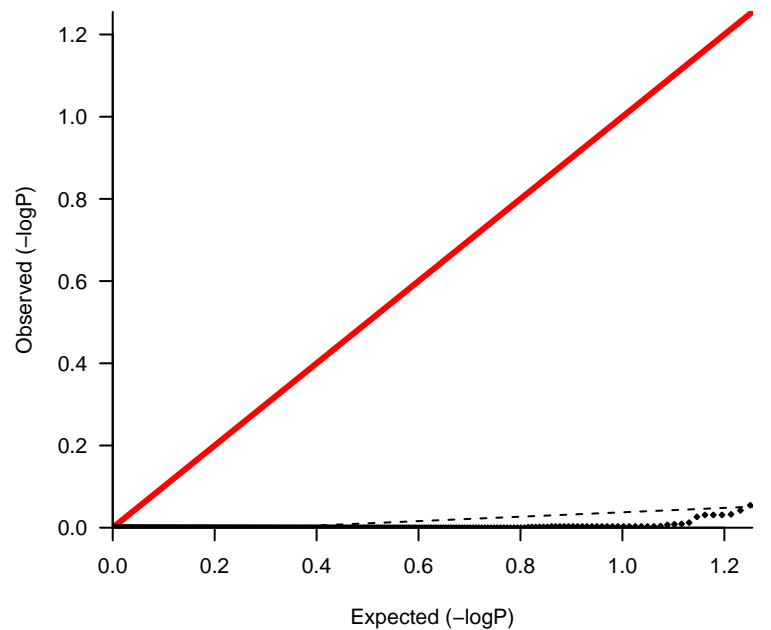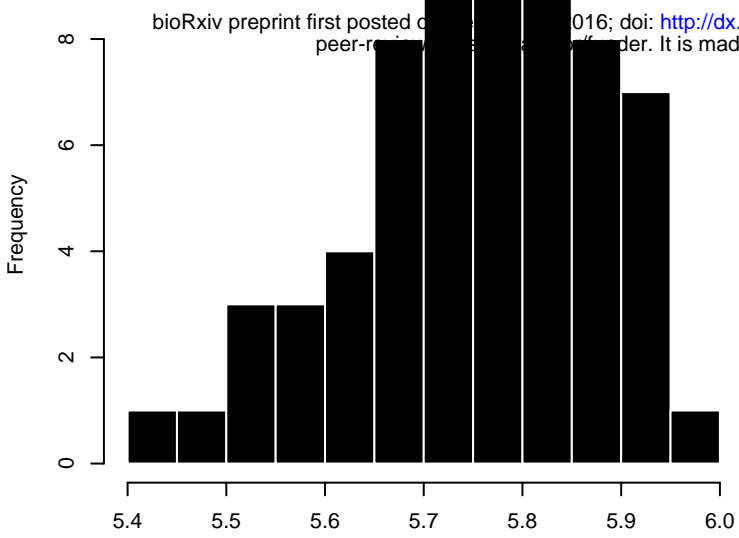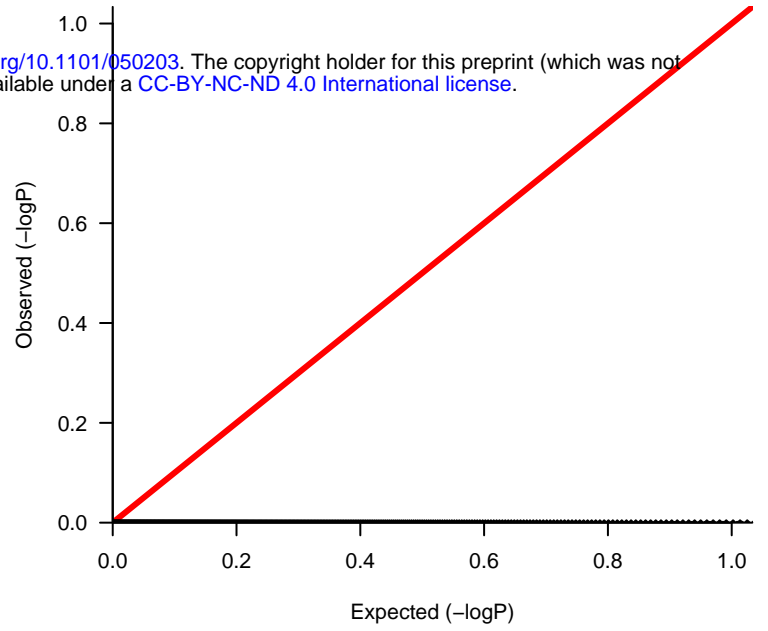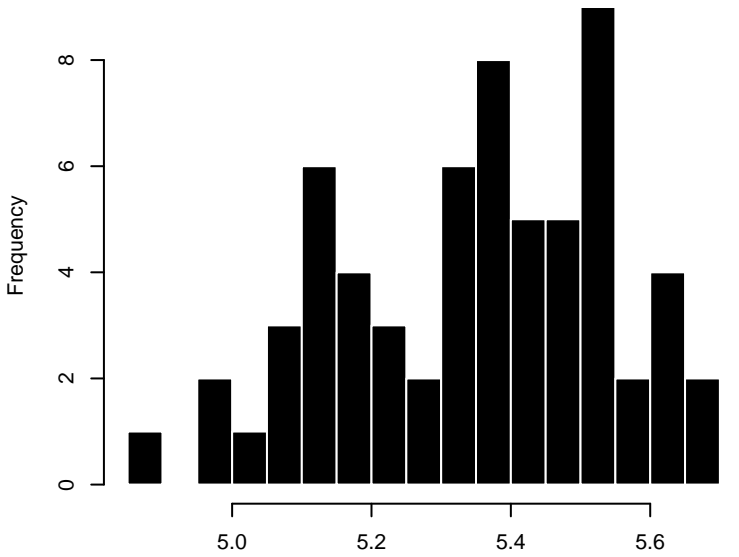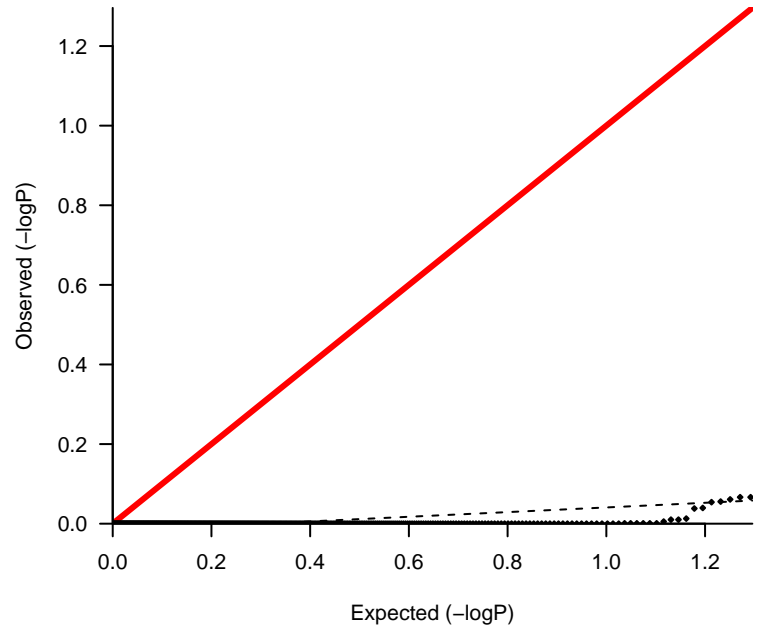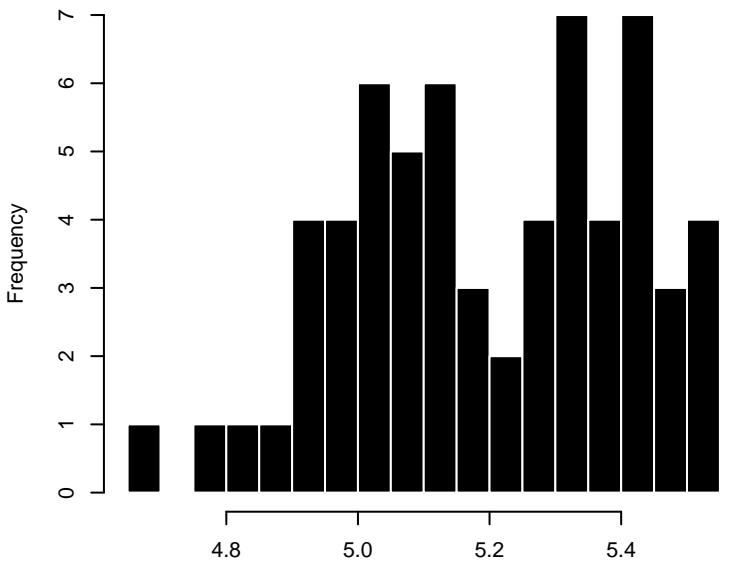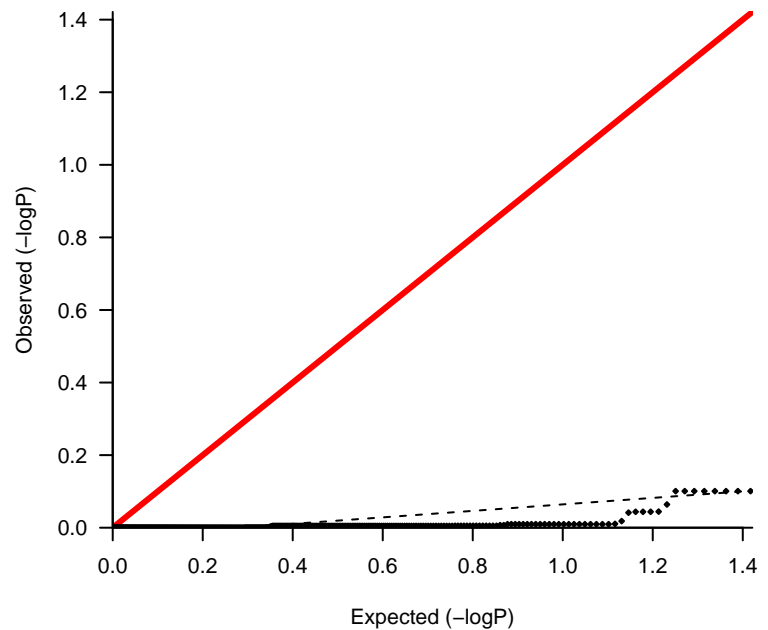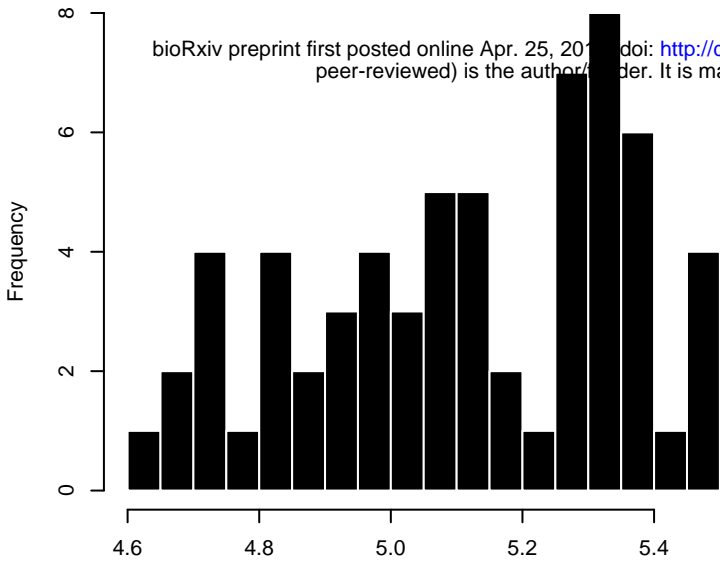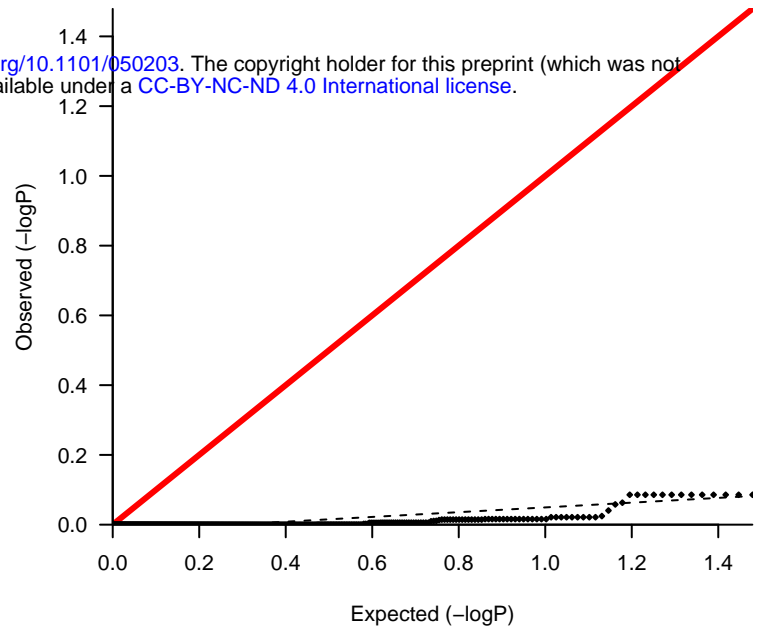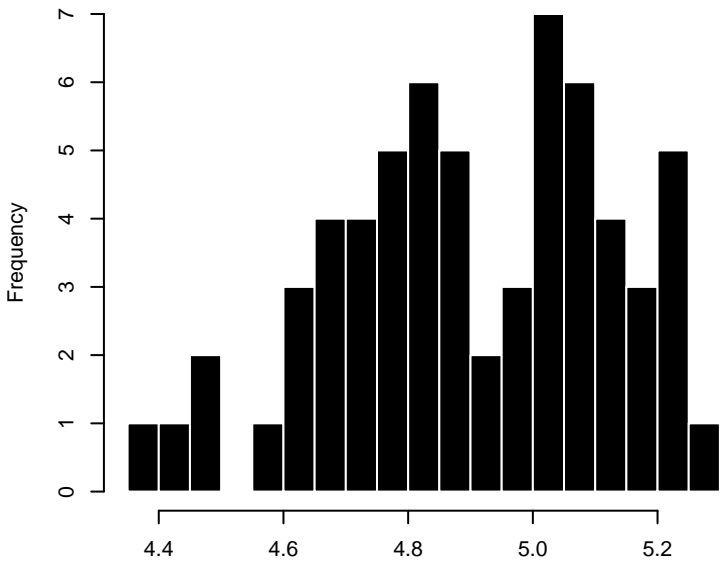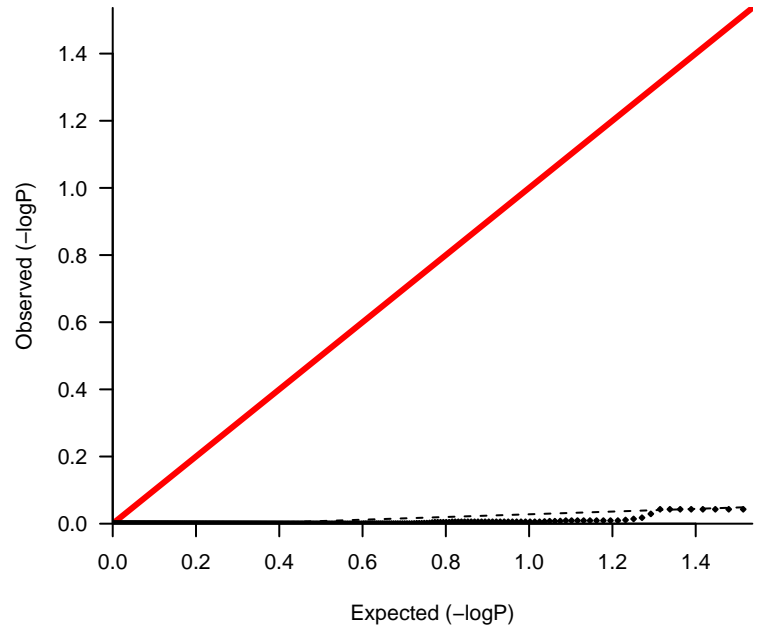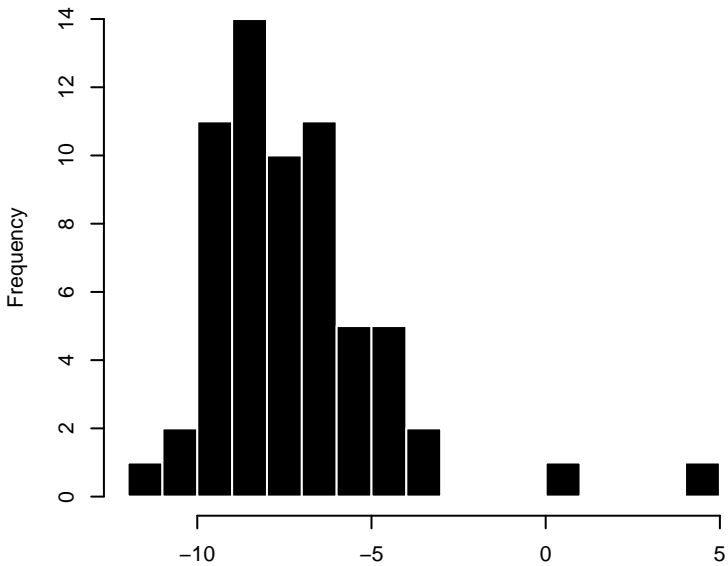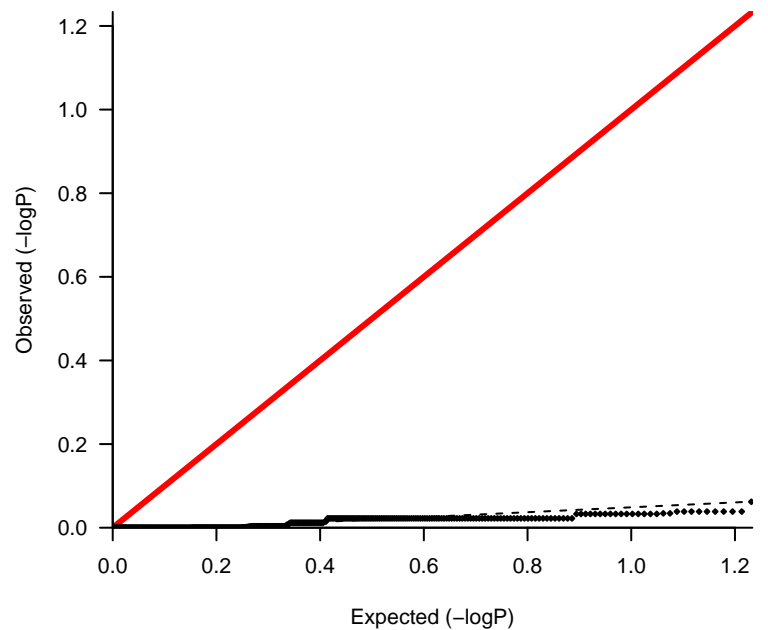
gravitropicScore
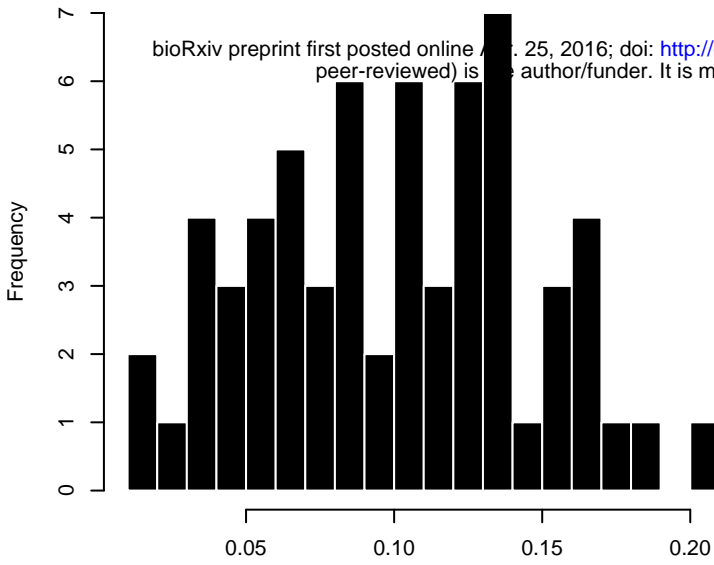
lambda 0.478
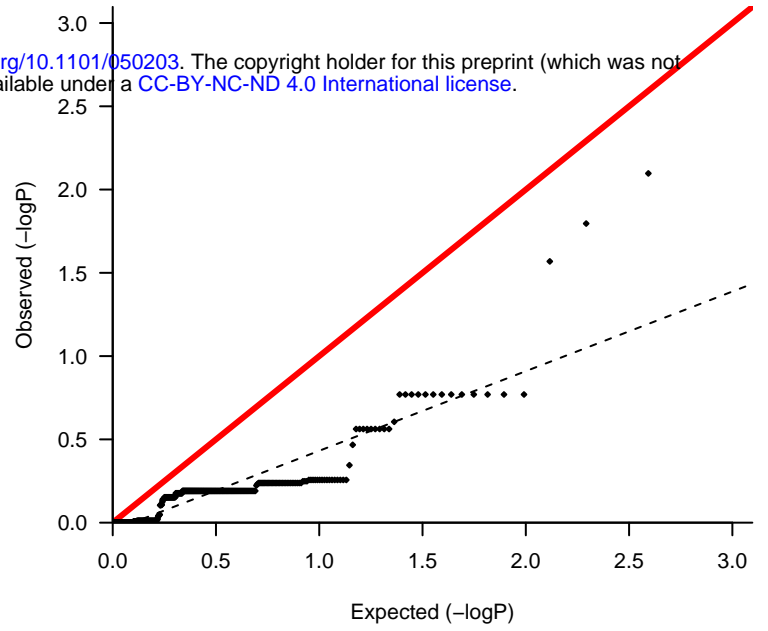
TotLen.EucLen
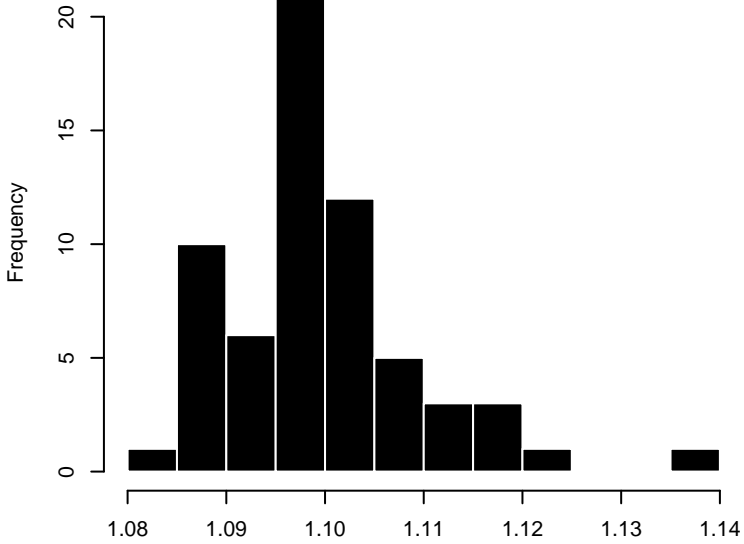
lambda 0.685
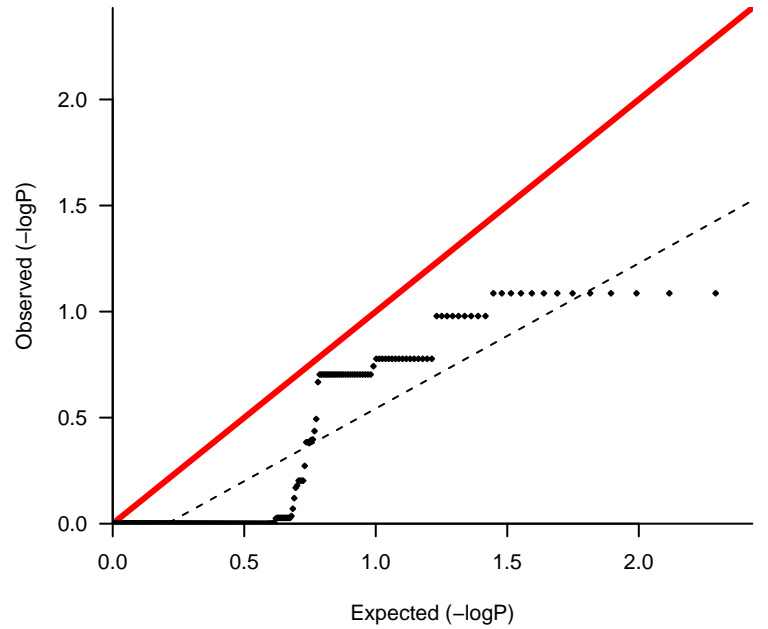
GR.TL
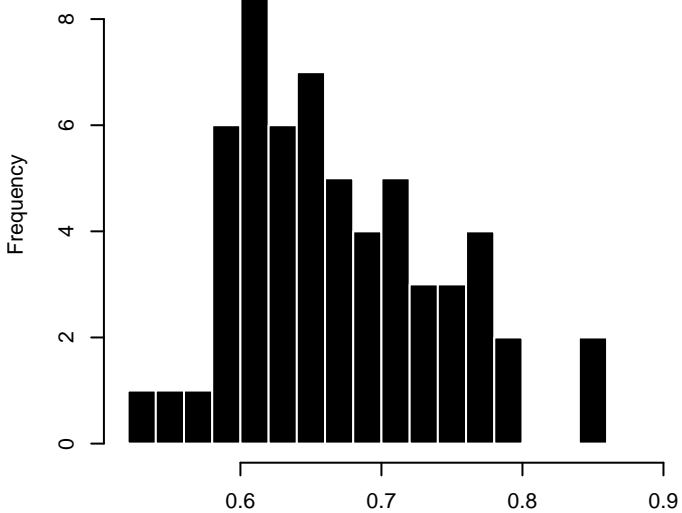
lambda 0.036
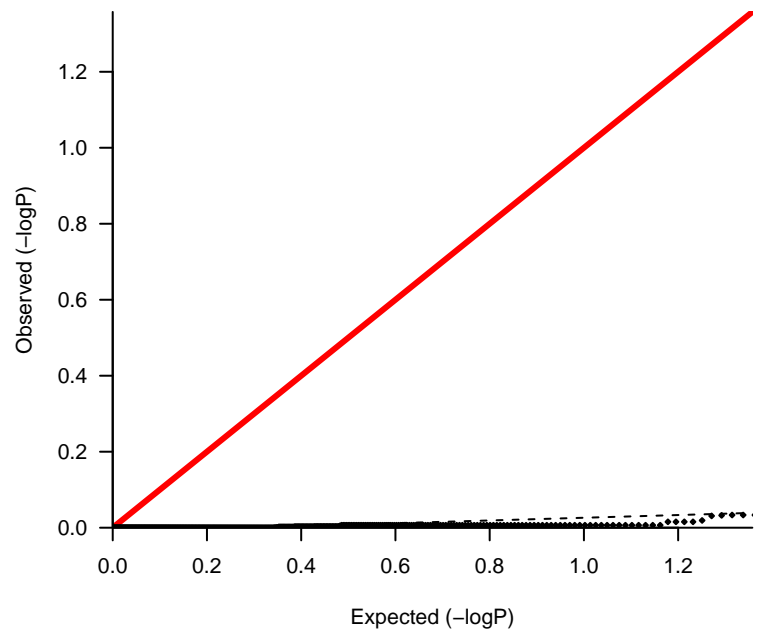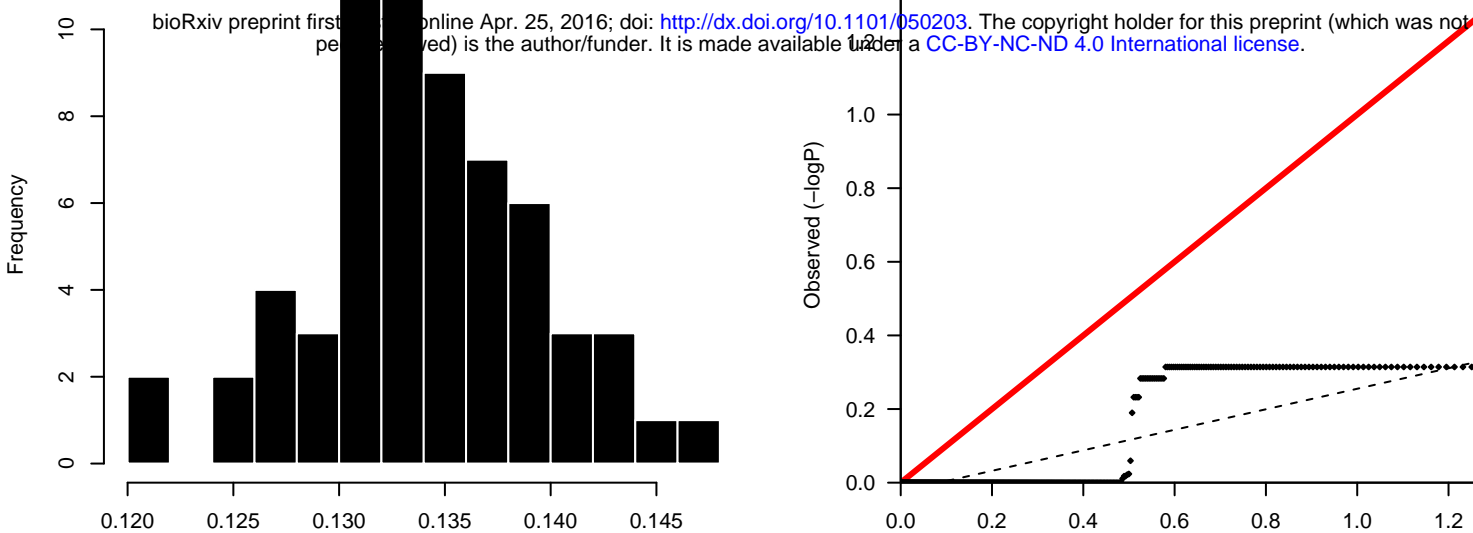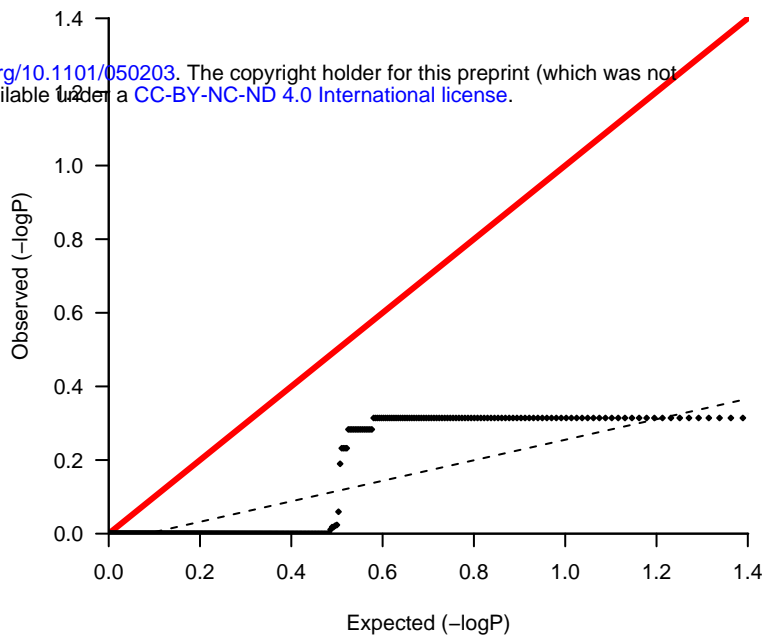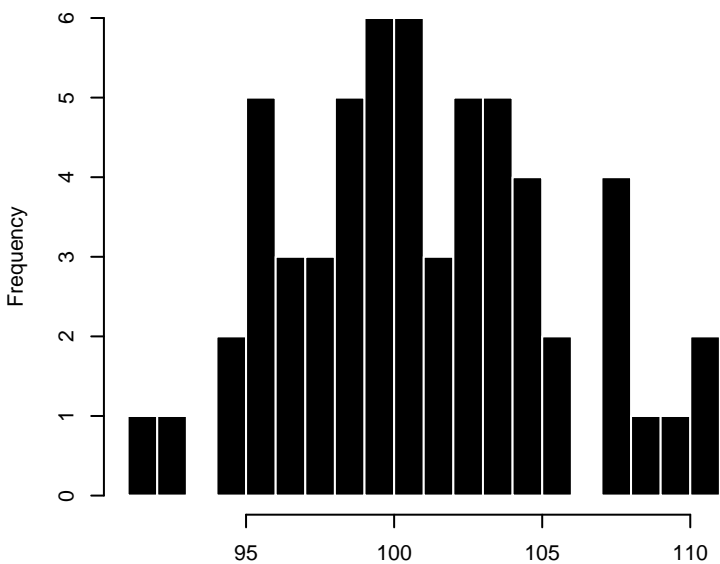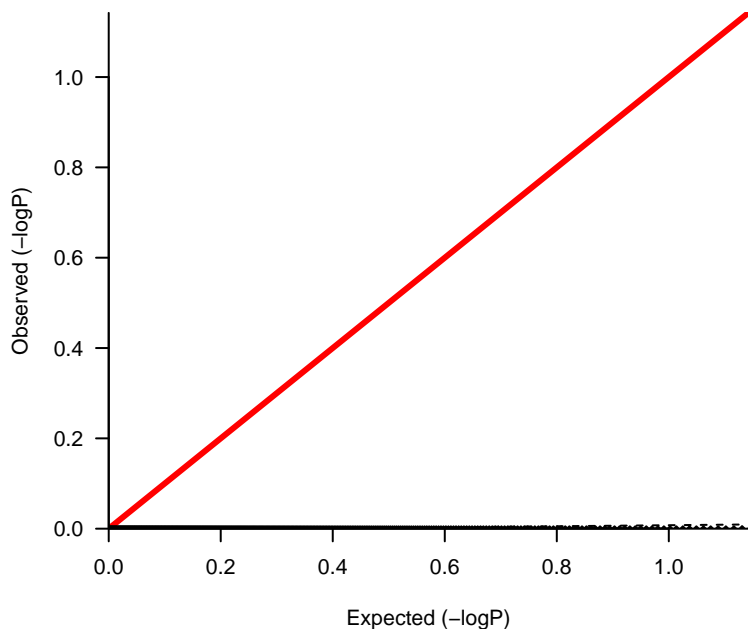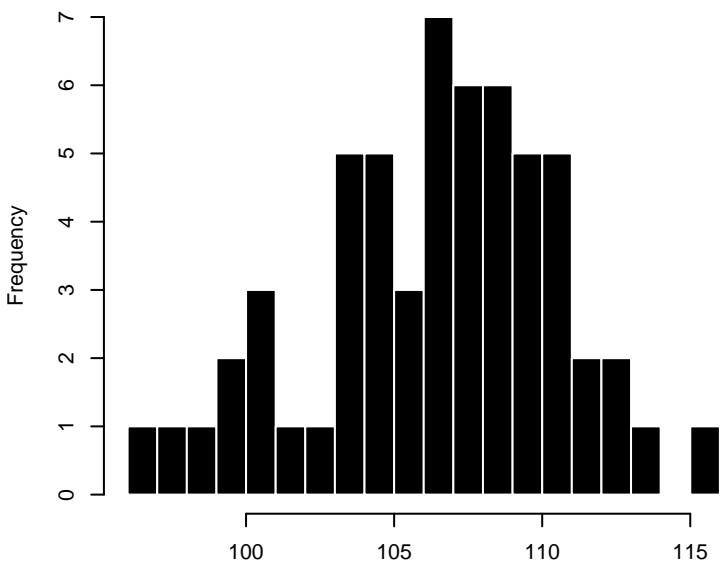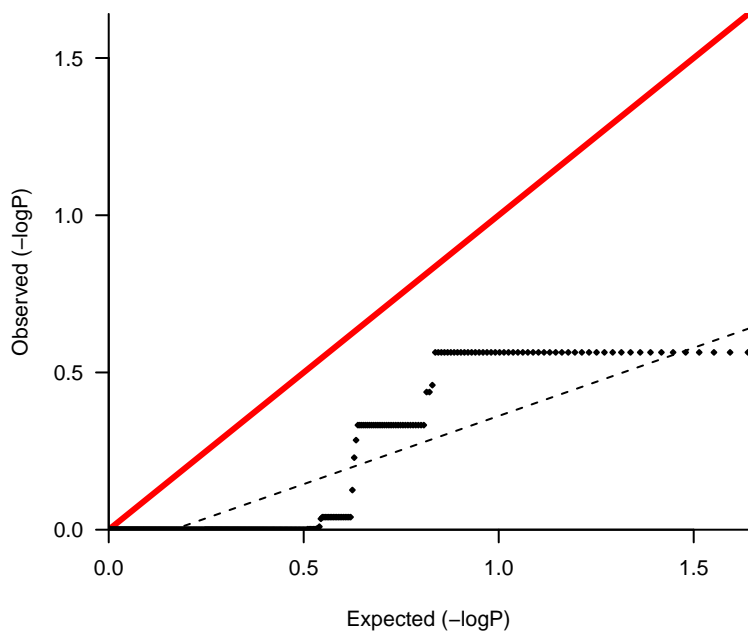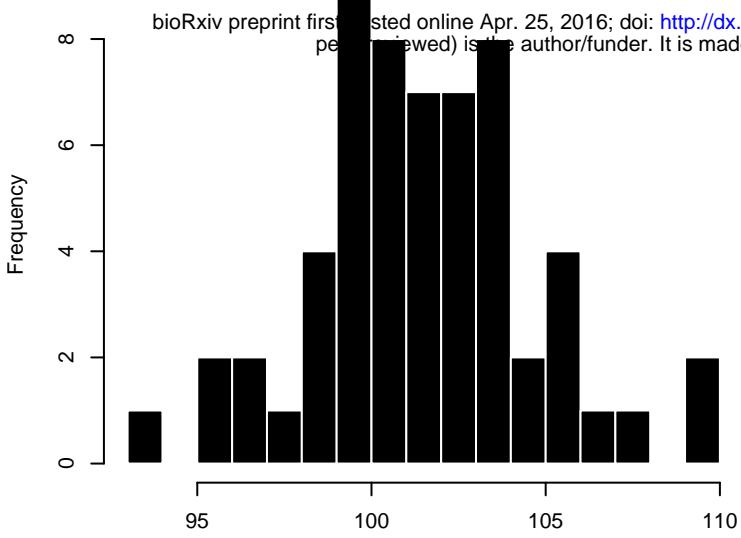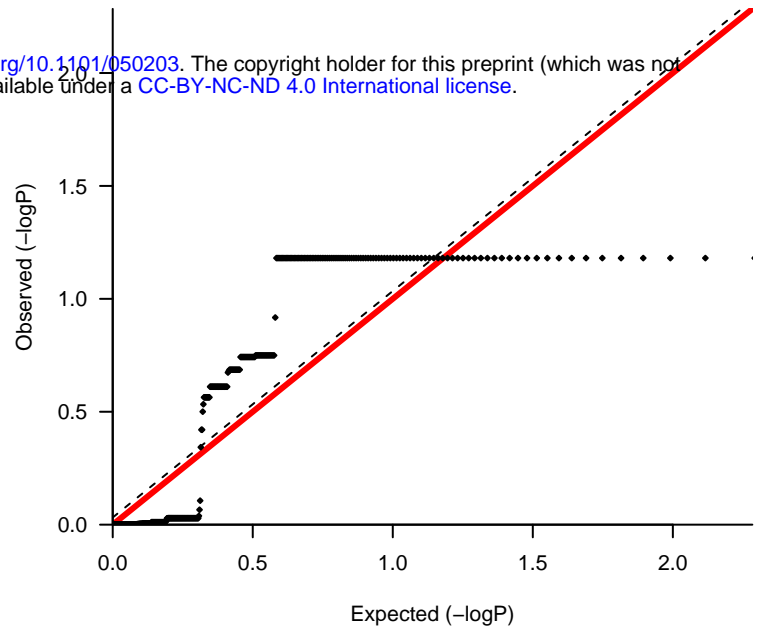
fecundity

lambda 0.879
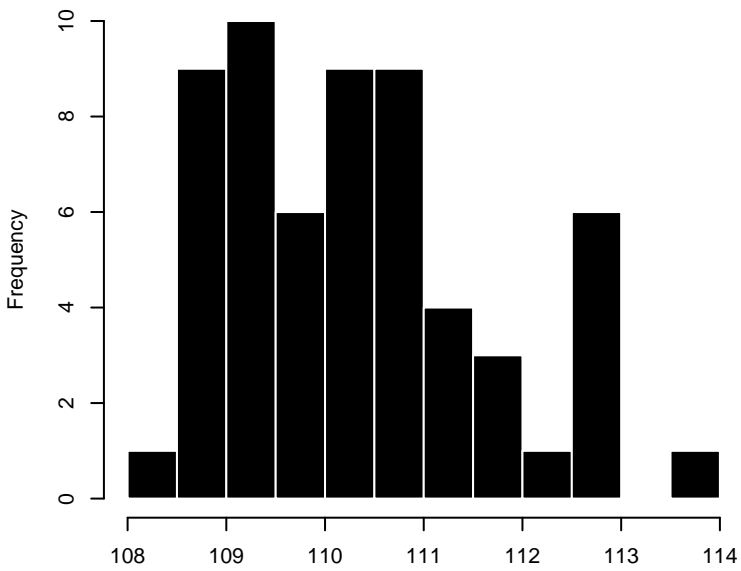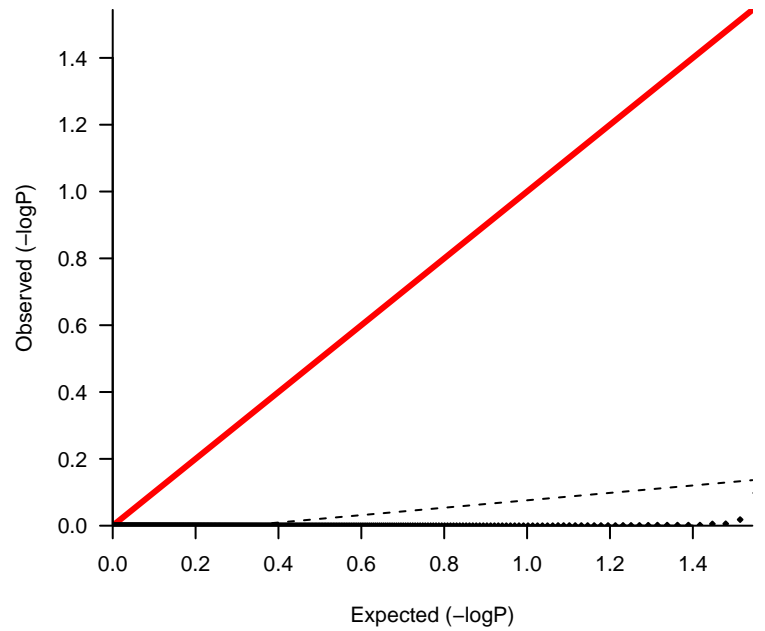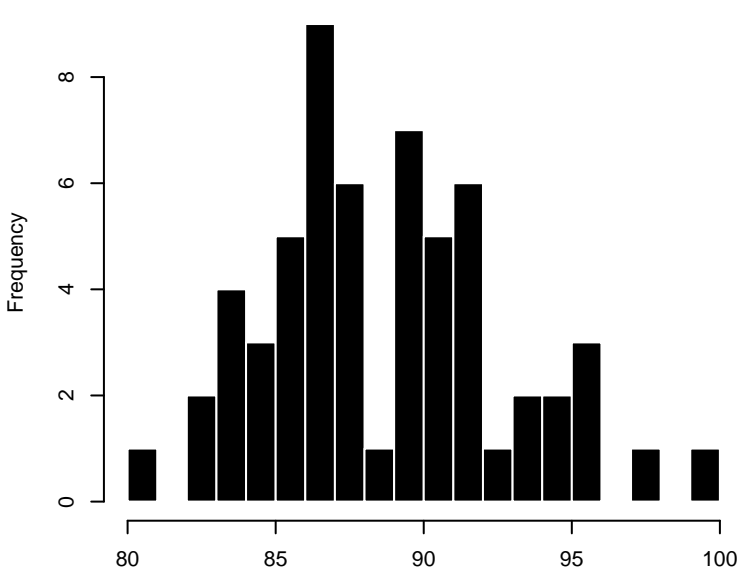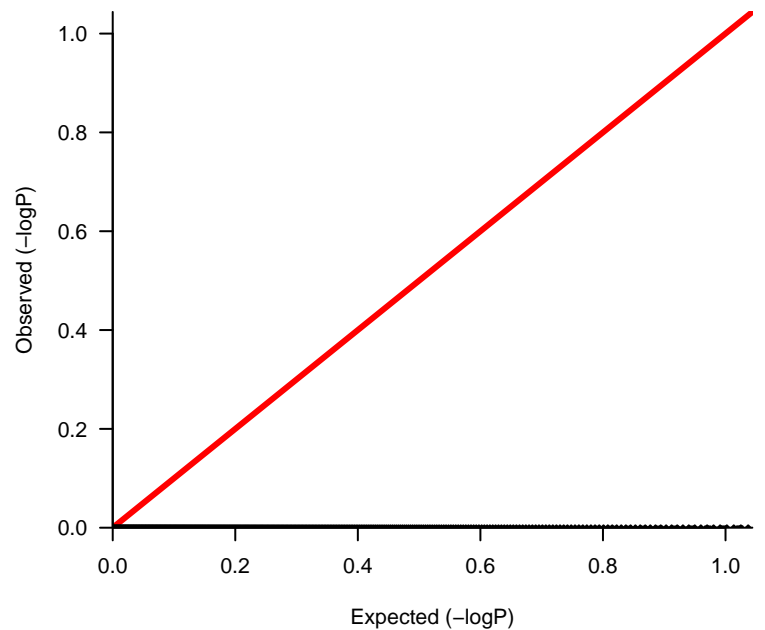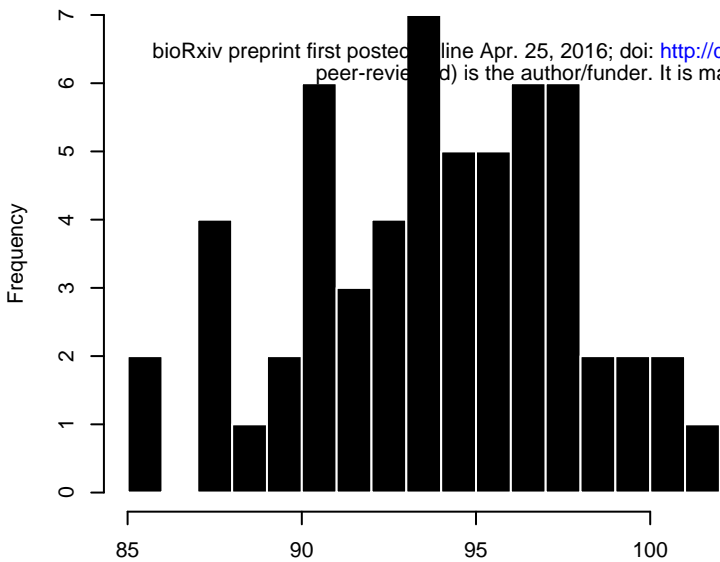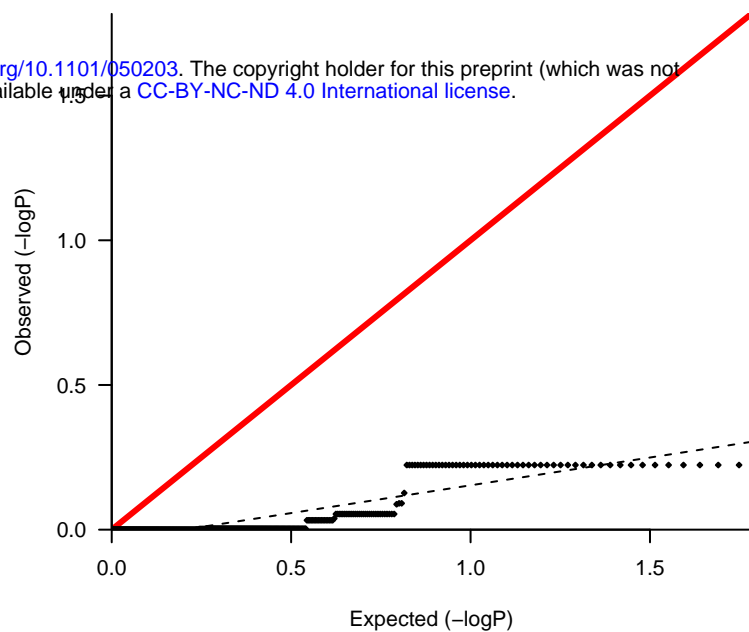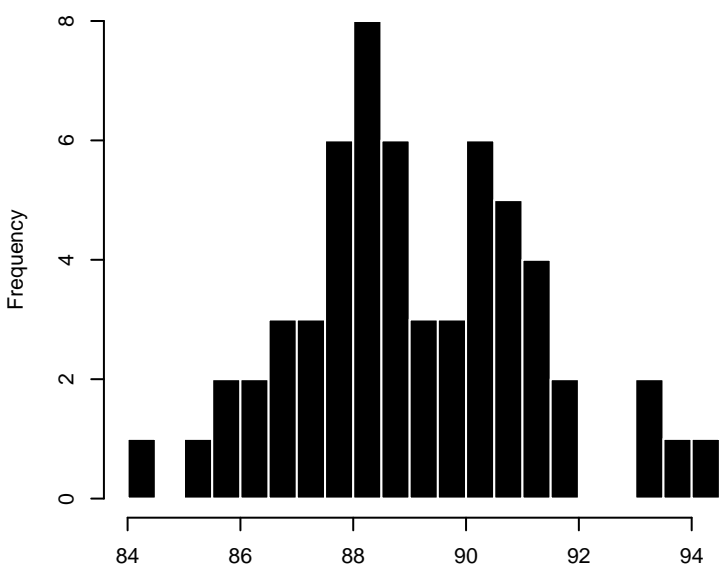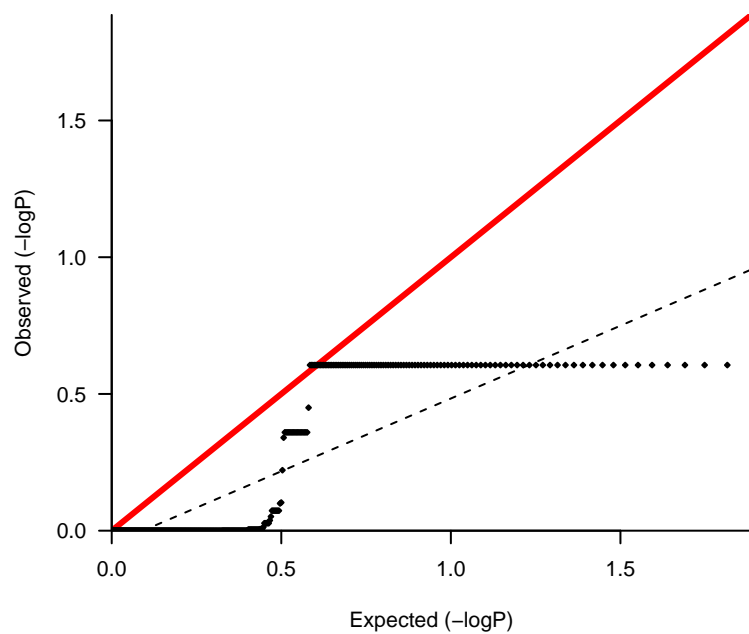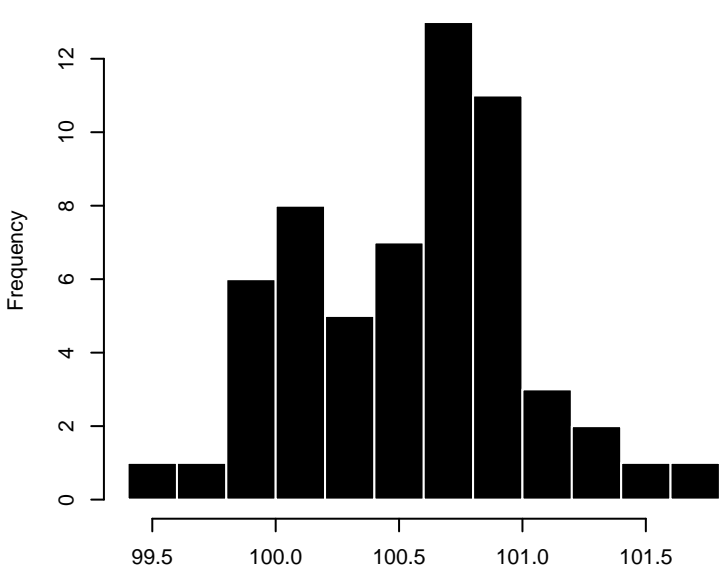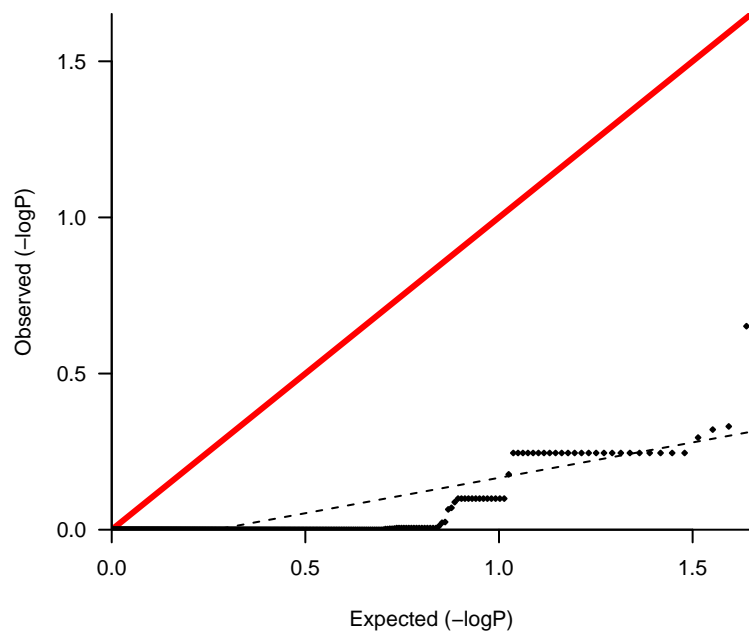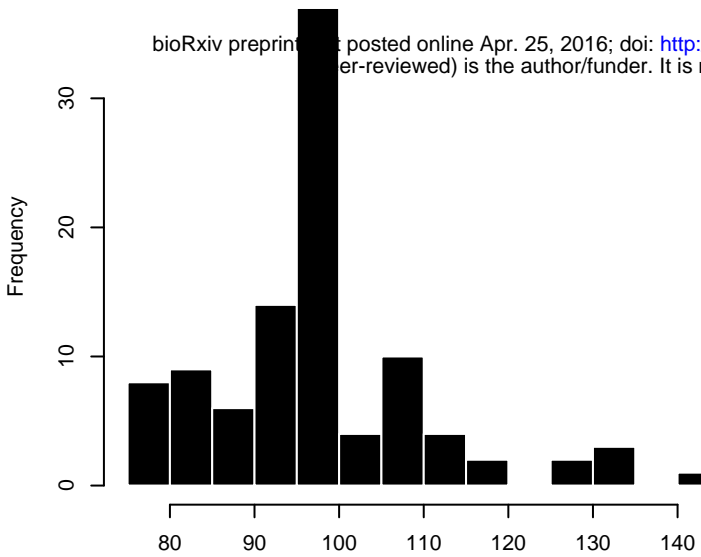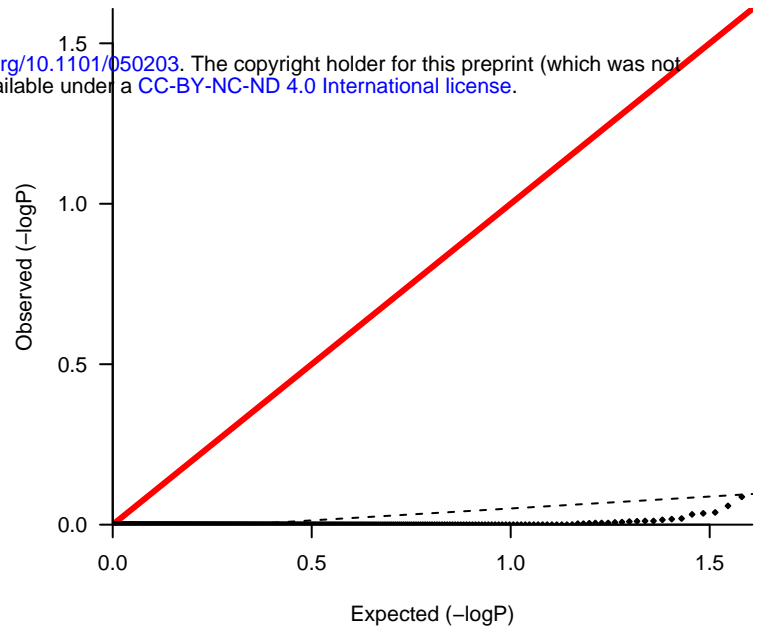
bio1

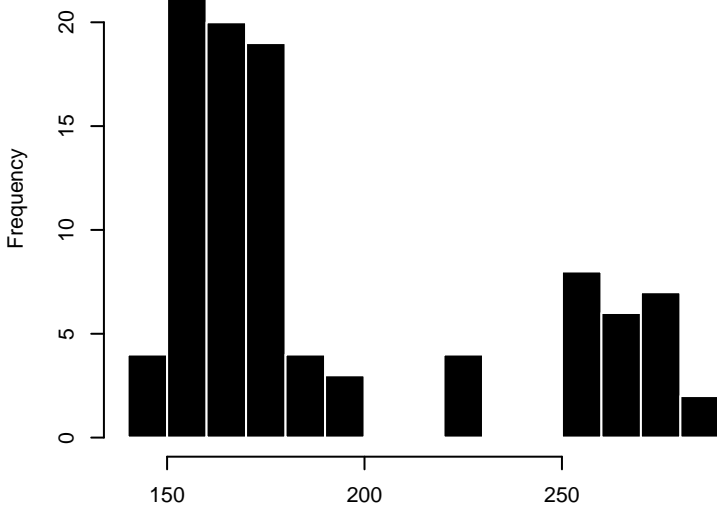**lambda 0.074**

bio2
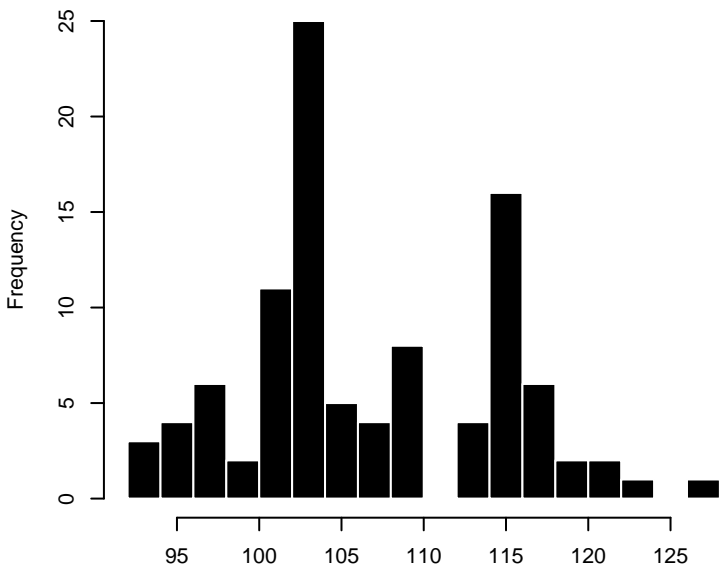
lambda 0.024

bio3

lambda 0.138

bio19

lambda 0.032